

Department of  
Medicine and Surgery

PhD program in Neuroscience, Experimental Neurology Unit, Cycle XXXIV

Curriculum in Experimental Neuroscience - 90R – 2

**Glycan-coated nanoparticles as inhibitors of  
specific lectins, a new neuroprotective  
therapeutic strategy for brain injury caused by  
ischemia**

Erol Gizem

852063

Tutor: Dr. Marco Gobbi

Co-tutor: Dr. Stefano Fumagalli

Supervisor: Dr. Silvia Cocco

Coordinator: Dr. Rosa Maria Moresco

ACADEMIC YEAR 2022-23

## Acknowledgement

---

As every good journey, the journey of my PhD also included challenges, fails, success, travels but most importantly great people who supported and encouraged me to keep going. Even though doing PhD is hard by its nature, I enjoyed the most thanks to all the people who provide such a working place with all the understanding, creativity, respect, share, and fun.

Foremost, I would like to sincerely thanks to my supervisors Dr. Marco Gobbi and Dr. Stefano Fumagalli and alumni supervisor Dr. Maria-Grazia De Simoni, for giving me this opportunity, their trust, continues support, guidance, advice and all their time that they spare for me, listening my questions and ideas. I am truly feeling grateful that they were my mentors during this journey which carries me from being a student to become a scientist, I would not succeed without them.

Next, I would like to thank all my fellow lab mates who contribute this thesis with their work and/or support, starting from Marco's group: Dr. Marten Beeg, Dr. Claudia Fracasso, Dr. Jacopo Lucchetti, Alessia Porta and alumni members Arianna Piotti and Elisabetta Battocchio for teaching, sharing their love and dealing with my problems, questions which always start with "*one question!*". As a prove of my luckiness, not only one family like crew, I had two ones. Therefore, with a same cordial way, I would like to thanks my fellows in Stefano's group: Domenico Mercurio, Alessia Valente, Joe Paul Kelk, Serena Seminara, Chantal Dembech, our alumni members and collaborators; Laura Neglia, Dr. Marco Oggioni, Dr. Carlo Perego, Dr. Franca Orsini, Dr. Katarzyna Popiolek-Barczyk, Dilan Bozanoglu for sharing, teaching, helping and making this journey much more fun being "*best!*" with their unique sides.

I would like to thank University of Milano-Bicocca and my supervisor Dr. Silvia Cocco for accepting me for the PhD program in neuroscience and European Union for being sponsor of my PhD project, NanoCarb which is funded under the H2020 work program, under the Marie Skłodowska Curie European Training Network scheme. I would like to thank all the colleagues in NanoCarb project making this project possible and specially to Dr. Laura Polito and group of Attana AB. (SE) for hosting me in their research facilities for my secondments and NanoCarb ESRs; Alessia Pancaro, Patricia Perez Schmidt and Marko Dobricic for sharing their knowledge and support being my secondment lab mates.

Last but not least, without the support and love of my family and friends close or far away, I know I could not have accomplished my PhD. A big thank goes to my dear Karim Mansour, for believing, encouraging, guiding me and the most for his endless support and love. I am deeply grateful to my family; my father Sener Erol, mother Yesim Erol and brother Yener Erol, for loving, and supporting me all the time throughout my life.

## Abstract

---

Glycans are chain-like structures of many monosaccharides which create the carbohydrate portion of glycoconjugates such as a glycoproteins, glycolipids, or proteoglycans, and are involved in many physiological functions. Glycans exposed on the surface of pathogens (pathogen-associated molecular patterns, PAMPs) are recognized by the lectin pathway of the complement system, one of the key components of innate immune system, through carbohydrate-binding lectins, such as mannose binding lectin (MBL) or ficolin. Experimental and clinical evidences indicate that MBL also drives secondary pathogenic thrombo-inflammation on the ischemic vasculature. MBL-mediated pathogenesis is initiated by its binding to the sugar moieties exposed on endothelial cell membranes after brain ischemia (damage-associated molecular patterns, DAMPs), e.g. induced by stroke.

Stroke is a major cause of disabilities and death worldwide and occurs by blockage or rupture of a brain artery (ischemic or hemorrhagic stroke), with lack of oxygen supply to brain tissues and sudden death of brain cells. Ischemic stroke is the most common type, i.e., 88% of all the cases. Pathological events on the ischemic vessels include the activation of coagulation, contact/kinin, and complement cascades. However, despite recent substantial progress in prevention and management, stroke still remains a large unmet medical need. Therefore, novel therapeutic strategies are needed and MBL inhibitors have been proposed as potential neuroprotective agents.

The main goal of this thesis was to identify potential MBL inhibitors, by developing and exploiting a robust pipeline of preclinical studies.

At first, an *in vitro* Surface Plasmon Resonance (SPR)-based assay was developed to identify MBL ligands/inhibitors and determine their affinities for MBL. The novel assay was extensively characterized and proved to be reliable and convenient. The results obtained with different ligands (e.g., monomeric mannose, a new glycan carrying nine mannose residues and mannose-coated gold nanoparticles (Man-GNPs) confirmed that multivalency markedly increases the affinity. Accordingly, Man-GNPs were selected as the best MBL-binding ligand for the following studies, which were carried out in a cell model mimicking the ischemic injury. i.e. immortalized human brain vascular endothelial cells (i-hBMECs) subjected to hypoxia and re-oxygenated in the presence of MBL. At first, a novel Quartz Crystal Microbalance (QCM)-based biosensor assay was developed which showed that mannose and N-acetylglucosamine —i.e., target sugars of MBL— are actually overexpressed by cells following hypoxic conditions. Consistently, it was observed that deposition of MBL on the cell surface is increased by hypoxia and this effect is counteracted by Man-GNPs, at non-toxic concentrations (20 ug/mL). Further studies showed that hypoxic cells overexpress inflammatory genes, in particular ICAM-1, in a MBL-dependent manner and this effect was prevented

by Man-GNPs. These results prompted to test Man-GNPs *in vivo*, in mice expressing human MBL (hMBL KI) and subjected to transient cerebral arterial occlusion, to have a mouse model of stroke. The administration of Man-GNPs to these mice did not result in toxic effects but also did not protect from the MBL-dependent stroke effects.

In conclusion, the work described in this thesis provides a full and robust pipeline for the preclinical studies of MBL inhibitors, with potential neuroprotective effect in stroke. Among MBL inhibitors, Man-GNPs were identified *in vitro* as the most promising one, and cell studies confirmed their ability to prevent MBL targeting to hypoxia-induced DAMPs, and the following inflammatory profile. However, the initial studies did not confirm efficacy *in vivo*, possibly for pharmacokinetic reasons which need to be further clarified.

## Riassunto

---

I glicani sono strutture composte da diversi monosaccaridi che formano la porzione di carboidrati tipica delle glicoproteine, dei glicolipidi o dei proteoglicani e sono coinvolti in diverse funzioni fisiologiche. I glicani che sono esposti sulla superficie dei patogeni (*pathogen-associated molecular patterns*, PAMP) rappresentano un segnale riconosciuto dalle lectine del sistema del complemento, una componente importante del sistema immunitario, tra cui ci sono le ficoline e *mannose-binding lectin* (MBL). Studi condotti in modelli sperimentali di ictus ischemico e studi clinici nei pazienti hanno dimostrato che MBL contribuisce al danno cerebrale endoteliale attivando cascate di tipo trombo-infiammatorio. Il riconoscimento di segnali di danno (*damage-associated molecular patterns*, DAMP) esposti sulle cellule endoteliali ischemiche è l'evento che scatena queste cascate tossiche.

L'ictus è una delle maggiori cause di mortalità e disabilità permanente nel mondo e dipende dalla rottura (ictus emorragico) o dall'occlusione (ictus ischemico) di un vaso cerebrale. L'ictus ischemico rappresenta il tipo più frequente e si verifica in circa 88% dei casi. Nonostante alcuni progressi nella cura, come l'introduzione della trombectomia meccanica, e nella prevenzione, la patologia rimane un problema medico irrisolto. Sarebbe quindi auspicabile l'identificazione di nuovi *target* terapeutici. In questo contesto MBL rappresenta un potenziale bersaglio farmacologico.

L'obiettivo principale di questa tesi è stato di identificare potenziali inibitori di MBL sviluppando ed utilizzando una robusta sequenza di test in vitro e in vivo.

Inizialmente abbiamo utilizzato un approccio in vitro mettendo a punto un saggio con *Surface Plasmon Resonance* (SPR) che ci ha permesso di identificare i ligandi zuccherini con miglior affinità di legame a MBL. Abbiamo dimostrato che l'aumento della multivalenza dei leganti disponibili, ottenuta avvalendoci di nanoparticelle d'oro funzionalizzate con residui di mannosio (Man-GNP), permette un'efficace *targeting* di MBL in vitro. Abbiamo quindi utilizzato cellule immortalizzate in coltura derivate da microvasi cerebrali umani (ihBMEC), dimostrando, con tecnica *Quartz Crystal Microbalance* (QCM), che le glicoproteine esposte sulla loro superficie cambiano se sottoposte ad uno stimolo ipossico, aumentando l'esposizione di residui di mannosio, il *target* principale di MBL. Abbiamo osservato che le ihBMEC ipossiche trattate con 20 µg/mL di Man-GNP hanno ridotto il loro profilo infiammatorio, con particolare riferimento all'espressione di ICAM-1 e MMP-2, due marcatori infiammatori vascolari. Questo effetto è stato accompagnato dalla riduzione della deposizione di MBL sulla superficie vascolare. Nell'ultima parte del progetto abbiamo testato l'efficacia del trattamento con Man-GNP in un modello murino di ictus ischemico, sfruttando un ceppo animale umanizzato, quindi delecto per le due isoforme murine di MBL e *knock-in* per quella umana. Il trattamento, quando confrontato con quello con GNP coniugate al glucosio, che non legano MBL, non ha però dimostrato

un effetto neuroprotettivo sui deficit sensorimotori dopo ischemia. In ogni caso la somministrazione sistemica delle Man-GNP si è dimostrata sicura e futuri esperimenti permetteranno di definire una strategia di trattamento migliore, volta ad aumentare la biodisponibilità della molecola.

In conclusione, questa tesi ha descritto una *pipeline* sperimentale per *screenare* diverse molecole con il potenziale di agire come inibitori di MBL, partendo da un approccio in vitro su chip (SPR), fino ad approcci in vitro su modelli cellulari ed in vivo su modelli animali di patologia. Gli studi in vitro indicano che le Man-GNP inibiscono MBL, ma la loro efficacia in vivo resta da dimostrare.

## Table of Contents

---

<b>Chapter 1 : Introduction.....</b>	<b>15</b>
<b>Chapter 2 : Method and materials .....</b>	<b>20</b>
2.1 Chemicals and reagents .....	20
2.2 Biological materials .....	20
2.3 Thiol-glyco-derivatives.....	21
2.4 Synthesis, functionalization and characterization of gold nanoparticles.....	21
2.5 Piranha/UV cleaning and chip surface coating .....	24
2.6 SPR binding assays.....	25
2.7 Western Blots.....	27
2.7.1 Native and recombinant MBL oligomerization .....	27
2.7.2 MBL protein corona formation .....	27
2.7.3 hMBL and mMASP-2 complexes of hMBL KI mice .....	27
2.8 Cell culture .....	28
2.9 QCM ischemic glycoprofiling assay .....	28
2.10 In vitro ischemia model assay with sugar-GNPs treatment.....	29
2.11 Immunofluorescence .....	30
2.11.1 In vitro cell assay .....	30
2.11.2 In vivo mouse model .....	30
2.12 Confocal microscopy and quantitative analysis .....	30
2.12.1 In vitro cell assay .....	30
2.12.2 In vivo mouse model .....	31
2.13 Reflectance confocal microscopy .....	31
2.14 Super-resolution microscopy. ....	31
2.15 Real-time RT-PCR.....	32
2.16 Mice .....	32

2.17 Focal cerebral ischemia: Transient middle cerebral artery occlusion .....	33
2.18 Treatments .....	34
2.19 Neurologic deficits .....	34
2.20 Elevated plus maze (EPM).....	35
2.21 Plasma collection.....	35
2.22 Brain collection.....	35
2.23 Lectin pathway activity assay.....	36
2.24 Statistical analysis.....	37
<b>Chapter 3 : Result .....</b>	<b>38</b>
3.1 In vitro binding studies .....	38
3.1.1 Defining optimum MBL binding surface.....	38
3.1.2 Recognizing MBL inhibitors in buffer .....	46
3.2 Hypoxia altered glycolyx of i-hBMECs.....	52
3.2.1 Introduction .....	52
3.2.2 Overexpression of glycans after hypoxia .....	53
3.3 Screening potential effect of GNPs in in vitro cell assay .....	55
3.3.1 Toxicity .....	55
3.3.2 Defining protective dose of sugar-GNPs .....	59
3.4 In vivo ischemic mouse model .....	64
3.4.2 Characterization of hMBL knock-in (KI) mice .....	65
3.4.3 In vivo protective effect Man-GNPs on the ischemic mouse model .....	70
<b>Chapter 4 : Discussion.....</b>	<b>72</b>
<b>Chapter 5 : Conclusion .....</b>	<b>77</b>
<b>Chapter 6 : References.....</b>	<b>78</b>



## Table of Figures

Figure 1 Pipeline of the pre-clinical studies for MBL-inhibitors.....	17
Figure 2 The Man9 glycan structure has three antennae that are capped with alpha 1,2 linked mannoses, based on the NMR analysis .....	21
Figure 3 Structure of the synthetic glyco-derives, Man-EG <sub>6</sub> C <sub>11</sub> S (A), Glc-EG <sub>6</sub> C <sub>11</sub> S (B).....	21
Figure 4 TEM images.....	22
Figure 5 Synthesis of mannose and glucose-capped GNPs .....	23
Figure 6 UV-Vis spectroscopy to characterize citrate-capped GNPs and glyco-capped GNPs .....	24
Figure 7 Parallel flow channels of ProteOn XPR36 SPR chip surface.....	26
Figure 8 Protocol of ischemia on i-hBMECs to profile glycocalyx of ischemic endothelium. ....	28
Figure 9 Experimental schema of i-hBMECs exposing hypoxia to investigate MBL interaction with sugar-GNPs on ischemic endothelium. ....	29
Figure 10 Representative figures for focal cerebral ischemia with transient middle cerebral artery occlusion (tMCAo).....	33
Figure 11 Schema of Mannan-assay for C3 deposition .....	36
Figure 12 Working principle of The ProteOn XPR36 SPR instrument. ....	38
Figure 13 Overview of SPR assay principle .....	39
Figure 14 Functionalization of the SPR chip surface in the instrument.....	40
Figure 15 Diagrammatic scheme of piranha/UV cleaning and the chip surface coating cycle. ....	41
Figure 16 Comparison of different cleaning approaches to reclaim the used SPR chip.....	42
Figure 17 Sensorgrams obtained on the same chip after sequential cleaning with piranha/UV, surface coating with Man-EG <sub>6</sub> C <sub>11</sub> S outside the SPR instrument as indicated, and injection of rhMBL.....	43
Figure 18 Concentration-dependent binding of rhMBL obtained by simultaneous injections of four dilutions of rhMBL (0.03-1 µg/mL).....	44
Figure 19 MBL specifically bound to Man-EG <sub>6</sub> C <sub>11</sub> S-coated SPR chip surface. ....	44
Figure 20 Detection of specific homogenous hMBL binding.....	45
Figure 21 Evaluation of quenching effect of MBL binding in presence of sera.....	46

Figure 22 Proof of principle for screening inhibitors of MBL binding to a Man-EG <sub>6</sub> C <sub>11</sub> S -coated SPR chip surface. ....	46
Figure 23 Inhibitory multivalency effect of M9 Glycan on MBL binding over Man-EG <sub>6</sub> C <sub>11</sub> S -coated SPR chip surface .....	47
Figure 24 Inhibition of MBL binding on Man-EG <sub>6</sub> C <sub>11</sub> S -coated SPR chip surface by sugar-capped GNPs. ....	48
Figure 25 MBL binding signals after pre-incubation with inhibitory sugar-capped GNPs. ....	49
Figure 26 Recombinant and human endogenous MBL showed different oligomerization. ....	50
Figure 27 MBL was found on hard corona of mannose-capped GNPs (Man-GNPs) but not glucose-capped GNPs (Glc-GNPs).....	51
Figure 28 Inhibition of MBL binding by sugar-capped GNPs in human serum.....	52
Figure 29 Diagrammatic scheme of LNB-CC/COP chip preparation for glycoprofiling of ischemic i-hBMECs endothelium and lectin binding assay on altered glycocalyx of i-hBMECs within the Cell A200 QCM instrument.....	53
Figure 30 Hypoxia altered glycoprofile of i-hBMECs endothelium.....	54
Figure 31 High concentration of sugar-GNPs (mannose-capped GNPs (Man-GNPs); glucose-capped GNPs (Glc-GNPs)) did not affect cell viability. ....	55
Figure 32 Hypoxic and normoxic i-hBMECs undergone re-oxygenation with or without in the presence of 40 µg/mL sugar-GNPs in 30% HS labelled with phalloidin (F-actin) to stain the cytoskeleton.....	56
Figure 33 Set up and test of reflectance confocal microscopy to visualize sugar-GNPs using a confocal microscope.....	57
Figure 34 Mannose-capped gold nanoparticles (Man-GNPs) were localized inside i-hBMECs with or without exposure of hypoxia. ....	58
Figure 35 Cytoskeletal organization of i-hBMECs was not altered in presence of Man-GNPs.....	59
Figure 36 Characterization of hypoxia-induced inflammatory genes in i-hBMECs after 4h of re-oxygenation in presence of 30% of human serum. ....	60
Figure 37 Normoxic (CTRL) or hypoxic (HYPX) i-hBMECs undergone re-oxygenation in the presence of 5, 20 or 40 µg/mL Man-GNPs in 30% HS (w/Man-GNPs) and analysed for inflammatory gene expression. ....	61

Figure 38 MBL deposition was significantly increased on endothelium after hypoxia and this deposition was decreased with a re-oxygenation in the presence of 5 and 20 $\mu\text{g/mL}$ Man-GNPs in 30% HS. ....	62
Figure 39 No-colocalization was found between MBL and of 5, 20 or 40 $\mu\text{g/mL}$ Man-GNPs on hypoxic and normoxic (CTRL) i-hBMECs.....	63
Figure 40 Evolutionary differences in MBL isoforms between rodents and humans.....	65
Figure 41 Human MBL has little changes in oligomerization and was consumed after tMCAo .....	66
Figure 42 hMBL expressed by hMBL KI mice was circulating with mMASP-2 after tMCAo.....	67
Figure 43 Brain glycoalyx characterization via mannose staining with fluorescent Concanavalin-A (ConA).....	68
Figure 44 hMBL targeted the brain vessels pertinent to the ischemic territory .....	69
Figure 45 Systemic activation of the complement system after 48h, 90' and 2d of tMCAo in wild and hMBL KI mice. ....	70
Figure 46 Evaluation of behavioural deficits, neuroscore after 48 h and EPM after 8d of reperfusion in hMBL KI mice with a treatment of sugar-GNPs (20 $\mu\text{g/mL}$ ).....	71

## List of Table

---

Table 1 Characterization by DLS of citrate and glycol-capped GNPs. ....	23
---	----

## List of Abbreviation

---

**AhR:** aryl hydrocarbon receptor

**ConA:** concanavalin A

**DAMPs:** damage-associated molecular patterns

**DLS:** dynamic light scattering

**GlcNAc:** N-Acetylglucosamine

**GNPs:** gold nanoparticles

**HIF-1:** hypoxia Inducible Factor 1

**HS:** human serum

**IC50:** the half-maximal inhibitory concentration

**ICAM-1:** intercellular adhesion molecule 1

**IL-1alfa:** interleukin 1

**i-hBMECs:** immortalized human brain microvascular endothelial cells

**K<sub>D</sub>:** equilibrium dissociation constant

**KI:** knock-in

**LCA:** lens culinaris agglutinin

**LP:** lectin pathway

**MBL:** mannose binding lectin

**MMP-2:** matrix metalloproteinase 2

**Neu5Ac:** N-acetylneuraminic acid (SialicAcid)

**PAMPs:** pathogen-associated molecular patterns

**PHAL:** phytohemagglutinin leucoagglutinin

**RAGE:** receptor for advanced glycation end products

**rhFicolin-1:** recombinant ficolin-1

**rhMBL:** recombinant human mannose binding lectin

**RU:** resonance units

**RCA:** ricinus communis agglutinin

**SAM:** self-assembled monolayer

**SNA:** sambucus nigra lectin

**SPR:** surface plasmon resonance

**TEM:** transmission electron microscopy

**TMD1:** trastuzumab emtansine

**WGA:** wheat germ agglutinin

# Chapter 1 : Introduction

Glycans are sugar-based polymers, composed of many monosaccharides linked by glycosidic bonds which forms chain-like structures on cells and most proteins. They present in many key physiological and pathological processes including<sup>1</sup> modulation of structural and functional properties of biomolecules, e.g. for detection of many infectious agents, cell adhesion, receptor activation, signal transduction, endocytosis. As carbohydrate binding proteins, lectins are the major interacting partners of the glycans. Lectins are proteins having different affinity to varieties of sugars carrying mono-, di-, or multivalent carbohydrate binding sites<sup>2-4</sup>, and can either be free or exposed on the cell surfaces. Lectins are endogenously found in microbes<sup>5-7</sup>, plants<sup>8-10</sup>, animals and humans<sup>11-15</sup>, and are involved in various biological processes, such as cellular development and interactions, signaling pathways and immune responses. Therefore, the interaction between lectins and glycans plays fundamental role in many human physio-pathological processes.

In humans, over 20 distinct types of lectins were detected including selectins, galectins and lectin pathway initiators<sup>11,14</sup>. The lectin pathway (LP) is part of the complement system, an arm of innate immunity triggered when lectin proteins, e.g. mannose binding lectin (MBL) or ficolin, bind to specific carbohydrates—and carbohydrate patterns—on the surface of pathogens (pathogen-associated molecular patterns, PAMPs) or expressed by damaged self-cells (damage-associated molecular patterns, DAMPs)<sup>16</sup>. While the complement activation consequent to the lectin binding to pathogens has a protective role, the consequences of their binding to DAMPs may be deleterious<sup>17</sup>. Among all the lectins, particularly MBL shows a key pathogenic role after myocardial<sup>18,19</sup>, renal<sup>20</sup>, gastrointestinal<sup>21</sup> and cerebral ischemic injury<sup>22-25</sup>. In all these conditions but especially for cerebral ischemic injury (stroke), MBL appears to contribute to tissue injury, as also confirmed by the fact that genetic deletion or pharmacological inhibition of MBL are protective<sup>22,23,26</sup>.

Stroke is the third leading cause of disabilities and second leading cause of death worldwide<sup>27-30</sup>. Among the different types of strokes, the ischemic one is the most frequent (88% of all strokes) and can be treated by the use of a thrombolytic agent and endovascular thrombectomy. Despite recent progress in prevention and management, stroke remains a medical issue considering that the available therapies present some limitations like a short therapeutic window and increased risk of hemorrhages. As such around 40% of ischemic stroke patients are untreated and the rate of patient treated with reperfusion is closer to <20% in Europe which is however showing a limited efficacy in some patients, even if a successful reperfusion is achieved, the so-called futile reperfusion<sup>31</sup>. Better

understanding of the pathological mechanisms of MBL on ischemic brain tissues and the development of MBL inhibitors represent promising research areas to address this unmet medical need.

As in every drug discovery, drug candidates should be developed and characterized in pre-clinical *in vitro* and *in vivo* studies for their efficacy, toxicity, pharmacokinetics and safety information.

In this thesis, convenient and robust pre-clinical assays were set up and applied to test MBL inhibitors and to evaluate their effects in cellular and *in vivo* models of secondary ischemic brain injuries.

It is important to recall that MBL has an oligomeric structure with multiple carbohydrate recognition domains (CRD), allowing multiple interactions with arrays of polyglycosylated targets with high avidity<sup>4,32</sup>. Thus, to effectively interfere with these multivalent interactions, multivalent inhibitors such polymannosylated compounds<sup>23,24,33</sup> are required to benefit more from this multivalency effect, in this project it was focused on nanoparticles.

Nanoparticles is an important application of nanobiotechnology to medicine and there are already many commercially available examples e.g. Copaxone for multiple sclerosis; Zevalin for lymphoma; Abraxane for cancer<sup>34,35</sup>. Their unique properties, and in particular the possibility to functionalize them with labels or ligands, allows their applications for molecular diagnostics and targeted drug delivery, with the aim of avoiding side effects and improving therapeutic window<sup>36,37</sup>.

In this study, different sugar-capped gold nanoparticles (sugar-GNPs) i.e. mannose-capped gold nanoparticles (Man-GNPs) and glucose-capped gold nanoparticles (Glc-GNPs) were screened as potential MBL inhibitors.<sup>38</sup>

This project was based on a stepwise approach with the following main aims:



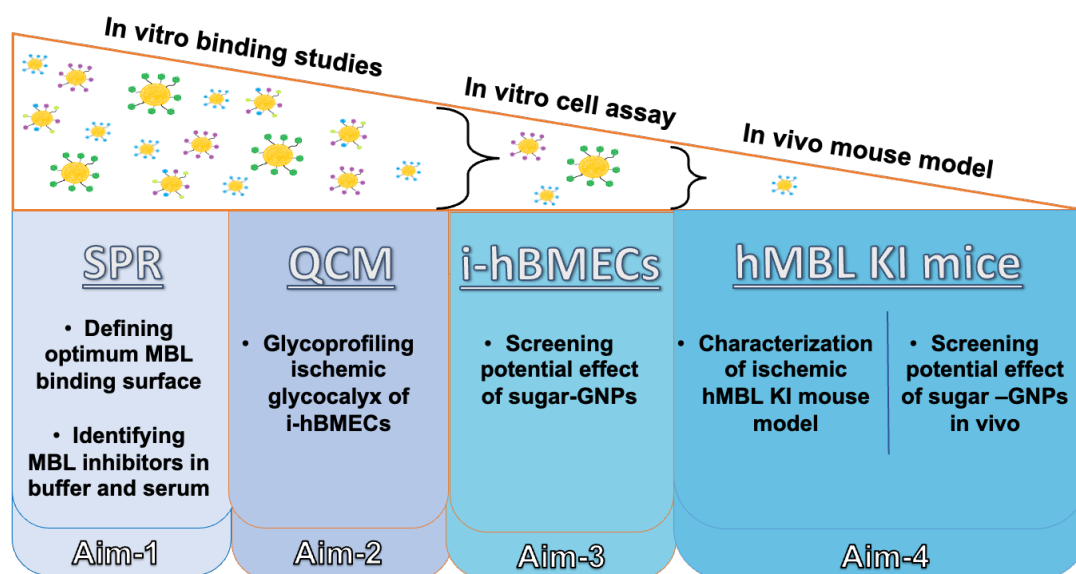


Figure 1 Pipeline of the pre-clinical studies for MBL-inhibitors

1) **The first aim** was to design a Surface Plasmon Resonance (SPR) assay to investigate binding of human MBL (in solution) to a mannose-exposing sensor chip by mimicking glycocalyx, and to apply it for the identification and characterization of inhibitors of this binding, supporting translational studies.

Previously, the so-called “mannan assay”<sup>39,40</sup> was used to study the binding of monovalent carbohydrates to MBL. However, it requires long incubation and washing steps which may affect the accuracy and precision of the measurements. For this, SPR was preferred in the present study, being the most common and well-established label-free technology, providing real-time measurements in a microfluidic system. The main application of SPR is for the characterization of biomolecular interactions in terms of on and off rates (kinetics) and binding strength<sup>41</sup> although its versatility allows many other uses<sup>42-45</sup>.

In order to screen putative MBL binders, a direct SPR design was used at first in which the compounds were flowed onto recombinant MBL immobilized on the sensor chip<sup>23</sup>. However, immobilization of MBL can alter its binding properties, and also makes this configuration different from the physiological condition, in which MBL is the circulating protein.

Thus a different SPR design was developed to mimic the real conditions more closely<sup>33</sup>. This involved MBL-containing solutions, with or without inhibitors, flowing over a sensor chip coated with mannosylated albumin. This enabled us to identify compounds that could prevent the binding of murine MBL isoforms to immobilized mannose residues. Although it gave satisfactory results with murine MBL, this approach did not work with native human MBL<sup>33</sup> thus limiting its application. Therefore, in the present work<sup>38</sup>, a new SPR assay was developed for in vitro screening of compounds

interfering with the binding of native human MBL to an appropriate chip surface functionalized with a pattern of sugar moieties mimicking DAMPS. Also, a novel procedure to regenerate the chip surface was characterized, accomplished by sequential cleaning with piranha solution followed by UV exposure.

**2) The second aim** of this project was to gain a better understanding of the mechanisms associated to the MBL deposition on ischemic vessels. Although MBL deposition has been demonstrated on kidney<sup>46,47</sup>, heart<sup>48</sup>, intestine<sup>49</sup> and brain<sup>19,22,23</sup> in several *in vitro* and *in vivo* studies with ischemic reperfusion injury, the specific MBL-binding molecules expressed by damaged endothelial cells remain unclear. Since MBL is a sugar binding protein, the experimental evidence<sup>50</sup> points that MBL could recognize the changes on sugar profile on glycocalyx—carbohydrate portion of glycoconjugates on surface of damaged endothelium, such as a glycoprotein, glycolipid, or proteoglycan<sup>1</sup>— and binding them to activate the complement cascade. In literature, it is shown that hypoxia altered endothelium glycosaminoglycans (GAG) i.e. heparan sulfate (HS), chondroitin sulfate (CS), and hyaluronan (HA), of different organs; kidney<sup>51,52</sup>, heart<sup>53,54</sup>, cremaster<sup>55</sup>, liver<sup>56</sup>, lung<sup>57</sup> and brain<sup>58,59</sup> but to our knowledge, this alteration has not investigated at the level of monovalent sugars.

To this aim, it was planned to develop a novel glycoprofiling assay for ischemic brain endothelium.

First assay is based on label-free sensors, and among them Quartz Crystal Microbalance (QCM)-based sensors is the only one allowing to study molecular interactions on the cell surfaces<sup>60–63</sup>. Unlike traditional methods, where multiple steps are required to obtain ligand molecule from the cells by isolating and purifying them to immobilize onto the biosensor chip surface<sup>64</sup>, Attana QCM technology provides a platform for a label-free, direct measurement of biomolecular interactions in their native environments. In this way, not only the studies become less laborious and time-consuming but also keep native form of the structures on cell which provide more accurate binding data. QCM cell biosensors have been exploited to investigate protein-carbohydrate interactions in real-time previously<sup>60–62,65,66</sup>. However, the study for real-time analysis of biomolecular interactions directly on immortalized human brain microvascular cell surfaces with a novel hypoxic model by using QCM biosensor have not been reported. In this thesis, the effect of hypoxia on glycocalyx alteration in monovalent sugar level was investigated by measuring the binding of selected lectins to i-hBMECs seeded on QCM chip, for the first time to the best of our knowledge.

This aim was accomplished with further studies based on lectin/immunohistochemistry<sup>67–69</sup> using fluorescent plant lectins with different affinities to sugars to stain the sugars on the endothelium of ischemic i-hBMEC and ischemic brain tissues of mouse model which had a surgery of middle cerebral artery occlusion (mcao).

**3) The third aim** was carried out using a cell model of endothelial ischemic injury, to investigate the toxicity and efficacy of Man-GNPs. Previously<sup>22</sup>, it was shown that cells exposed to hypoxia, and re-oxygenated with human serum (HS) or recombinant MBL (rhMBL) had an increased MBL deposition (+93%) and complement system activation in comparison with normoxic cells. The presence of MBL in cells caused hypoxia-induced altered cytoskeletal organization and reduced viability (-25%) compared to conditions without MBL, showing a direct toxic effect of MBL. In this study, the same ischemic model with i-hBMECs was used to screen the potential protective effect of Man-GNPs.

**4) The fourth and last aim** of this project was to explore the protective effects of Man-GNPs in an in vivo mice model of ischemia.

The role of MBL in mouse model of ischemia has been widely studied<sup>23,70,71</sup>. For this, mice are subjected to transient middle cerebral artery occlusion (tMCAo) in order to mimic stroke. Smaller ischemic lesion, better vascular function and improved neurological deficits were observed in MBL knock-out mice or in mice treated with anti-MBL molecules<sup>23,70</sup>. A specific deposition of MBL was found on ischemic endothelium, followed by complement activation and vascular inflammation. This deposition of MBL lasted up to 48 h post-stroke, driving expansion of the ischemic lesion and pointing to circulating MBL as a promising therapeutic target. In fact, MBL is synthesized by liver but not brain cells, and the presence of MBL in the brain is due to circulating MBL which suggests the potential of systemic injection of MBL inhibitors. For the present studies, mice expressing human MBL were used (human MBL knock-in) to have better clinical translation of preclinical data. In fact, humans and rodents carry different isoforms of MBL. While rodents have two functional MBL isoforms (MBL-A and MBL-C), humans have only one<sup>39,71</sup>.

This thesis provides a complete pre-clinical pipeline, with a multidisciplinary approach, for the development of MBL inhibitors as potential anti-stroke drugs.

## Chapter 2 : Method and materials

---

### 2.1 Chemicals and reagents

All chemicals were of analytical grade, used without further purification. All water was double-distilled, supplied in house by a Milli-Q system (Millipore, Bedford, MA, USA). Hydrogen peroxide solution (30% w/w) and D- (+)-mannose were purchased from Merck Millipore (Overijse, Belgium). Tween 20 was from Sigma-Aldrich (Milan, Italy). 2- Mercaptoethanol (14.2 M) and cleaning reagents (0.5% SDS, 50 mM NaOH and 100 mM HCl) were from the ProteOn Regeneration Kit (Bio- Rad, California, USA).

### 2.2 Biological materials

Recombinant human MBL protein (rhMBL) (9086-MB) and recombinant human Ficolin-1 protein, carrier-free (rhFicolin-1) (4209-FC) were purchased from R&D Systems (Minneapolis, MN, USA). Soybean agglutinin (SBA) unconjugated was purchased from Vector Laboratories (L-1010). Human serum (from male AB clotted whole blood), USA origin, sterile-filtered (H6914) was purchased from Merck Life Science S.r.l. MBL, human, mAb 3E7 (HM2061) was purchased from Hycult Biotech.

MBL-depleted human serum was prepared according to a method described previously<sup>72</sup>. Briefly, a 5 mL column containing 2 mL of mannan-agarose (Sigma-Aldrich, Belgium) as depleting beads was equilibrated with Veronal buffer (Lonza, Allendale, New Jersey, US) containing calcium chloride (3 mM) and magnesium chloride (10 mM). Human serum was passed through the column, and the flow-through was collected. The depletion of MBL was confirmed by Human MBL Quantikine ELISA (DMBL00; R&D Systems, bio-technie Ltd. Abingdon, UK) showing  $\geq 95\%$  depletion efficiency.

M9 Glycan (High mannose or oligo mannose N glycan with a di-N- acetylglucosamine core and 9 mannose residues) 95% purity, was provided by Ludger Ltd. (Figure 2).

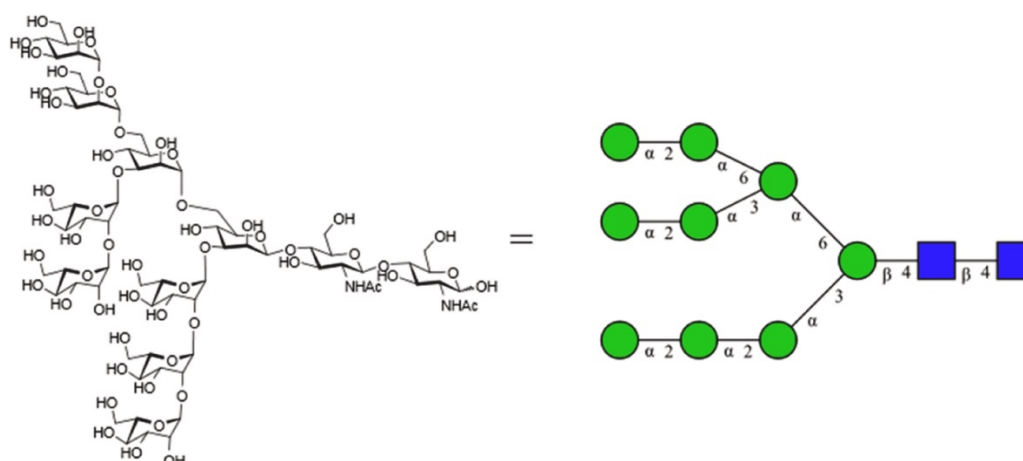


Figure 2 The Man<sub>9</sub> glycan structure has three antennae that are capped with alpha 1,2 linked mannoses, based on the NMR analysis

## 2.3 Thiol-glyco-derivatives

Synthetic glyco-derivatives, Man-EG<sub>6</sub>C<sub>11</sub>S, Glc-EG<sub>6</sub>C<sub>11</sub>S (Figure 3) were prepared according to the reference method<sup>73,74</sup> by Midatech (Bil-bao Spain) and dissolved in water.

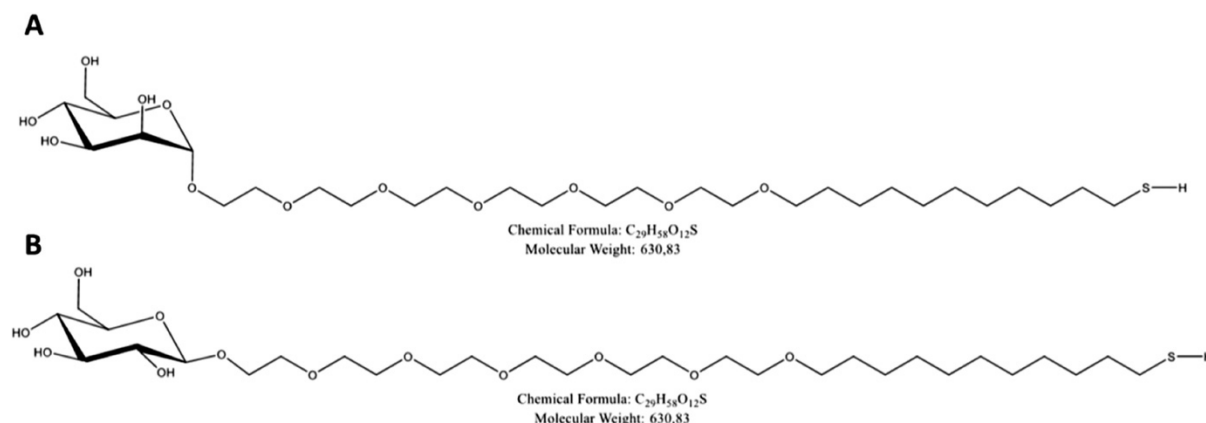


Figure 3 Structure of the synthetic glyco-derivatives, Man-EG<sub>6</sub>C<sub>11</sub>S (A), Glc-EG<sub>6</sub>C<sub>11</sub>S (B)

## 2.4 Synthesis, functionalization and characterization of gold nanoparticles

Gold nanoparticles (GNPs) were synthesized and characterized as previously described<sup>75</sup>. Briefly, sodium citrate (9 mL, 68 mM), HAuCl<sub>4</sub> (7.5 mL, 10 mM) and AgNO<sub>3</sub> (490 μL, 5.9 mM) were mixed and stirred for 6 min at room temperature. Then the solution was added into 250 mL of boiling water in a 500 mL flask and stirred (750 rpm) for 1 h at 100 °C, allowing the formation of the seeds. The seed solution was cooled to room temperature, 5 mL of glycerol was added, and the solution was left stirring for 10 min

A second mixture of sodium citrate (10 mL, 34 mM),  $\text{HAuCl}_4$  (7.5 mL, 10 mM) and  $\text{AgNO}_3$  (426  $\mu\text{L}$ , 5.9 mM) was pre-mixed for 6 min and then added to the seed solution, followed immediately by the addition of hydroquinone (8 mL, 91 mM). The solution was left stirring at 750 rpm for 1 h to age and improve homogeneity.

Synthesized citrate-capped GNPs were purified by centrifuging, using Millipore Amicon Ultra-4 Centrifugal Filter Units, 30KDa cut-off, at 6000 rpm for 4 min and stored as colloidal solution in water (12 mL, Au content 14 mg). These citrate-capped GNPs are stable in water for months, and their core diameter is  $14.1 \pm 2.1$  nm, determined by transmission electron microscopy (TEM) images (Figure 4). No evidence of residual silver on the gold surface was found, checked by TEM and energy dispersive X-ray.

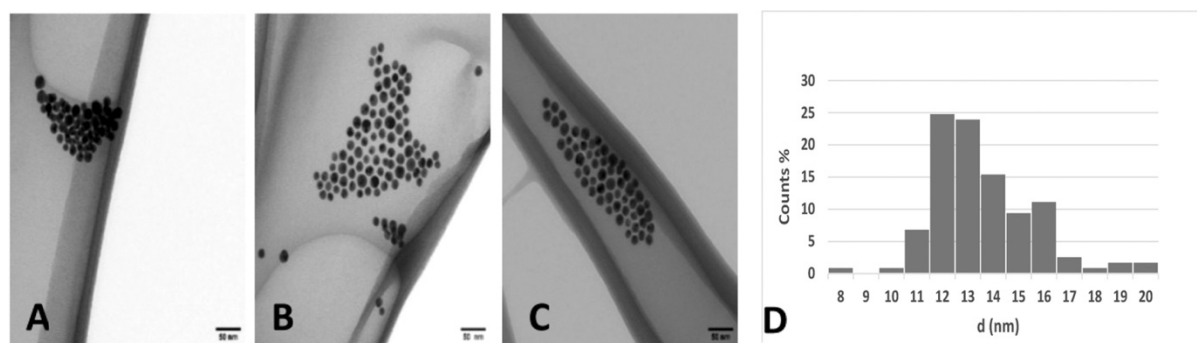
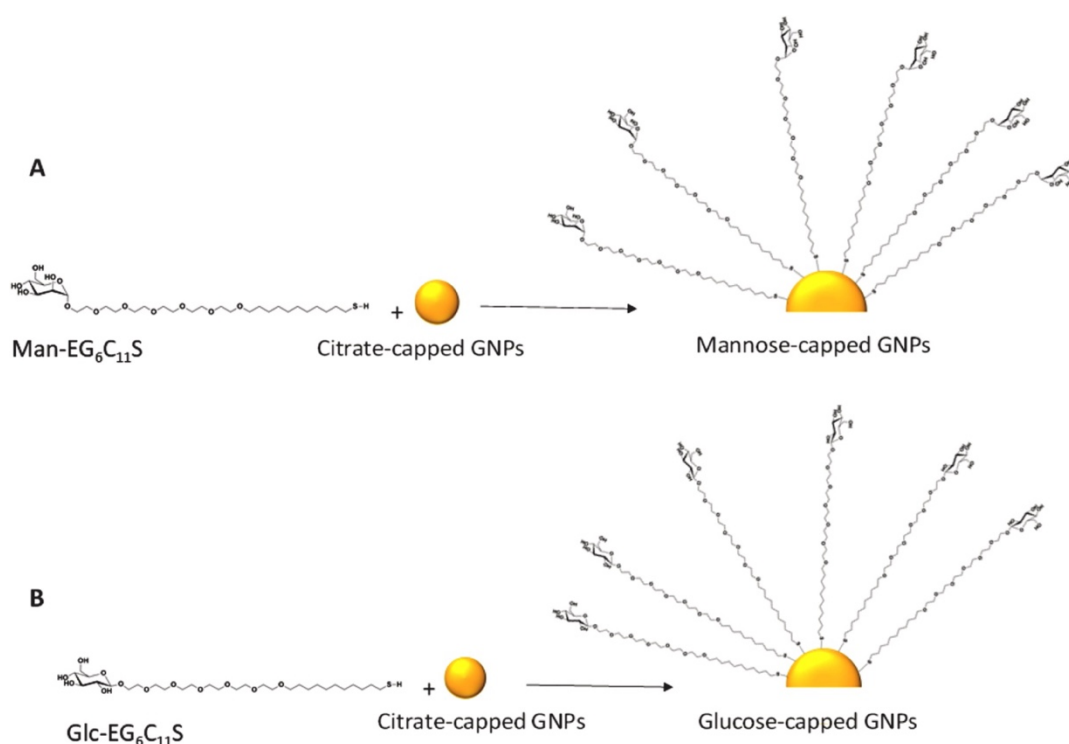


Figure 4 TEM images

A) Citrate-capped GNPs; B) Mannose-capped GNPs; C) Glucose-capped GNPs; D) Statistical distribution of particle diameters:  $d(\text{average}) = 14.1 \pm 2.1$  nm. There were no differences in core size distributions after functionalization with mannose and glucose derivatives.

GNPs were functionalized by capping the metal surface with thiol- glyco-derivatives, exploiting the strong thiol-gold bond and allowing a self-assembled monolayer on the gold surface (Figure 5).



**Figure 5** Synthesis of mannose and glucose-capped GNPs

First, 15  $\mu\text{L}$  of 10  $\mu\text{g}/\text{mL}$  thiol-glyco-derivatives, Man-EG<sub>6</sub>C<sub>11</sub>S or Glc-EG<sub>6</sub>C<sub>11</sub>S, were added to 85  $\mu\text{L}$  of water and 500  $\mu\text{L}$  of citrate-capped GNPs (1.16  $\text{mg}/\text{mL}$ ) were added dropwise to the solution, then shaken overnight at 4  $^{\circ}\text{C}$  in the dark. The samples were centrifuged at 13000 rpm (16.1 ref) for 25 min at 15  $^{\circ}\text{C}$ . After centrifugation, the supernatant was removed and the GNPs were re-dispersed in 600  $\mu\text{L}$  of water. This step was repeated three times. After the final cycle the particles were dispersed in 300  $\mu\text{L}$  of water.

Citrate-capped GNPs and glyco-functionalized GNPs were fully characterized by: 1) dynamic light scattering (DLS) and  $\zeta$ -Potential, to determine their hydrodynamic diameter and assess their colloidal stability (Table 1).

**Table 1** Characterization by DLS of citrate and glycol-capped GNPs.

Gold Nanoparticles	Hydrodynamic diameter (nm)	Polydispersity index	$\zeta$ -Potential (mV)
Citrate-GNPs	33 $\pm$ 9	0.201 $\pm$ 0.03	-26 $\pm$ 5
Man-GNPs	28 $\pm$ 7	0.173 $\pm$ 0.03	-19 $\pm$ 2
Glc-GNPs	29 $\pm$ 7	0.177 $\pm$ 0.01	-9 $\pm$ 2

DLS was done with a 90 Plus Particle Size Analyzer from Brookhaven Instrument Corporation (Holtville, NY, USA) operating at 15 mW of a solid-state laser ( $\lambda$  661 nm), using a  $90^\circ$  scattering angle. The  $\zeta$ -potential was determined at 25 °C, using the same instrument equipped with an AQ-809 electrode, operating at an applied voltage of 120 V. The  $\zeta$ -potential was calculated from electrophoretic mobility based on the Smoluchowski theory. 2) UV-Vis spectroscopy to characterize the plasmon band was done with an Agilent 8453 instrument equipped with a disposable cuvette with 1 cm optical path length (Figure 6) and a concentration of NPs calculated with the Beer-Lambert law. 3) Inductive coupled plasma optical emission spectroscopy (ICP-OES) to analyze the metal content was done with ICP-OES iCAP 6200 Duo upgrade, Thermofisher. Samples were acid-digested on a hotplate with aqua regia (HCl: HNO<sub>3</sub> 3:1) solution, diluted with water. 4) TEM was done on a specimen prepared by dropping the GNP solution onto supported lacey-carbon copper TEM grids, using a ZEISS LIBRA200FE microscope equipped with an in-column  $\Omega$ -filter spectrometer/filter, operating at 200 kV (Figure 4).

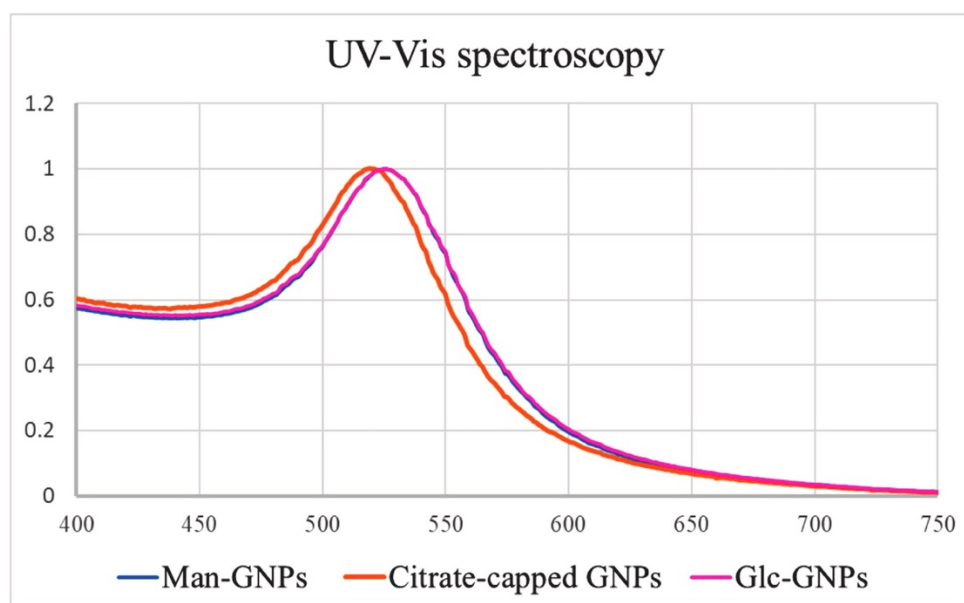


**Figure 6** UV-Vis spectroscopy to characterize citrate-capped GNPs and glyco-capped GNPs

Man-EG<sub>6</sub>C<sub>11</sub>S-coated GNPs (Man-GNPs) and Glc-EG<sub>6</sub>C<sub>11</sub>S-coated GNPs (Glc-GNPs). Milli-Q water was used as blank and automatically subtracted from all the samples. Uv-Vis spectra are normalized on a 0–1 scale.

## 2.5 Piranha/UV cleaning and chip surface coating

For these studies, GLC and GLM sensor chips from BioRad were used, after the removal of the alginate polymer layer which originally coated the gold surface. For this, the chips were taken out of the housing (Figure 15) and their surface was immersed in sequence in SDS (0.5%), NaOH (50 mM)



and HCl (100 mM) for a min each, with intermediate washes with water, then dried under a nitrogen stream. After this pre-cleaning, the bare gold surface of the chip was obtained by immersing the chip for 5 min in freshly prepared piranha solution [ $\text{H}_2\text{O}_2:\text{H}_2\text{SO}_4$  1:5] pre-cooled to room temperature for 15 min under a magnetic-induction stirrer. Immediately after, the chip was immersed in water to remove residual piranha solution, and rinsed again with water (150 mL), followed by 96% ethanol (50 mL), then dried under a nitrogen stream. After that, the chip was placed horizontally under the biohazard safety VBH sterile hood and exposed to the germicidal UV light of the hood for 1 h.

The cleaned chips were then either used immediately for in-situ surface coating or used ex-situ for thiol-mediated immobilization of the SH-glyco-derivatives. For this, inside the sterile hood the chip was again rinsed with water (150 mL) and 96% ethanol (50 mL) and placed in a homemade sealed parafilm box. The dried surface of the chip was covered with freshly prepared SH-glyco-derivative solution (800  $\mu\text{g}/\text{mL}$ ) diluted in 50% ethanol, and left for 24 h on a circular shaker in the dark. Then the surface was gently rinsed with water (50 mL) and 96% ethanol (5 mL), dried under a nitrogen stream, and re-inserted into the chip housing. All the above steps (chip cleaning and ligand immobilization) were carried out in sequence.

## 2.6 SPR binding assays

All the SPR analyses were done with the ProteOn XPR36 SPR. The running and dilution buffer was TBST with  $\text{Ca}^{2+}$  10 mM Tris buffer [pH 7.4], with 150 mM NaCl, 0.005% Tween-20 and 1.2 mM  $\text{CaCl}_2$ .

For initial binding studies different concentrations of rhMBL (0.125–20 nM) were injected for 300 s at a rate of 30  $\mu\text{L}/\text{min}$ , over chips coated directly with different SH-glyco-derivatives, as described above. Representative sensorgrams (i.e., the time course of the SPR signal in resonance units (RU)) were obtained from parallel spots of the SPR chip surfaces (Figure 7).

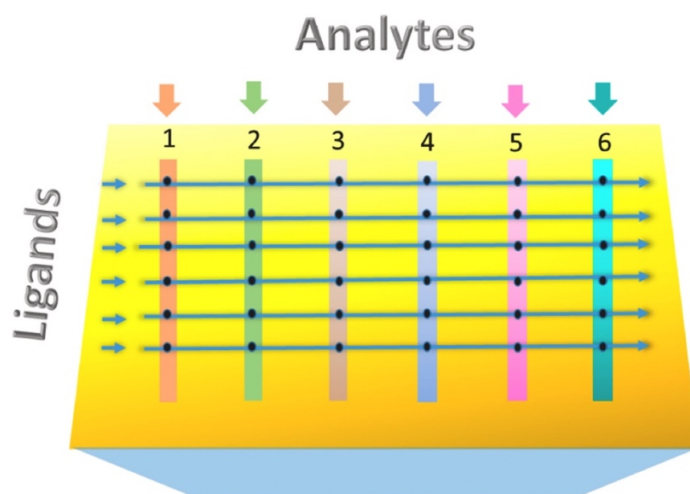


**Figure 7 Parallel flow channels of ProteOn XPR36 SPR chip surface**

The ProteOn XPR36 SPR instrument has six parallel flow channels and can define six parallel strips of the same sensor chip. These flow channels can serve to inject six different analytes. For each strip, the SPR signal is measured in six spots, indicated by dots

For inhibition studies, 1  $\mu\text{g}/\text{mL}$  (5 nM) rhMBL was pre-incubated with monovalent mannose (10 mM and 30 mM) or M9 glycan (100–200  $\mu\text{M}$ ) for 1 h, as indicated, at 25 °C on an orbital shaker, and the solutions were then injected over the chip, for 150–300 s at 30  $\mu\text{L}/\text{min}$ .

In another set of experiments, 1  $\mu\text{g}/\text{mL}$  rhMBL was preincubated with or without Man-EG<sub>6</sub>C<sub>11</sub>S-functionalized GNPs (25, 12.5, 6.25  $\mu\text{g}/\text{mL}$ ) or Glc-EG<sub>6</sub>C<sub>11</sub>S-functionalized GNPs (25  $\mu\text{g}/\text{mL}$ ) for 1 h at 25 °C on an orbital shaker. The solutions were injected over the chip surface for 5 min at 30  $\mu\text{L}/\text{min}$  or centrifuged at 13000 rpm (16.1 rcf) for 25 min at 4 °C to precipitate the NPs, and the supernatants were injected as above.

To evaluate the binding of native MBL, 50-fold-diluted human serum was preincubated with or without Man-EG<sub>6</sub>C<sub>11</sub>S- or Glc-EG<sub>6</sub>C<sub>11</sub>S- functionalized GNPs (25  $\mu\text{g}/\text{mL}$ ) for 1 h at 25 °C on an orbital shaker. Then the solutions were centrifuged at 13000 rpm (16.1 rcf) for 25 min at 4 °C, to precipitate the NPs, and the supernatants were injected over the chip surface, for 800 s at 30  $\mu\text{L}/\text{min}$ . In parallel MBL-depleted human serum with or without the addition of rhMBL were used.

The injection of diluted sera was immediately followed by injection of anti-hMBL 3E7 antibody (10  $\mu\text{g}/\text{mL}$  at a rate of 30  $\mu\text{L}/\text{min}$  to specifically recognize the MBL captured by the immobilized sugars.

## 2.7 Western Blots

### 2.7.1 Native and recombinant MBL oligomerization

The i-hBMECs that underwent 16h of hypoxia (HYPX) or normoxia (CTRL), were then re-oxygenated in presence of human serum 30% (HS) and 10 µg/mL recombinant hMBL (rhMBL) in MBL depleted human serum 30% (MBL Dep. HS 30%) for 4 h. HS and hMBL Dep. HS were diluted in medium without FBS and applied to cells. Four hours after reoxygenation media were collected and immediately stored at -20 °C. Equal amounts of proteins (10 µg/sample) were electrophoresed on Tris-Acetate 3-8% gradient gels (EA3735, Invitrogen) and without denaturation (0.1% of SDS) in Tricine-SDS running buffer (Novex LC1675, Invitrogen) and transferred to polyvinylidene fluoride membranes using Tris-glycine 20% MeOH. Membranes were incubated overnight at 4°C with hMBL mouse antibody (clone 3E7) (1\_1000; Hycult Biotech) followed by anti-mouse HRP-conjugated antibody (1:10000, goat anti-mouse IgG specific light chain, Jackson ImmunoResearch) for 1h at room temperature (RT). Immunocomplexes were visualized by chemiluminescence using the IMMOBILON western blot substrate (Merck KGaA). Images were acquired by ChemiDoc Imaging Systems (Bio-Rad).

### 2.7.2 MBL protein corona formation

Protein corona formed by 1h of incubation of sugar-GNPs (80 µg/mL) in 30% HS diluted in TBST/Ca<sup>+2</sup>. Soft corona gradually removed by four consequent washing – centrifugation steps in TBST/Ca<sup>+2</sup> at 13 rcf, 40 min. Samples were immediately stored at -20 °C. Presence of MBL composition on soft corona (Soft C. ManNP/GlcNP) and hard corona (Hard C. Man/Glc) revealed with western blot analysis. Equal volume of protein corona sample (10 µl/sample) were electrophoresed on 12% sodium dodecyl sulfate polyacrylamide gel and with denaturation in a mixture including 2% SDS and boiling for 5 min at 96 °C and transferred to polyvinylidene fluoride membrane. hMBL mouse antibody (clone 3E7) (1:1000; Hycult Biotech) followed by anti-mouse HRP-conjugated antibodies 1:10000, goat anti-mouse IgG specific light chain, Jackson ImmunoResearch) were used. Immunocomplexes were visualized by chemiluminescence using the IMMOBILON western blot substrate (Merck KGaA).

### 2.7.3 hMBL and mMASP-2 complexes of hMBL KI mice

Plasma samples from hMBL KI mice at -2d, 90min and 48h after tMCAo were collected and immediately stored at -80°C. Equal amounts of plasma proteins (10 µg/sample) were electrophoresed on Tris-Acetate 3-8% gradient gels (EA3735, Invitrogen) in 1% SDS loading buffer using Tricine-SDS running buffer (Novex LC1675, Invitrogen) and transferred to nitrocellulose membranes by

TransBlotTurbo system (Bio-rad). Membranes were incubated overnight at 4°C with a mix of hMBL mouse antibody (clone 3E7) (1\_1000; Hycult Biotech) and hMASP-2 rat antibody 1:1000 (clone 8B5). Membranes were then incubated for 1h at RT with a-mouse IRDye800 (1:10000, LI-CORE Bioscience) together with an a-rat Alexa 647 (1:5000, Invitrogen), used for hMBL and MASP-2 staining respectively. Immunocomplexes were visualized by fluorescence using ChemiDoc Imaging Systems (Bio-Rad). Quantifications were done with Image Lab Software (Bio-Rad) and results were standardized using the total protein loaded (Ponceau solution).

## 2.8 Cell culture

Immortalized hBMECs (Innoprot) were cultured in rectangular canted neck cell culture flask (Corning). Flask was coated overnight before use, with fibronectin (Sigma) 15 mg/mL in Dulbecco's phosphate buffer saline (DPBS, Euroclone). Cells were cultured in culture medium, prepared with MCDB 131 (Gibco) supplemented with 5% fetal bovine serum (FBS, Euroclone), 2 mM L-glutamine (Gibco), penicillin/streptomycin (P: 100 U/mL-S: 100 U/mL, Sigma), 1 mg/mL hydrocortisone (Sigma), 50 mg/mL endothelial cell growth supplement (ECGS, Sigma), and kept at 37°C, with 5% CO<sub>2</sub> and 90% humidity.

## 2.9 QCM ischemic glycoprofiling assay

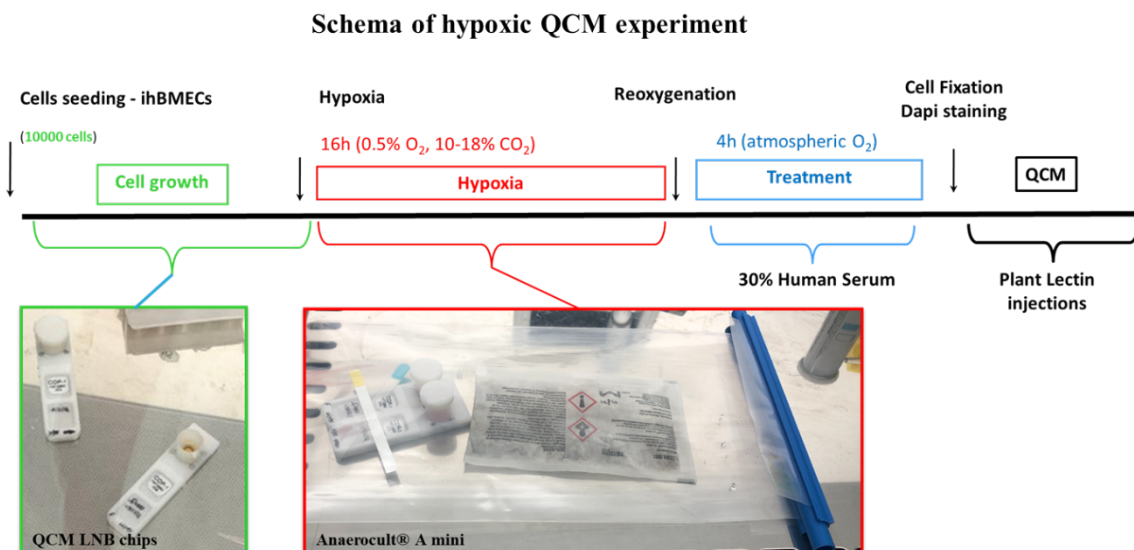


**Figure 8 Protocol of ischemia on i-hBMECs to profile glycocalyx of ischemic endothelium.**

i-hBMECs were either captured ( $10^5$  cells/cm<sup>2</sup>) or seeded ( $10^5$  cells/cm<sup>2</sup>) on QCM LNB-CC and LNB-COP chips, respectively. After i-hBMECs captured on LNB-CC for 15 min or seeded—to have monolayer cell distribution—on LNB-COP for 2 days, cells underwent 16h of hypoxia (HYPX, 0.5%

O<sub>2</sub>, 10-18% CO<sub>2</sub>) in anaerocult A mini kit (Merck KGaA) (Figure 8) or to normoxia (CTRL) in incubator. Then, cells were treated with human serum 30 % diluted in culture medium (30% HS) for 4 h and fixed with paraformaldehyde 4%. Cells were checked with nuclei staining (DAPI).

CTRL and HYPX LNB-CC/COP chips pairs were inserted in Cell A200 QCM instrument. Different plant lectins (PHAL, RCA, WGA, SNA, ConA, LCA) with different sugar affinities, were injected at four different concentration (0.7-2-6-18 µg/mL) for 250s at 10 µL/min over CTRL and HYPX i-hBMECs on LNB-CC or LNB-COP chips. Regeneration was done between each injection of lectins with TBST buffer without Ca<sup>+2</sup> and two glycine pH1.5 injections, respectively.

## 2.10 In vitro ischemia model assay with sugar-GNPs treatment

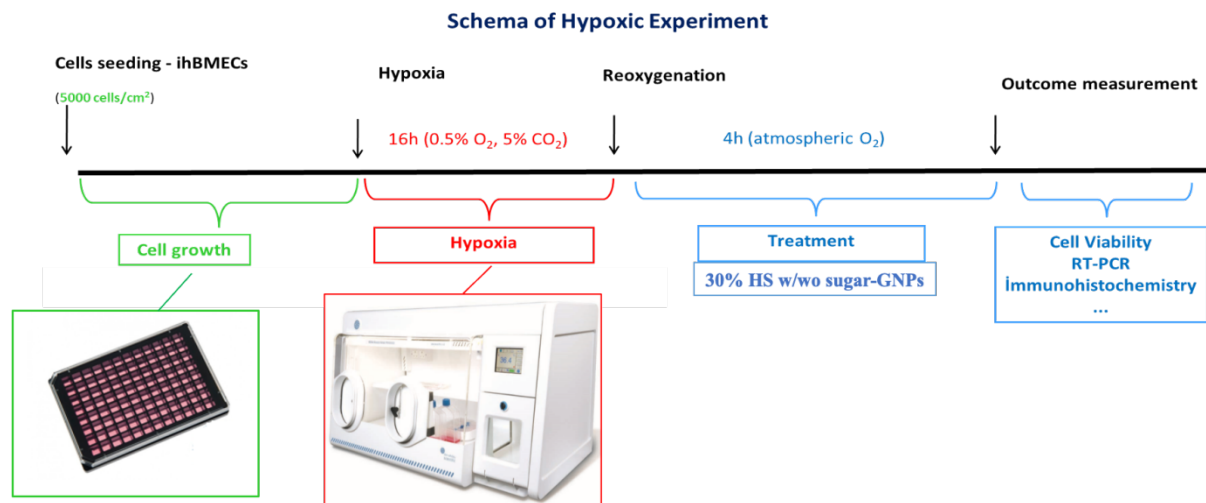


**Figure 9** Experimental schema of i-hBMECs exposing hypoxia to investigate MBL interaction with sugar-GNPs on ischemic endothelium.

i-hBMECs (5000 cells/cm<sup>2</sup>) (Innoprot) were seeded on black 96-well m-plates (ibidi, Germany) with optically clear flat bottom, suitable for fluorescence microscopy. Plates were coated overnight before use, with fibronectin (Sigma) 15 mg/mL in Dulbecco's phosphate buffer saline (DPBS, Euroclone). Cells were cultured in culture medium (MCDB-131 supplemented as described above; 0). Once cells formed monolayer, they were transferred into a hypoxic chamber (Whitley H35 Hypoxystation, Don Whitley Scientific, UK) at 37C, and maintained in deoxygenated culture medium at the following gas concentrations: O<sub>2</sub> 0.5%, CO<sub>2</sub> 5% and N<sub>2</sub> 94.5% for 16 h. Deoxygenated culture medium was obtained by leaving growth medium in a Petri dish inside the hypoxic chamber for 7 h before use. Control cells were maintained in fresh culture medium in a normoxic incubator. After 16 h, hypoxic cells were taken out of the hypoxic chamber, washed twice with DPBS and re-oxygenated for 4 h in a normoxic incubator. During re-oxygenation, normoxic and hypoxic cells were exposed to 30% HS (Innovative Research) with or without sugar-GNPs (40-20-5 µg/mL) or MBL depleted human serum

30% (MBL Dep. HS 30%, obtained as described above; 2.2). All serums were diluted in culture medium (not supplemented with FBS). At the end of re-oxygenation, media of all conditioned collected and immediately stored at -20°C. Cells were either fixed with 4% paraformaldehyde (PFA) in DPBS RT for 15 min or scratch and collected with lysis buffer (PureLink RNA miniKit, Invitrogen, CA, USA) containing 1% of 2-mercaptoethanol. Fixed cells were stored in 0.01M NaN<sub>3</sub> in PBS 0.01M at 4°C until immunofluorescence analysis, collected cells were stored at 20°C until RT-PCR analysis.

## 2.11 Immunofluorescence

### 2.11.1 In vitro cell assay

Immunofluorescence was done on fixed cells. Nuclei were stained with DAPI (1 mg/mL, Invitrogen). For MBL staining, after a blockade with 1% normal goat serum for 1 h, fixed cells were incubated overnight with mouse antihuman MBL (1:100, Hycult Biotechnology). Cells were then incubated with biotinylated anti-mouse (1:200) for 1 h followed by incubation with streptavidin Alexa 647-conjugated (1:100) for 30 min. For F-actin staining, fixed cells were blocked with 1% bovine serum albumin for 30 min, then incubated with phalloidin Alexa 488-conjugated (1:100, Invitrogen).

### 2.11.2 In vivo mouse model

**MBL Deposition:** Twenty-micron thick coronal sections were incubated with mouse antihuman MBL (1:100, Hycult Biotechnology). Alexa 546 fluoro-conjugated goat-anti-rat IgG (1:500, Molecular Probes) was used as a secondary antibody. Brain vessels and nuclei were stained with Alexa488 fluoro-conjugated isolectin (IB4, 1:200, Invitrogen) and DAPI (1 µg/ml, Invitrogen), respectively.

**Glycoprofiling:** The same sections of mouse brains were incubated for 2h with Alexa 546 fluoro-conjugated Concanavalin A (ConA, 1:250, Sigma Aldrich) and Hoechst for the staining of nuclei.

## 2.12 Confocal microscopy and quantitative analysis

### 2.12.1 In vitro cell assay

Images for MBL and phalloidin layer occupancy on normoxic and hypoxic i-hBMECs treated with sugar-GNPs, were obtained by acquiring a 2.5 mm field in the center of each well. Acquisitions were done by microscopy with a confocal scanning A1 unit (Nikon), managed by 'NIS-elements' software. Cells were illuminated with 405 nm (nuclei), 640 nm (MBL) and 488 nm (F-Actin) lasers; 512 pixel images were acquired with a 20x objective, over a 10 mm stack, with 2.65 mm step size, and stitched with 15% overlay. To avoid bleed-through effects, a sequential scanning mode was used. After

background subtraction, the fluorescent signal for MBL and F-actin was quantified by ImageJ software. Graphic elaboration of images was done with GIMP software.

### **2.12.2 In vivo mouse model**

Images were acquired by confocal microscopy using a scanning sequential mode to avoid bleed-through effects by an IX81 microscope equipped with a confocal scan unit FV500 with 3 laser lines: 405 nm (nuclei), 488 nm (Vessels) and 546 nm (MBL) lasers and a UV diode. Three-dimensional images were acquired over a 10  $\mu\text{m}$  z-axis with a 0.23  $\mu\text{m}$  step size and processed using Imaris software (Bitplane) and Photoshop CS2 (Adobe Systems Europe Ltd).

For the quantification of the ConA signal, confocal microscopy was done using a sequential scanning mode to avoid bleed-through effects by an A1 Nikon confocal microscope with an excitation at 405 nm for DAPI and 561 nm for ConA signals. Large view images were acquired by a 20x 0.5 NA objective, with pixel size 0.62  $\mu\text{m}$  and automatically stitched with 10% overlap. Large view images served as reference to identify the cortical regions of interest for subsequent analysis. Four three-dimensional volumes sized 210 x 210 x 12  $\mu\text{m}$  were acquired with a 40x 0.75 NA objective. Digital image analysis was done using originally developed ImageJ plugins. Briefly, the image was corrected for background noise and then the raw integrated density of pixels calculated over all focal planes. The sum of focal planes' raw integrated density was used for statistical analysis.

## **2.13 Reflectance confocal microscopy**

Reflectance confocal microscopy was set up to visualize Sugar-GNPs. Man-GNPs, Glc-GNPs and Alexa488-conjugated beads were dropped on different microscope slides. Focus and background adjustment were illuminated with 488 nm (Alexa488-conjugated beads) lasers and Sugar-GNPs were excited with 561 nm (HV: 100, laser power: 0.5) changing the dichroic to the transmitted/reflectance mirror (BS20/80) with pinhole adjustment. Images were acquired with a 100x 1.49 NA oil immersion objective. Same setting then applied on normoxic and hypoxic i-hBMECs treated with 30% HS in presence of Man-GNPs to visualize nanoparticles. Images were obtained by acquiring a 2.5 mm field in the center of each well.

## **2.14 Super-resolution microscopy.**

Structured illumination microscopy (SIM) was done on a Nikon SIM system with a 100x 1.49 NA oil immersion objective (for F-actin quantification), managed by NIS elements software. Cells were imaged at laser excitation of 405 for nuclei, 488 for F-actin with a 3D-SIM acquisition protocol. Fourteen-bit images sized 1024 pixels with a single pixel of 0.030  $\mu\text{m}$  (100) or 0.036  $\mu\text{m}$  (60) were

acquired in a gray level range of 0–4000 to exploit the linear range of the camera (iXon ultra DU-897U, Andor) at 14-bit and to avoid saturation. Raw and reconstructed images were analyzed with the SIM check plugin of ImageJ. For cytoskeletal organization, 12 cells from four wells per condition were acquired and analyzed with F-actin touches on 1  $\mu$ m-spaced grid superimposition. SIM images were quantified with ImageJ. Briefly, a region of interest was drawn including the cell cytoplasm but not the nucleus. Background noise was normalized throughout the samples and F-actin filaments were selected by signal segmentation followed by the skeletonize function.

## 2.15 Real-time RT-PCR

Total RNA was extracted from cells at the end of the 4 h re-oxygenation using the PureLink RNA miniKit (Invitrogen, CA, USA) according to the manufacturer's instructions. Samples of total RNA (100 ng) were treated with DNase (Applied Biosystems, Foster City, CA, USA) and reverse-transcribed with random hexamer primers using multiscribe reverse transcriptase (TaqMan reverse transcription reagents, Applied Biosystems, Foster City, CA, USA). Primers were designed to span exon junctions in order to amplify only spliced RNA, using PRIMER-3 software (<http://frodo.wi.mit.edu/>) based on GenBank accession numbers ( $\beta$ -actin: NM\_001101.5, MBL2: NM\_000242.2). The same starting concentrations of cDNA template were used in all cases. Real-time PCR was done using Power SYBR Green according to the manufacturer's instructions (Applied Biosystems).  $\beta$ -actin was used as reference gene and relative gene expression levels were determined according to the Ct method (Applied Biosystems). Data are presented with individual values. Primer sequences: AhR fwd: cagtactgccaggccaaca, rev: tgtgtgtagtctgagtgtattatg; IL-1 $\alpha$  fwd: tgaagaagacagtctccattg, rev: cttcatggagtggccatag; MMP-2 fwd: atccgccttaactggag rev: ggaagccaggatccatttc; ICAM-1 fwd: tgatgggcagtcaacagcta rev: ggtaaggtcttgcccactgg; RAGE rev: accgagtcctgtctaccag fwd: tcctctgacacacatgtcc; TMD1 fwd: gttgtgcgtcgtgtctc rev: actcgcagaggaagccatc HIF-1 fwd: ttaccatgccccagattcag rev: ggtgaactttgtctagtgtcca ; Caludin-5 fwd: cctgegaggcgttgataa rev: gacgtccgaggagcctg;  $\beta$ -actin fwd: ccagctcaccatggatgatg, rev: atgccggagccgttctc.

## 2.16 Mice

Procedures involving animals and their care were conducted in conformity with institutional guidelines in compliance with national and international laws and policies. Our project involving animals received ethical approval by the local ethic committee and by the Italian Ministry of Health (Autorizzazione n° 383/2021-PR, project number 9F5F5.194). Male and female C57BL/6 J mice were used at 10-13 weeks old and weighting 26–28 g, either WT or hMBL KI, kindly provided by Dr. Gregory Stahl, Harvard Medical School, Boston, US, and colonized at the Mario Negri Institute). The



protocols and details of this report are in accordance with the ARRIVE guidelines (<http://www.nc3rs.org.uk/page.asp?id=1357>, see the list provided as a supplementary file).

## 2.17 Focal cerebral ischemia: Transient middle cerebral artery occlusion

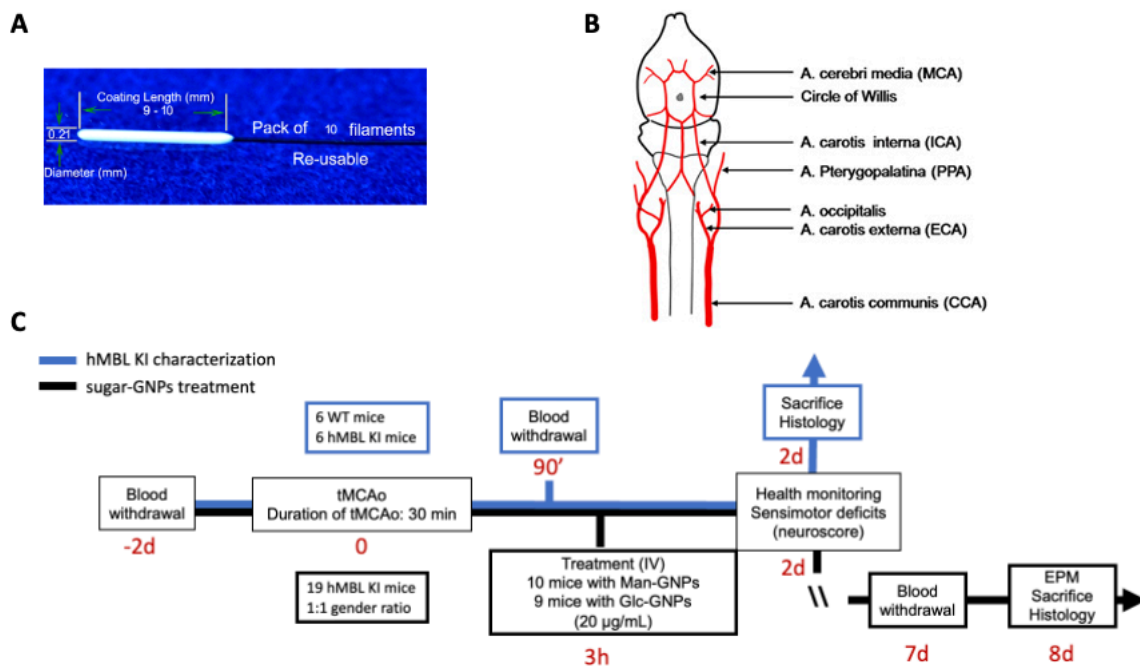


**Figure 10** Representative figures for focal cerebral ischemia with transient middle cerebral artery occlusion (tMCAo)

Siliconized filament (Docol Corporation, A) and scheme of the vessel architecture supplying the brain (depicted in background) in the mouse (B). Experimental schema of two different tMCAo experiments: hMBL KI mice characterization (blue line) and sugar-GNPs treatment (black line). Panels show the timeline (see red numbers) for tMCAo, treatment and post-tMCAo evaluations (C).

Focal cerebral ischemia was induced by transient middle cerebral artery occlusion (tMCAo) as previously reported by our group<sup>71</sup>. Anesthesia was induced by 3% and maintained by 1.5% isoflurane inhalation in an N<sub>2</sub>O/O<sub>2</sub> (70/30%) mixture. Transient ischemia (60 minutes) was achieved using the filament model. A silicone coated monofilament nylon suture (sized 7-0, diameter 0.06-0.09 mm, length 20 mm; diameter with coating 0.23 mm; coating length 10±1 mm, Docol Corporation, Redlands, CA, USA) was introduced into the common carotid artery (appropriately isolated) and advanced to block the middle cerebral artery (MCA). After 30 minutes, blood flow was restored by carefully removing the filament. During surgery body temperature was kept at 37°C by a heating pad.

During MCA occlusion, mice were awakened from anesthesia, kept in a warm box and tested for intras ischemic deficits (for inclusion/exclusion criteria, see below). Analgesia was achieved by local application of an ointment (EMLA, containing 2.5% lidocaine and prilocaine, Aspen Pharma) where the skin was opened. Animals were monitored after surgery according to the IMPROVE guidelines<sup>76</sup> and treated subcutaneously with 0.1 mg/kg buprenorphine if developing severe signs of distress (IMPROVE's amber category of clinical signs).

#### Inclusion/exclusion criteria

Mice were included in the study if successfully induced with ischemia, i.e., filament correctly positioned in the MCA. Thus, ischemic animals were included if presenting  $\geq 3$  of the following intras ischemic deficits:

1. the palpebral fissure had an ellipsoidal shape (not the normal circular one)
2. one or both ears extended laterally
3. asymmetric body bending on the ischemic side
4. limbs extended laterally and did not align to the body.

Mice were excluded if:

1. they died during MCA surgery
2. they had a decrease in body weight  $< 35\%$  before sacrifice compared to baseline

## 2.18 Treatments

Mice received by intravenous (IV) bolus injection in the tail vein at 3h after onset of tMCAo, while under anesthesia, 20  $\mu\text{g}/\text{mL}$  (40  $\mu\text{g}/\text{mouse}$ ) Man-GNPs and Glc-GNPs (injected volumes maximally 100  $\mu\text{L}/\text{mouse}$ ). Ten mice for Man-GNPs and nine mice for Glc-GNPs treatment were used with 1:1 gender ratio.

## 2.19 Neurologic deficits

Forty eight hours after the induction of ischemia, each mouse was rated on two neurologic function scales unique to the mouse. The general deficit scale evaluates hair (0–2), ears (0–2), eyes (0–4), posture (0–4), spontaneous activity (0–4), and epileptic behavior (0–12), whereas the focal deficit scale evaluates body symmetry (0–4), gait (0–4), climbing on a surface held at 45° (0–4), circling behavior (0–4), front limb symmetry (0–4), compulsory circling (0–4), and whisker response to a light touch (0–4). Scores range from 0 (healthy) to 56 (the worst performance in all categories) and

represent the sum of the results of general and focal deficits (13 categories). Results are expressed as composite neurological score. All mice meeting the criteria (intraischemic deficits) were included. If sacrificed for humane endpoint, they were given the worst behavioral score. A trained investigator who was blinded to the experimental conditions performed experiments.

## 2.20 Elevated plus maze (EPM)

The EPM measures disinhibition and anxiety-like behaviours. The test consists of two open and two closed arms (each 35 cm × 5.5 cm), and a central platform (5.5 cm × 5.5 cm), elevated 60 cm above the ground. Mice were acclimatized in the room for 1 h prior to testing, then placed in the central platform facing an open arm and their movements were recorded for 5 min. Video recording and time spent in the closed and open arms were measured by Ethovision XT, 514.0 (Noldus Information Technology, Wageningen, The Netherlands). All mice meeting the criteria (intraischemic deficits) were included. If sacrificed for humane endpoint, they were given the worst behavioral score. Data were expressed as percentage of time spent on the open arms (OA) over the total time the mouse spent on the maze [open arm time % = 100 × (OA time/total time)].

## 2.21 Plasma collection

Blood (≈50 μL) was obtained from the submandibular vein (cheek pouch) -2d, 90 min and 48h after tMCAo. Drops of blood were exude from the stick point and were collected into a suitable sample container. Blood was centrifuged at 2000 g for 15 minutes at 4°C and the plasma was stored at -80 °C for subsequent analyses.

## 2.22 Brain collection

Mice were anesthetized with 300 μL of ketamine (150 mg/kg) plus medetomidine (2 mg/kg) intraperitoneally before sacrifice.

Mice were transcardially perfused with 30 mL of phosphate buffered saline (PBS) 0.1 mol/L, pH 7.4, followed by 60 mL of chilled paraformaldehyde (4%) in PBS. The brains were carefully removed from the skull and post-fixed for 6 h at 4 °C, then transferred to 30% sucrose in 0.1 mol/L phosphate buffer for 24 h until equilibration. The brains were frozen by immersion in isopentane at -45 °C for 3 min and stored at -80 °C until use.

## 2.23 Lectin pathway activity assay

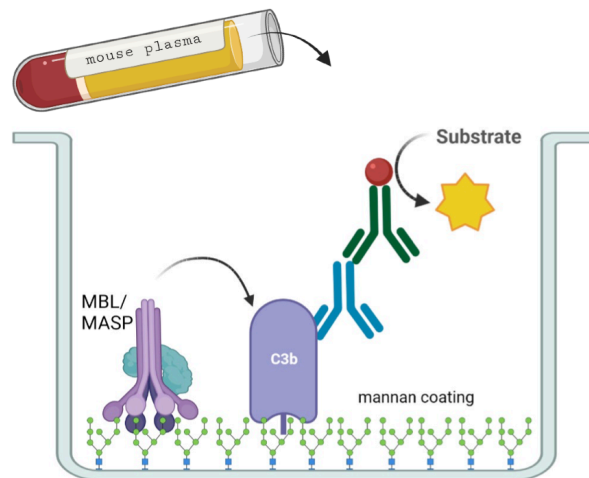


**Figure 11** Schema of Mannan-assay for C3 deposition

A lectin pathway specific C3 deposition ELISA was prepared on a Maxisorp ELISA plate (NUNC™). Plate was coated with 10 µg/mL mannan diluted in coating buffer (15 mM Na<sub>2</sub>CO<sub>3</sub>, 35 mM NaHCO<sub>3</sub>, pH 9.6) and incubated overnight at 4°C. Residual protein binding sites were saturated by incubating the plate with 1% BSA-TBS blocking buffer (0.1% (w/v) BSA in 10 mM Tris-CL, 140 mM NaCl, 1.5 mM NaN<sub>3</sub>, pH 7.4) overnight at 4°C. The plate was then washed with washing buffer (TBS with 0.05% Tween 20 and 5 mM CaCl<sub>2</sub>). EDTA-plasma samples collected from hMBL KI -2d, 90 min and 48h after tMCAo, were thawed on ice and suspended in barbital buffered saline (BBS; 4 mM barbital, 145 mM NaCl, 2 mM CaCl<sub>2</sub>, 1 mM MgCl<sub>2</sub>, pH 7.4), to a final plasma concentration of 6%. Wells receiving only BBS buffer were used as negative controls. Plasma solutions were incubated on the coated plate at 37°C for 1 h 30 min (40 µL/well). The plate was washed and incubated for 1 h 30 min at RT with a polyclonal anti-human C3c antibody (Dako, A0062) diluted 1:5,000 in washing buffer. After washing, the plate was incubated with an alkaline-phosphatase labeled goat anti-rabbit IgG antibody (Sigma A-3812) diluted 1:5,000 in washing buffer for 1 h 30 min at RT. Following washing, the assay was developed by adding 100 µL substrate solution (Sigma Fast p-Nitrophenyl Phosphate tablets, Sigma). The absorption at OD405 nm was then measured using the Infinite M200 spectrofluorometer managed by Magellan software (Tecan, CH). Plates were washed and incubated for 1 h 30 min at RT with a polyclonal antihuman-C3c antibody (Dako, A0062) diluted to 2.4 µg/mL in wash buffer. After washing, plates were incubated with an alkaline phosphatase-labeled goat anti-rabbit IgG antibody (Sigma A-3812) diluted to 1 µg/mL in wash buffer for 1 h 30 min at RT. After washing, the assay was developed by adding 100 µL of substrate solution (Sigma Fast p-Nitrophenyl Phosphate Tablets, Sigma). The absorbance at 405 nm

was then measured using the Infinite M200 spectrofluorometer managed by Magellan software (Tecan, CH).

## 2.24 Statistical analysis

Wells containing cells were randomly allocated to treatments. Subsequent immunohistological evaluations were done by blinded investigators. Data are reported as bar plots with mean  $\pm$  SD. Groups were compared by analysis of variance (ANOVA) and post hoc test, as indicated in each figure legend. The parametric or non-parametric test was selected after a Kolmogorov–Smirnov test for normality to assess whether groups met normal distribution. The constancy of variances was checked by Bartlett’s test. Data with equal variances were analyzed with two-way ANOVA followed by Tukey’s and Sidak’s multiple comparison, one-way ANOVA followed by Tukey’s multiple comparisons or unpaired t-test. Welch’s corrected t-test was used for normally distributed data with unequal variances. Group size for in vitro studies was defined pre hoc using the formula:  $n = 2s^2 f(a,b)/2$  (sd in groups = s, type I error a = 0.01, type II error b = 0.2, percentage difference between groups = 200 (2 time fold-change in the hypoxic group)). The standard deviation between groups was calculated based on a pilot experiment presented in 36 measuring the overexpression of *ICAM-1* due to hypoxia, and resulted in s = 42, yielding n = 4).

Group size for in vivo studies was defined pre hoc using the formula:  $n = 2s^2 f(a,b)/2$  (sd in groups = s, type I error a = 0.05, type II error b = 0.2, percentage difference between groups = 25). The standard deviation between groups was calculated based on previous experiment with neuroscore at 48h as primary endpoint, and resulted in s = 22, yielding n = 12).

## Chapter 3 : Result

### 3.1 In vitro binding studies

#### 3.1.1 Defining optimum MBL binding surface

##### 3.1.1.1 Introduction

Surface plasmon resonance (SPR) is a label-free sensor which allows to detect biomolecular interactions in real-time, measuring binding kinetic rate constants (association rate constant  $k_{on}$ ; dissociation rate constant  $k_{off}$ ) and the equilibrium dissociation constant ( $K_D$ , a measure of affinity or binding strength) (Figure 12).

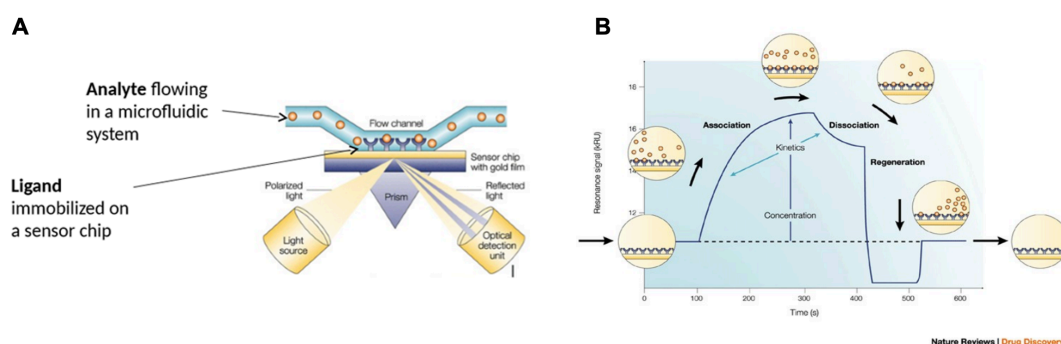


**Figure 12 Working principle of The ProteOn XPR36 SPR instrument.**

SPR technology allows to characterize biomolecular interactions between two unlabelled molecules, one immobilised on a sensor chip (referred to as the “ligand”), the other (the “analyte”) flowing through a microfluidic system over the chip surface (A). The interaction between the flowing analyte and the immobilized ligand is measured directly in real-time. The output of a typical SPR experiment is a sensorgram, in which the SPR binding signal is shown in function of time, distinguishing the association and the dissociation phases, i.e., during and after the flow of the analyte, respectively (B).

In this section, a new, convenient and robust SPR-based protocol was developed for in vitro screening of compounds interfering with the binding of native human MBL to an appropriate chip surface functionalized with a pattern of sugar moieties mimicking DAMPs (Figure 13). The SPR method is based on the specific binding of human recombinant MBL or native MBL present in human serum to the immobilized sugar moieties, to screen and identify inhibitors of this binding. This assay also includes the procedure to regenerate the chip surface after each experimental session, accomplished by sequential cleaning with piranha solution followed by UV exposure.

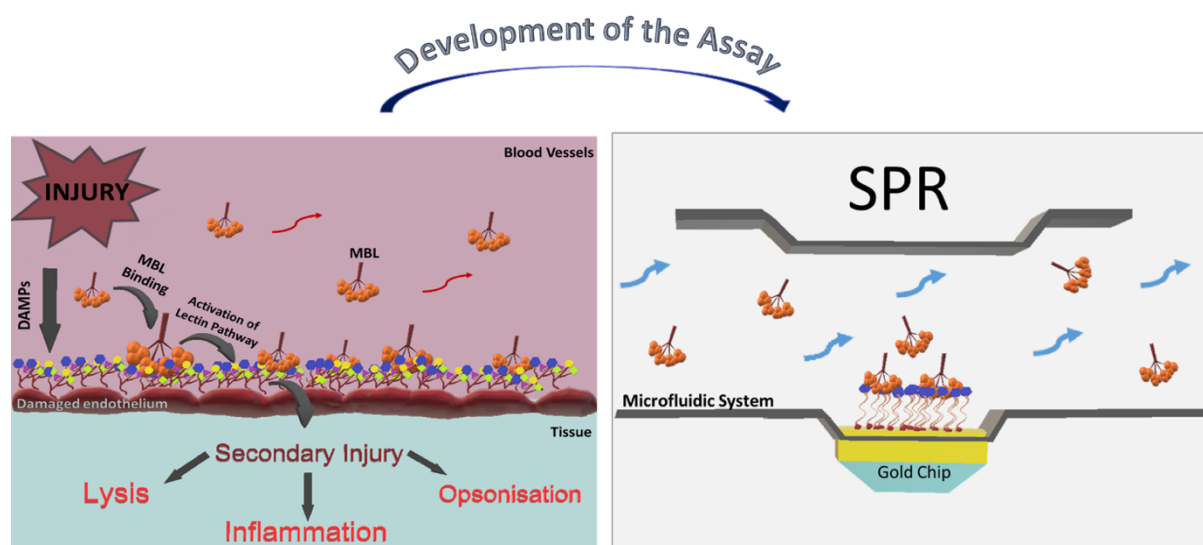
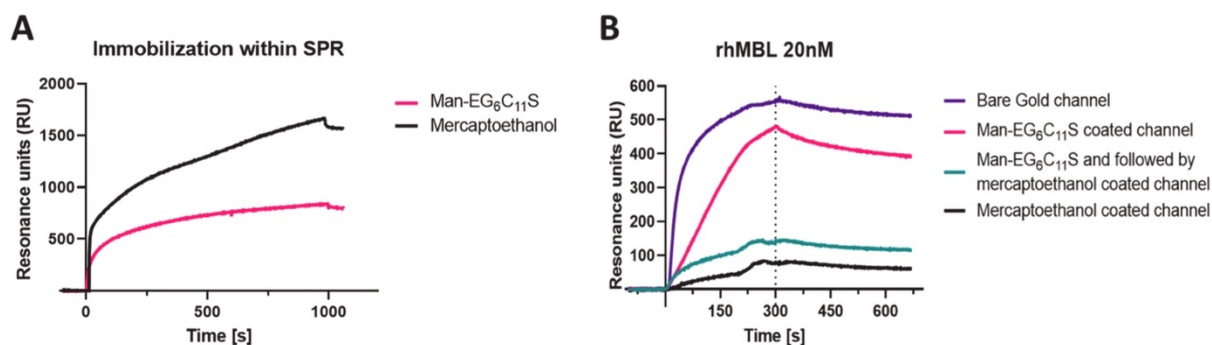


Figure 13 Overview of SPR assay principle

### 3.1.1.2 In-situ functionalization of the SPR chip is not efficient

At first, it was attempted to immobilize the SH-glyco-derivatives *in the SPR instrument*, i.e., flowing the SH-molecules over the bare gold surface. This would have allowed to immobilize different SH-glyco-derivatives in parallel lanes of the same sensor chip (Figure 7) and would have given more control of the level of immobilization.

Figure 14A shows the sensorgrams obtained when flowing Man-EG6C11SH (800  $\mu\text{g}/\text{mL}$ ) or mercaptoethanol 1 M (used as a control SH-molecule) on the bare gold surface for 980 s, indicating that both of them could be immobilized at high levels. The signal of Man-EG6C11SH was lower than with mercaptoethanol, despite the higher MW, indicating that the number of immobilized Man-EG6C11SH molecules is about 15 times lower than the number of immobilized mercaptoethanol molecules.



**Figure 14 Functionalization of the SPR chip surface in the instrument.**

(A) Immobilization of mercaptoethanol 1 M (black) and man-EG<sub>6</sub>C<sub>11</sub>SH (800 µg/mL) in two strips of the same chip. (B) Injection of rhMBL (20 nM) onto these functionalized strips with sequential injection of SH-glycopolymer with (green) or without (red) mercaptoethanol. rhMBL binding on bare gold, shown in purple, and binding on the mercaptoethanol-coated channel is in black.

Figure 14B shows the binding signals of rhMBL on the prepared surfaces. The response was good on the Man-EG<sub>6</sub>C<sub>11</sub>SH-immobilized surface but not on the mercaptoethanol-immobilized surface; however, rhMBL binding was even greater on the unfunctionalized bare gold, probably due to the cysteine groups of the protein. It is therefore hypothesized that mercaptoethanol efficiently coated the whole surface, while the immobilization of Man-EG<sub>6</sub>C<sub>11</sub>SH was not so efficient, leaving some unfunctionalized gold-surface to which rhMBL can bind.

To confirm this, the Man-EG<sub>6</sub>C<sub>11</sub>SH-immobilized surface was subjected to an intermediate flow of mercaptoethanol for 980 s, followed by rhMBL injection. In this condition, the binding of rhMBL was substantially lower (green), supporting the notion that in-instrument immobilization of Man-EG<sub>6</sub>C<sub>11</sub>SH is not sufficient to saturate the whole surface.



### 3.1.1.3 Ex-situ functionalization of the SPR chip is efficient and reproducible

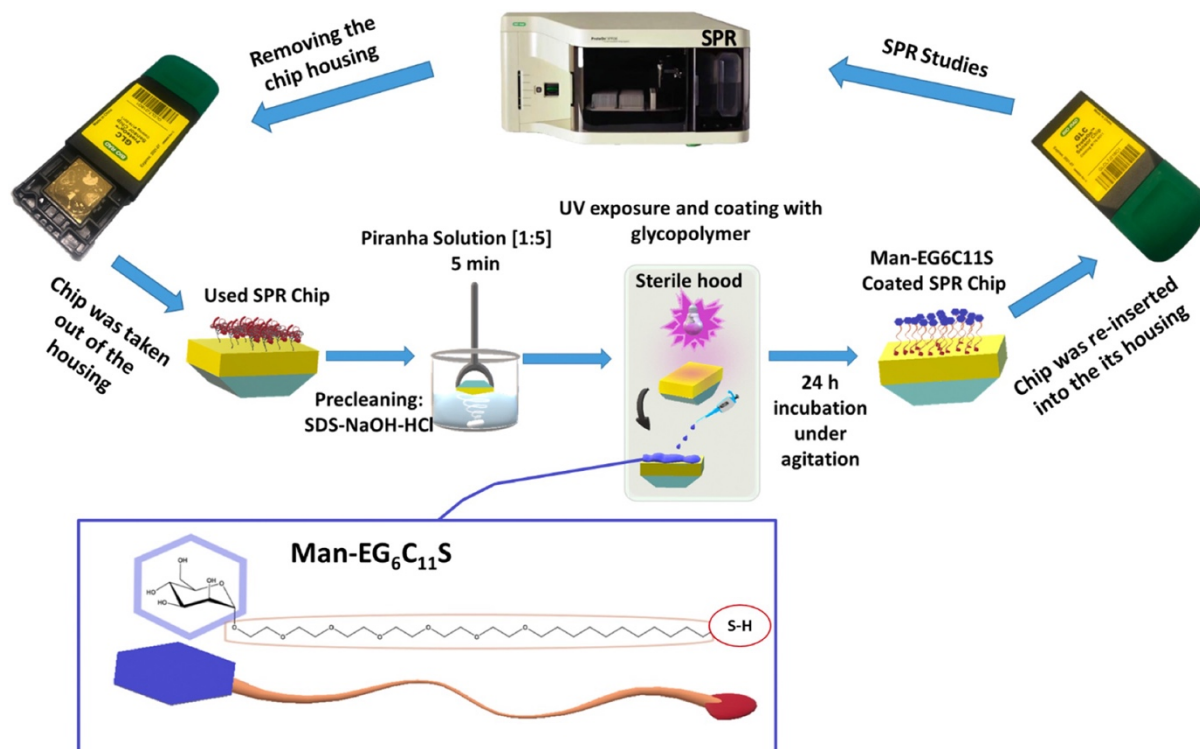
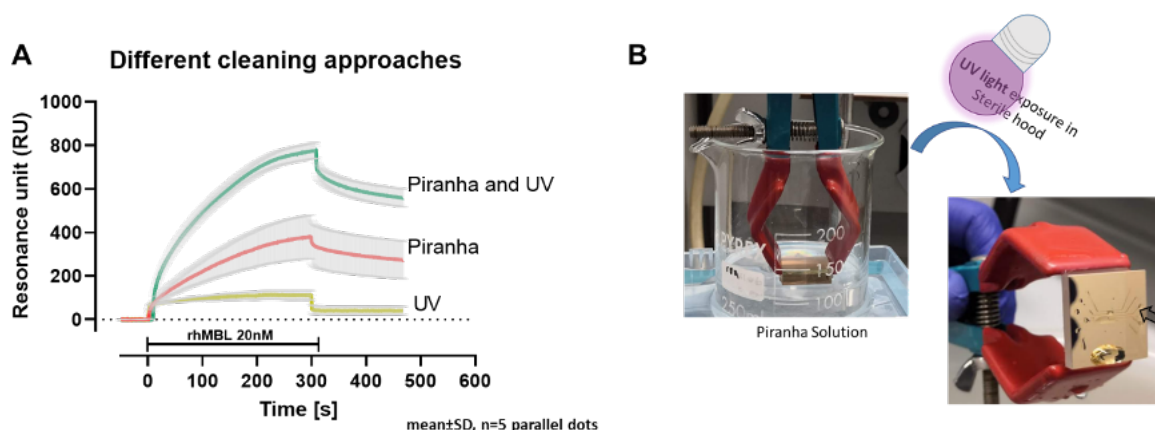


Figure 15 Diagrammatic scheme of piranha/UV cleaning and the chip surface coating cycle.

To overcome the low functionalization efficiency *in the instrument*, the SH-glyco-derivatives were immobilized on the bare gold surface *outside the SPR instrument*. This meant that the incubation time could be extended to 24 h, with the aim of allowing a complete functionalization. After this incubation, the chip is inserted into the SPR instrument (Figure 15) to evaluate the MBL-binding to the functionalized surfaces.

To be feasible, this approach needed a suitable method for chip regeneration. Therefore different cleaning strategies (Figure 16A) were tested to remove the immobilized ligands, e.g. dextran matrices or SH-glyco-derivatives, and identified the combination of immersion in piranha solution followed by exposure to UV as the best (Figure 16B).



**Figure 16 Comparison of different cleaning approaches to reclaim the used SPR chip.**

Chips were cleaned as indicated and functionalized with Man-EG<sub>6</sub>C<sub>11</sub>S outside of the SPR instrument. rhMBL (20 nM) was flowed for 300 secs. The panel A show the sensorgrams (i.e., time course of SPR signal in RU) expressed as mean±SD of five detection spots of the same chip. SPR Chip cleaning with Piranha and UV is showed in panel B, cleaned SPR chip microfluidic channels pointed with arrow.

Further studies were carried out to evaluate the performances of the same chip after sequential regenerations. Figure 17 shows that this enabled us to completely remove the immobilized Man-EG<sub>6</sub>C<sub>11</sub>S (compare panels A and B), while maintaining the surface properties for subsequent functionalizations (compare panels B and C, in which rhMBL binding is reinjected after regeneration and functionalization with Man-EG<sub>6</sub>C<sub>11</sub>S).

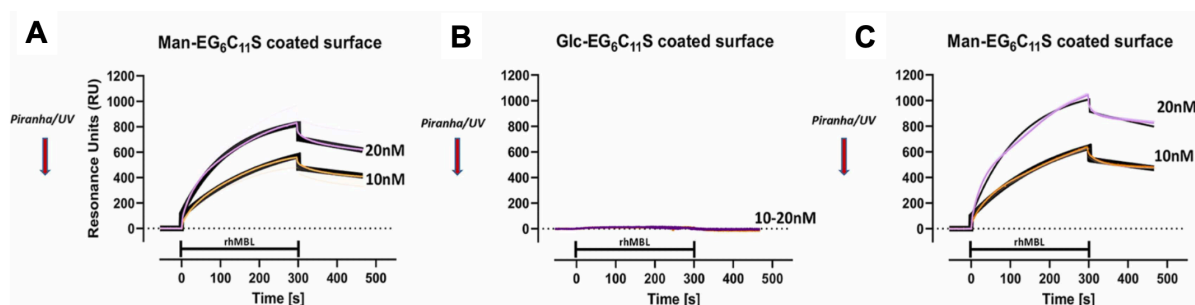


**Figure 17** Sensorgrams obtained on the same chip after sequential cleaning with piranha/UV, surface coating with Man-EG<sub>6</sub>C<sub>11</sub>S outside the SPR instrument as indicated, and injection of rhMBL.

The figures show the sensorgrams expressed as mean±SD of six detection spots of the same chip (for clarity only one side of SD is shown). Black lines show the fitting of the sensorgrams in panel A and C, with a common estimated K<sub>D</sub> of 2.3 nM (the small difference in the absolute RU values was accounted for small difference in the estimated R<sub>max</sub>, left free in the fitting, as expected for different immobilizations).

### 3.1.1.4 Characterization of the binding properties of Man-EG<sub>6</sub>C<sub>11</sub>S-coated surface in buffer and serum

Binding properties of the Man-EG<sub>6</sub>C<sub>11</sub>S-coated surface were characterized by using the conditions for surface cleaning and functionalization described previously (2.5).

Figure 18 shows the concentration-dependent binding of rhMBL to Man-EG<sub>6</sub>C<sub>11</sub>S previously immobilized on a cleaned GLC chip. The K<sub>D</sub> was  $0.46 \pm 0.03 \mu\text{g/mL}$ , calculated by a fitting of all the sensorgrams in Figure 18 with the Langmuir equation. Assuming a MW of rhMBL of 230 kDa (i.e. trimers of structural monomers, each made up of three identical 25.5 kDa polypeptide chains<sup>77</sup>), the estimated K<sub>D</sub> is  $2.3 \pm 0.13 \text{ nM}$  (mean±SD of six different detection spots) as in the literature<sup>32</sup>.

The mean K<sub>D</sub> from twelve injections of different concentrations of rhMBL over eight piranha/UV cleaned chips (up to four times) functionalized with Man-EG<sub>6</sub>C<sub>11</sub>S is  $2.3 \pm 0.33 \text{ nM}$  (association rate constant  $k_{\text{on}} 7.4 \pm 0.7 \times 10^5 \text{ M}^{-1} \text{ s}^{-1}$ ; dissociation rate constant  $k_{\text{off}} 1.3 \pm 0.2 \times 10^{-3} \text{ s}^{-1}$ ).

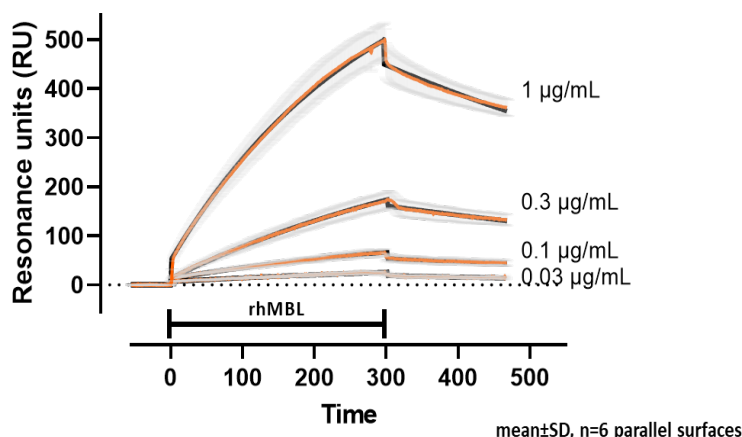


**Figure 18** Concentration-dependent binding of rhMBL obtained by simultaneous injections of four dilutions of rhMBL (0.03-1 µg/mL).

The variability of the sensorgrams obtained in six detection spots (SD shown as shaded area) with the fitting (black lines) obtained using the the Langmuir equation results in a  $K_D$  of 0.46 µg/mL.

As for the specificity of the binding, it was found that the Man-EG<sub>6</sub>C<sub>11</sub>S-coated surface did not bind Soybean-agglutinin and rh-Ficolin1 (Figure 19), in agreement with literature data showing no binding of these lectins to mannose<sup>78,79</sup>.

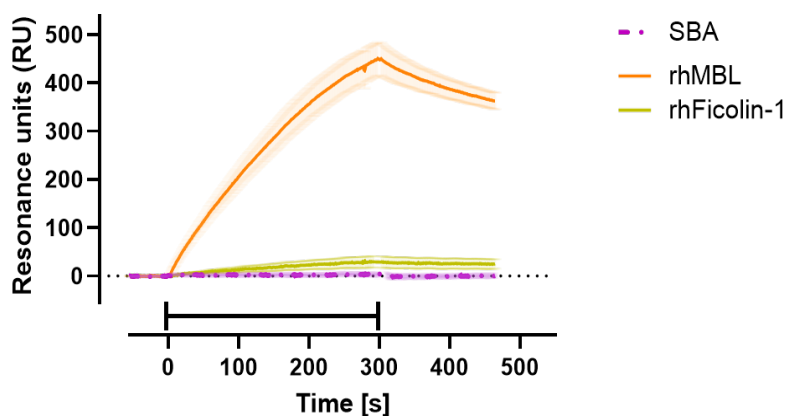


**Figure 19** MBL specifically bound to Man-EG<sub>6</sub>C<sub>11</sub>S-coated SPR chip surface.

Binding specificity was evaluated by injecting a fixed concentration (1 µg/mL) of different lectins: rhMBL(orange), rhFicolin-1 (green), Soybean Agglutinin (SBA) (pink) over Man-EG<sub>6</sub>C<sub>11</sub>S-coated SPR chip surface.

Then the binding of native MBL the Man-EG<sub>6</sub>C<sub>11</sub>S-coated surface was investigated. Human serum was diluted 50 times to reduce non-specific binding due to other serum proteins and injected over the Man-EG<sub>6</sub>C<sub>11</sub>S-coated surface. Diluted MBL-depleted serum was tested in parallel to estimate the non-specific binding.

Figure 20A shows the clear MBL-dependent binding, although there was also significant MBL-independent binding. To specifically visualize the MBL-dependent binding, a second injection with an anti-MBL antibody was added, immediately after the serum. The antibody injection specifically detected the MBL-dependent binding, since the signal was negligible for MBL-depleted serum (Figure 20B).

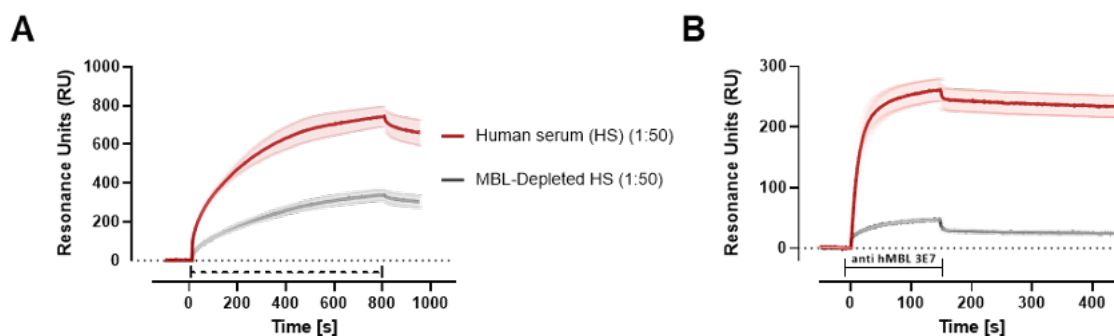


**Figure 20** Detection of specific homogenous hMBL binding

The graphs show representative sensorgrams, i.e., the time course of the surface plasmon resonance signal in resonance units (RU). Human serum (HS) or MBL-depleted HS was injected for 800 sec at the rate of 30  $\mu\text{g}/\text{mL}$  over chip surfaces coated with Man-EG<sub>6</sub>C<sub>11</sub>S (A). MBL-dependent binding was then determined by sequential injections of anti-hMBL 3E7 antibody (10  $\mu\text{g}/\text{mL}$ ) shortly after the sera (B). All sera were diluted 1:50 in TBST/ $\text{Ca}^{+2}$ . Data show the mean $\pm$ SD of the sensorgrams obtained in six detections spots.

To check for quenching of the MBL detection due to the matrix, rhMBL was added to MBL-depleted serum and compared the binding signal with those in buffer. Diluted serum had only a slight (13%) quenching effect (Figure 21A, B).

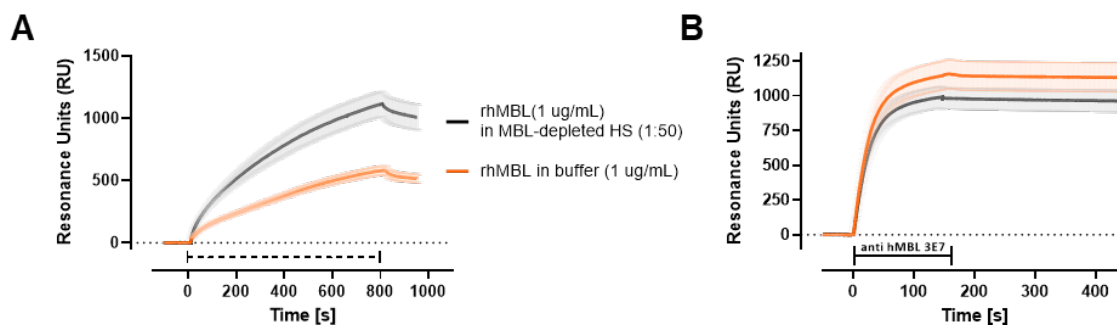


**Figure 21** Evaluation of quenching effect of MBL binding in presence of sera.

Injection of rhMBL (1  $\mu\text{g}/\text{mL}$ ) in TBST/ $\text{Ca}^{+2}$  buffer or in MBL-depleted HS over Man-EG<sub>6</sub>C<sub>11</sub>S (A). MBL-dependent binding determined by sequential injections of 3E7 antibody (10  $\mu\text{g}/\text{mL}$ ) shortly after rhMBL (B). All sera were diluted 1:50 in TBST/ $\text{Ca}^{+2}$ . Data show the mean $\pm$ SD of the sensorgrams obtained in six detections spots.

### 3.1.2 Recognizing MBL inhibitors in buffer

Preincubation of rhMBL for 1 h in buffer with 10 or 30 mM mannose (1.8 and 5.4 mg/mL) resulted in concentration-dependent inhibition of rhMBL binding to Man-EG<sub>6</sub>C<sub>11</sub>SH-coated surface, with IC<sub>50</sub> 5.1 mM (95% CI 5.45  $\pm$  2.35 mM) ( $\sim$  1 mg/mL) (Figure 22).

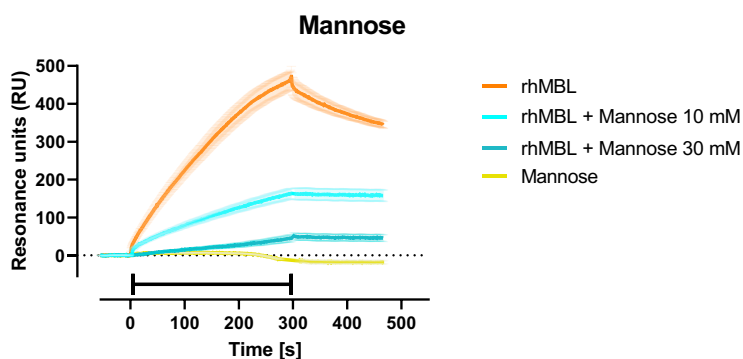


**Figure 22** Proof of principle for screening inhibitors of MBL binding to a Man-EG<sub>6</sub>C<sub>11</sub>S -coated SPR chip surface.

Sensorgrams shows the injections of rhMBL preincubated or not with monovalent mannose (10 and 30 mM) (blue), and mannose alone (yellow). All samples were prepared in TBST/ $\text{Ca}^{+2}$  Data show the mean $\pm$ SD of the sensorgrams obtained in 5-6 detections spots.

A glycan carrying nine mannose residues (M9), was then tested after 1 h preincubation of rhMBL in buffer (Figure 23). M9 was tested at 100 and 200  $\mu\text{M}$ , corresponding to 0.18 and 0.36 mg/mL. The glycan inhibited rhMBL binding to the Man-EG<sub>6</sub>C<sub>11</sub>SH-coated surface with an estimated IC<sub>50</sub> of 175  $\mu\text{M}$  (0.33 mg/mL). These data indicate that this oligo-mannose glycan increases the affinity of MBL by about 30 times, presumably due to the multivalency effect.

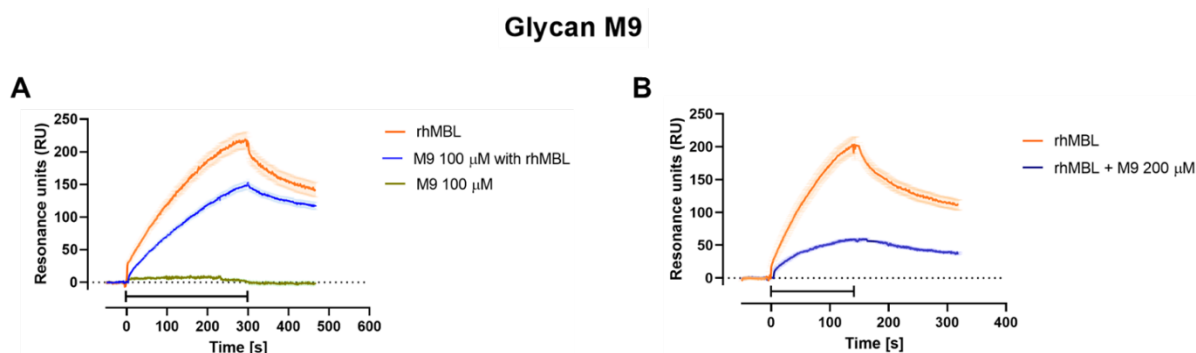


**Figure 23 Inhibitory multivalency effect of M9 Glycan on MBL binding over Man-EG<sub>6</sub>C<sub>11</sub>S-coated SPR chip surface**

Sensorgrams shows the injections of rhMBL binding after preincubation of M9 Glycan (100  $\mu\text{M}$ , blue (A), 200  $\mu\text{M}$ , blue (B)), rhMBL alone (orange) and M9 glycan 100  $\mu\text{M}$  (green)). All samples were prepared in TBST/Ca<sup>2+</sup>. Data show the mean $\pm$ SD of the sensorgrams obtained in 5-6 detections spots.

To benefit more from the multivalency effect, following studies focused on gold nanoparticles exposing many residues of mannose (Man-GNPs), or glucose (Glu-GNPs) as controls. These NPs were synthesized starting from citrate-capped GNPs with a core diameter of  $14.1 \pm 2.1$  nm (Figure 4). The citrate-GNPs and glyco- GNPs were fully characterized by TEM and UV-Vis (Figure 4-Figure 6) and by DLS in order to determine their hydrodynamic diameter and check their colloidal stability by measuring their  $\zeta$ -potentials (see Table 1).

For evaluation of the inhibitory effect of Man- or Glc-GNPs, rhMBL in TBST/Ca<sup>2+</sup> buffer was preincubated for 1 h with 3  $\mu\text{g/mL}$  of GNPs. The mixture including GNPs was injected, over the functionalized sensor surface.

The results indicated a relevant binding of GNPs themselves on the surface (Figure 24A), which made it necessary to perform a second injection with anti-MBL antibody (Figure 24B). Although suggesting an inhibitory effect of GNPs (Figure 24) the possibility that MBL bound to the GNPs might still be recognized by the antibody would make the interpretation of the results difficult.

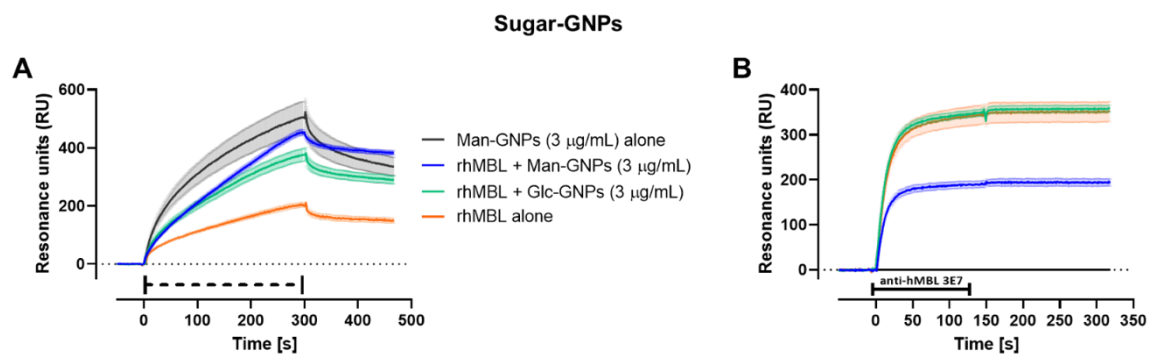


**Figure 24** Inhibition of MBL binding on Man-EG<sub>6</sub>C<sub>11</sub>S-coated SPR chip surface by sugar-capped GNPs.

rhMBL (1 µg/mL) was preincubated with and without Mannose-(blue, Man-GNPs) and Glucose-(green, Glc-GNPs) coated gold nanoparticles (3 µg/mL) for 1 hour. The preincubated solutions were injected for 300 sec. over parallel channels of the Man-EG<sub>6</sub>C<sub>11</sub>S-coated SPR chips (A). Specific MBL binding was determined by sequential injections of anti-hMBL 3E7 antibody (10 µg/mL) shortly after the injection of solutions (B). Each sensorgram shows the mean of six parallel sensor spots; SD is indicated as shaded area.

Since the aim here was to see whether GNPs actually bind MBL, the solution was centrifuged in order to pellet GNPs with bound MBL, injecting the supernatants (containing unbound rhMBL) over Man-EG<sub>6</sub>C<sub>11</sub>S-coated surfaces.

Figure 25 shows that Man-GNPs reduced the rhMBL-dependent binding signal in a concentration-dependent manner, with an extrapolated IC<sub>50</sub> of 1.1 µg/mL (95% CI 0.2–3.3 µg/mL) whereas Glc-GNPs had a much smaller inhibitory effect, with IC<sub>50</sub> > 25 µg/mL. The very small amount of NPs with an inhibitory effect (1.1 µg/mL) indicates that the avidity effect markedly raises the affinity of these multivalent mannose-based ligands of MBL by 2–3 orders of magnitude.



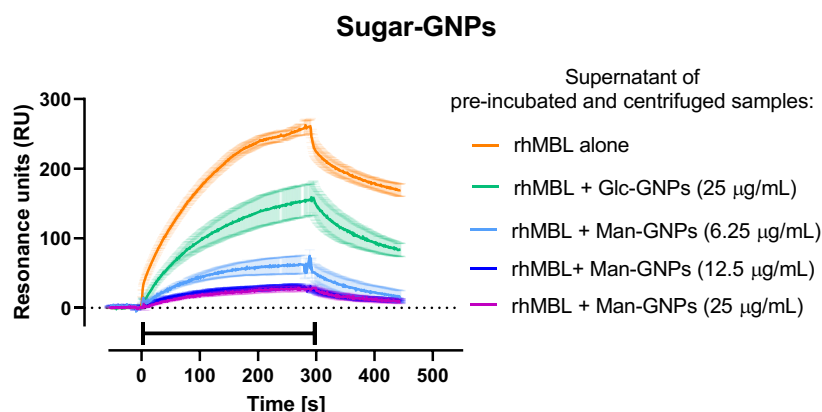


**Figure 25** MBL binding signals after pre-incubation with inhibitory sugar-capped GNPs.

Sensorgrams show the injections of rhMBL binding after preincubation of mannose-capped GNPs (6.5-25 µg/mL) (Man-GNPs, blue), or glucose-capped GNPs (25 µg/mL) (Glc-GNPs, green), rhMBL alone (orange). All samples were prepared in TBST/Ca<sup>2+</sup>. Data show the mean±SD of the sensorgrams obtained in 5-6 detections spots.

### 3.1.2.1 Different Oligomerization of hMBL

MBL is a folded molecule, forms a structural unit of three MBL monomers (MBL<sub>3</sub>), which are organized through higher order oligomers by interchain disulfide bridge formation<sup>80,81</sup>. Circulating MBL is a highly polydisperse molecule with the size of the oligomers ranging from three to eight structural units (3xMBL<sub>3</sub> - 8xMBL<sub>3</sub>)<sup>32</sup>. Due to this highly polydisperse structure of MBL, oligomerization of rhMBL and native hMBL were compared to evaluate better the affinity studies.

Western blot analysis (Figure 26), carried out in non-reducing conditions, showed that human endogenous MBL is present as high-order oligomers, with major distinct bands ranging 171-382 kDa. On the other hand, the major bands of rhMBL ranged from 25.5 kDa (monomers) to ~71 kDa (trimers).

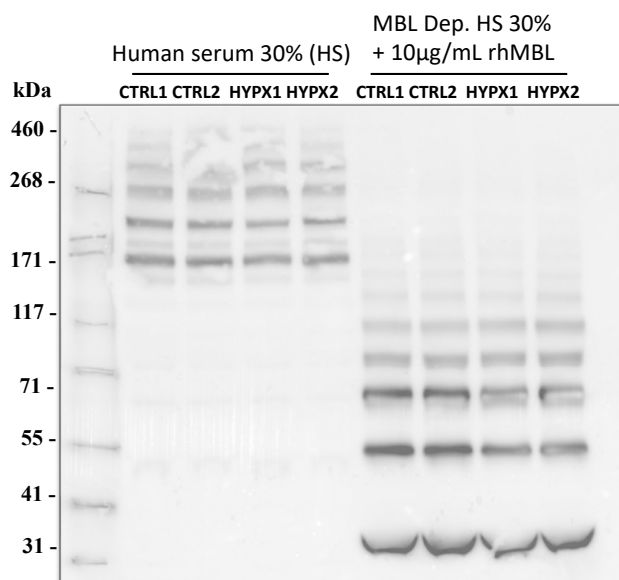


**Figure 26 Recombinant and human endogenous MBL showed different oligomerization.**

Western blot analysis for MBL oligomerization was run in non-reducing condition with media collected over immortalized human brain microvascular endothelial cells, exposed to hypoxia (HYPX) or not (CTRL), and then re-oxygenated in the presence of 30% human serum (HS) or 10 µg/mL recombinant hMBL (rhMBL) in MBL depleted human serum 30% (MBL Dep. HS 30%), as explained in 2.10. Human endogenous MBL presented in 30% HS, showed high oligomerization within major distinct band range of 171-382 kDa, whereas rhMBL majorly ranged in 31-71 kDa. No significant changes observed between the CTRL and HYPX groups. Four replications of the samples prepared for each condition.

### 3.1.2.2 Protein Corona formation on MBL inhibitors in serum

Protein corona is a natural interface between nanomaterials and biological surroundings, as biological molecules, including proteins, sugars, and lipids, forming “a corona” on the surface of all nanoparticles (NPs). This formation may confer a biological identity of the nanomaterials such that they can engage NPs interactions with living systems<sup>82</sup>. Surface of sugar-capped GNPs (sugar-GNPs) are attracted by both low affinity serum proteins which creates outer dynamic soft corona (see blue circle around the NPs) and high affinity serum proteins that strongly bound to particles to create inner hard corona (see red circle around the NPs) immediately after sugar-GNPs are introduced into human serum (Figure 27A).

Protein corona was formed by incubation of sugar-GNPs in 30%HS diluted in TBST/Ca<sup>+2</sup>. Soft corona was gradually separated from the hard corona by four consequent washings – centrifugation steps in TBST/Ca<sup>+2</sup> (Figure 27A). MBL was found on hard corona of Man-GNPs, which proves that protein corona formation does not interfere the binding of hMBL to Man-GNPs in serum. This binding is strong and sugar specific as no strong signal was detected on Glc-GNPs (Figure 27B).

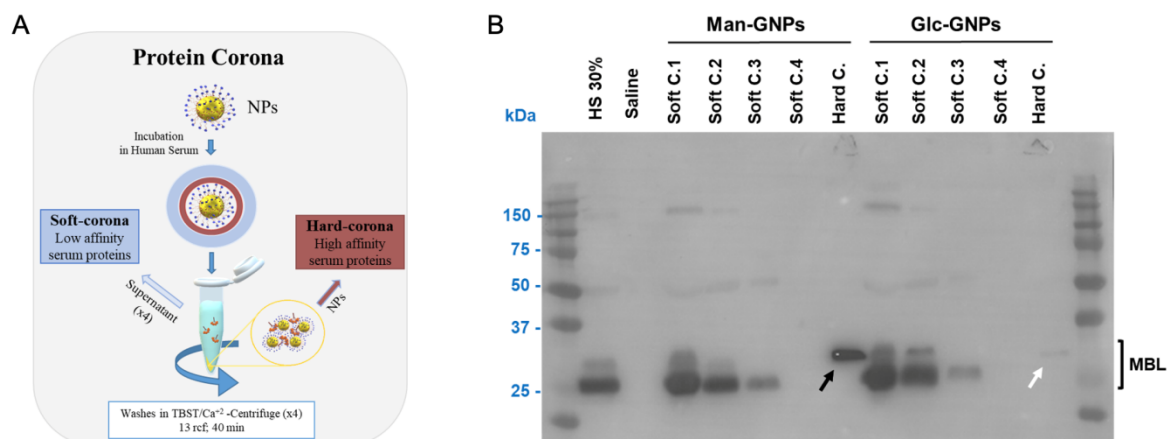


**Figure 27** MBL was found on hard corona of mannose-capped GNPs (Man-GNPs) but not glucose-capped GNPs (Glc-GNPs).

Scheme of MBL protein corona formation and separation of soft corona and hard corona (blue and red circle, respectively) (A). MBL signal decreased after first to third washes (Soft C1-3\_Man/Glc-GNPs) and no signal captured after additional washing step (Soft C.4\_Man/Glc-GNPs), meaning soft corona efficiently separated from hard corona. Hard Corona was analysed over loaded sugar-NPs (pointed with black arrow for Man-NPs, white arrow for Glc-GNPs). Sugar-GNPs remained on the top of the membrane, but only hard corona proteins run through the membrane. MBL was found only on hard corona of Man-GNPs, but no strong signal detected on Glc-GNPs (B).

### 3.1.2.3 Recognizing MBL inhibitors in serum

Studies were carried out to see whether the Man-GNPs also inhibits MBL binding in serum, i.e., to assess both the effect of protein corona formation on GNPs and high oligomerization of endogenous MBL which would affect Man-GNPs ability to bind MBL.

Man- or Glc-GNPs (6.25  $\mu\text{g}/\text{mL}$ ) were pre-incubated in 50-fold diluted HS for 1 h. The solutions were then centrifuged to pellet NPs, and the supernatants (containing unbound MBL) injected over the Man-EG<sub>6</sub>C<sub>11</sub>S-coated surface (Figure 28A). To clearly dissect the MBL-dependent binding, a second injection with an anti-MBL antibody was added, after the one with serum. Figure 28B shows that Man-GNPs completely inhibited the binding of native MBL (blue), while Glc-GNPs had negligible inhibitory effect (Figure 28B, green).

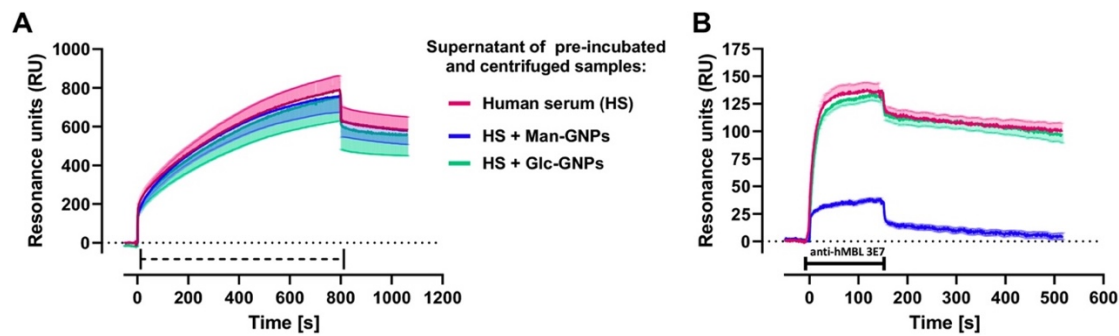


Figure 28 Inhibition of MBL binding by sugar-capped GNPs in human serum.

HS (1:50) was preincubated with and without Man- EG<sub>6</sub>C<sub>11</sub>S (blue) and Glc- EG<sub>6</sub>C<sub>11</sub>S (green) coated GNPs (6.25 µg/mL) for 1h, and precipitated by centrifugation (25 min). Only the supernatants were injected simultaneously for 800 s over parallel channels of the Man- EG<sub>6</sub>C<sub>11</sub>S coated SPR chip. (A) Specific MBL binding determined by sequential injections of anti-hMBL 3E7 antibody (10 µg/mL) shortly after the injection of sera. (B) Each sensorgram shows the mean of six parallel sensor spots; SD is indicated as shaded area (one side only for clarity).

## 3.2 Hypoxia altered glycolyx of i-hBMECs

### 3.2.1 Introduction

Quartz Crystal Microbalance (QCM) is a cell-based biosensor assay providing real-time pharmacodynamic analyses on tissues and cells in whole blood and sera.<sup>63,83</sup> QCM offers extended possibilities for understanding the biology including *in vivo*-effects, overcoming limitations of traditional biosensors as they require isolated and purified target molecules immobilized on the sensor surface where the target is not present in its natural context, possibly resulting in undesirable conformation alterations of the target molecule.

Attana Cell A200 QCM was used to investigate possible hypoxia related changes on glycolyx of i-hBMECs, mimicking the physiological conditions of ischemic brain injury. For that, either LNB-carboxyl sensor chip (LNB-CC), allowing cell capturing by immobilized PHAL lectins, and LNB-COP sensor chip, providing a surface for cell culturing, were used for glycoprofiling assay. Glycoprofiling was carried out by parallel injections of different concentrations of plant lectins—having affinities to different sugars<sup>84</sup> i.e. PHAL and RCA to galactose, WGA to GlcNAc, SNA to Neu5Ac, ConA and LCA to mannose— on normoxic and hypoxic i-hBMECs in Cell A200 QCM instrument (Figure 29).

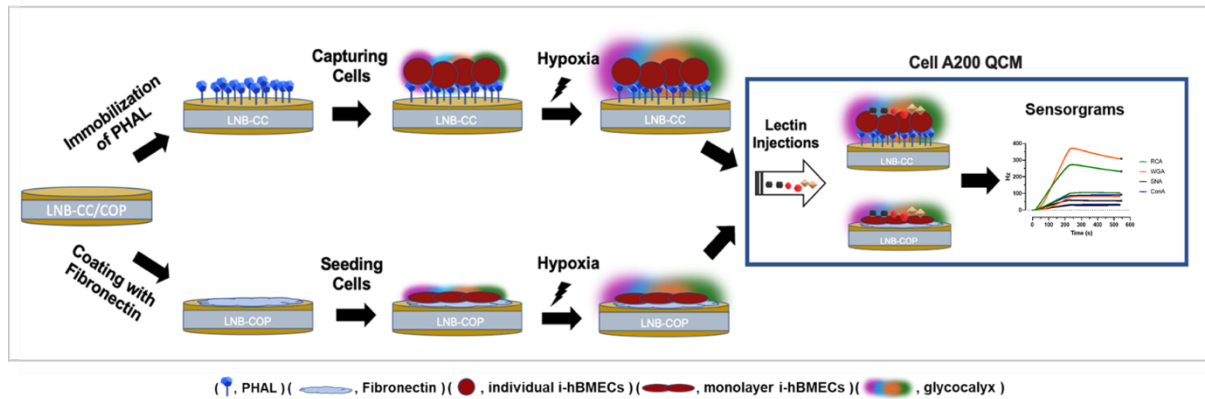
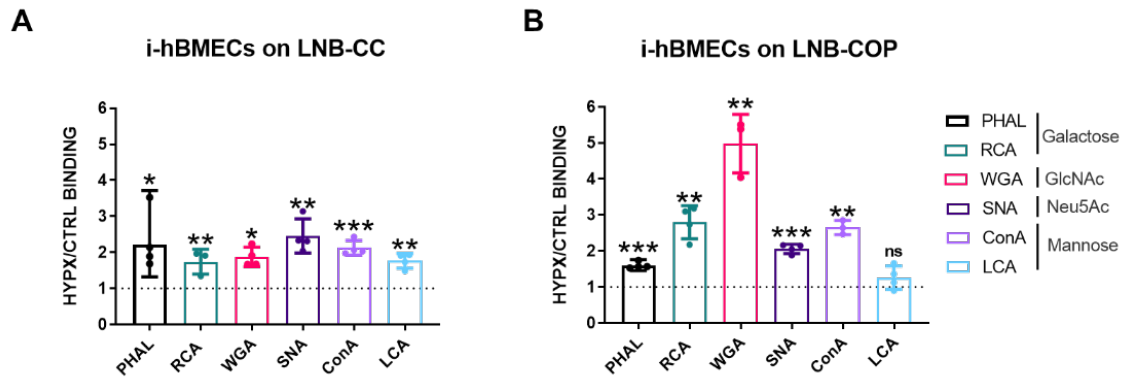


Figure 29 Diagrammatic scheme of LNB-CC/COP chip preparation for glycoprofiling of ischemic i-hBMECs endothelium and lectin binding assay on altered glycocalyx of i-hBMECs within the Cell A200 QCM instrument.

### 3.2.2 Overexpression of glycans after hypoxia

Plant lectins were bound more on ischemic (HYPX) endothelium of i-hBMECs than normoxic (CTRL) ones, contributing to the fact that hypoxia altered glycocalyx of endothelium and induced more sugar expression on cell surface (Figure 30). LNB-COP chip with i-hBMECs showed higher signal compared to LNB-CC chip, suggesting monolayer formation of endothelial cells provides better binding surface for lectins.



**Figure 30 Hypoxia altered glycoprofile of i-hBMECs endothelium.**

i-hBMECs captured on LNB-CC or seeded on LNB-COP surface were exposed to hypoxia (HYPX) or not (CTRL), and then re-oxygenated in the presence of 30% HS. Cells were fixed (4% PFA) and LNB chips inserted to Cell A200 QCM instrument. Different plant lectins, with different sugar affinities, were injected at four different concentration (0.7-2-6-18  $\mu\text{g}/\text{mL}$ ) for 250 sec. over CTRL and HYPX i-hBMECs on LNB-CC (A) or LNB-COP (B) chips. For each concentration, the ratio of the binding signals observed in HYPX vs CTRL cells was determined and is shown as single point in the graph. The bars show the mean with 95% CI (n=3-4). Statistical analysis was carried out using the original data, i.e., binding signals measured in CTRL and HYPX cells, and was a Ratio paired t-test: \* $p < 0.05$ , \*\* $p < 0.01$  HYPX vs CTRL.

### 3.3 Screening potential effect of GNPs in in vitro cell assay

#### 3.3.1 Toxicity

Potential effects of chosen MBL inhibitor i.e., Man-GNPs were investigated on hypoxic and normoxic i-hBMECs. For potential toxic effects, the normoxic and hypoxic cells were treated with high concentration (40  $\mu\text{g}/\text{mL}$ ) of Man-GNPs and as negative control with Glc-GNPs in presence of 30% HS. Cell viability assay were carried out by cell counting with DAPI staining. No significant changes were observed either by hypoxic model and high concentration of sugar-GNPs (Figure 31).

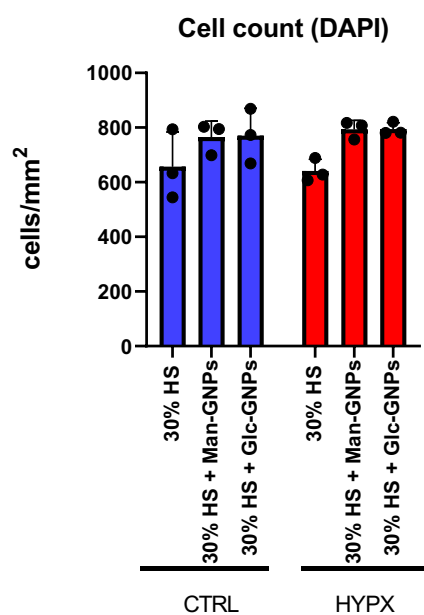


**Figure 31** High concentration of sugar-GNPs (mannose-capped GNPs (Man-GNPs); glucose-capped GNPs (Glc-GNPs)) did not affect cell viability.

i-hBMECs underwent 16h of hypoxia (HYPX, red) or normoxia (CTRL, blue). Then they were reoxygenated in presence of human serum diluted 30% in culture medium (30% HS) with or without 40  $\mu\text{g}/\text{mL}$  sugar-GNPs for 4h. Cells were counted after nuclei staining (DAPI). The data are shown as mean with individual values + SD ( $n = 3$ ). Two-way ANOVA followed by Tukey's post hoc, ns.

Cells were then examined for cytoskeleton organization. First, F-actin layers were labelled with phalloidin. Hypoxia induced structural damage, as indicated by a greater spacing between cells, less dense phalloidin staining for F-actin filaments. This effect was not antagonized by presence of 40  $\mu\text{g}/\text{mL}$  sugar-GNPs (Figure 32).

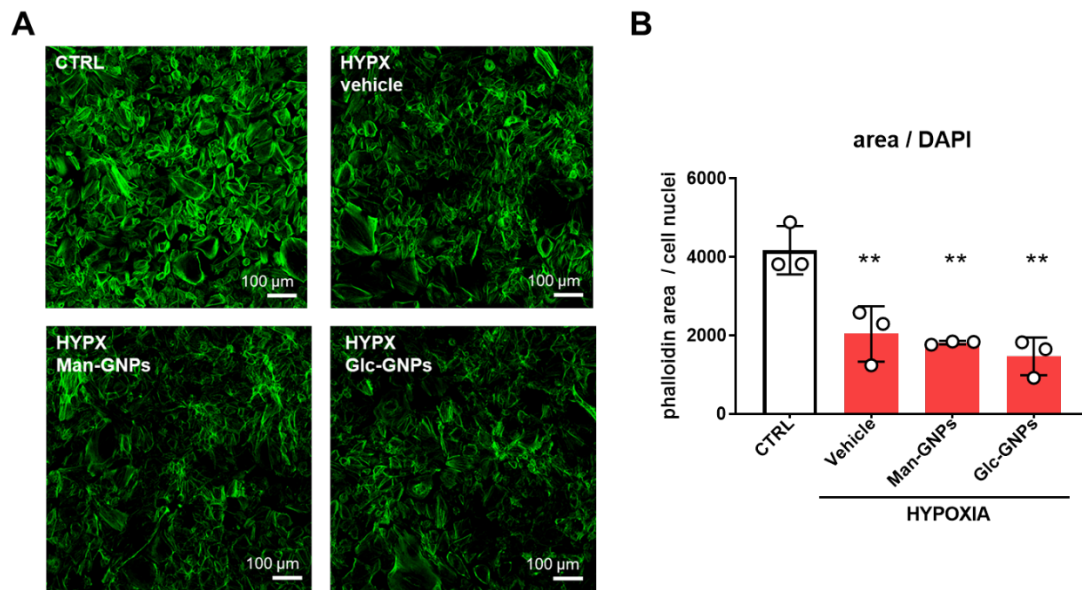


**Figure 32** Hypoxic and normoxic i-hBMECs undergone re-oxygenation with or without in the presence of 40 µg/mL sugar-GNPs in 30% HS labelled with phalloidin (F-actin) to stain the cytoskeleton.

F-actin staining (green) showed that normoxic (CTRL) i-hBMECs formed a regular layer, while hypoxic i-hBMECs had greater spacing between cells and less dense staining (A). Scale bars 100 µm. The effect of hypoxia was not antagonized by presence of 40 µg/mL sugar-GNPs (B). Data are reported as mean with individual values  $\pm$  SD (n=3). One-way ANOVA followed by Tukey's post hoc, \*\*p < 0.01 vs. CTRL.

To clarify more the non-toxic function of sugar-GNPs, it was aimed to visualize sugar-GNPs to understand if the particles were localised in cell or not. For this, reflectance confocal microscopy (RCM) was used thanks to optical properties of spherical gold nanoparticles. First, RCM was set up on microscope slides by exciting metallic surface of sugar-GNPs with a single-wavelength laser (561 nm) and then collecting the reflective laser with same wavelength. Focus of camera was adjusted by Alexa488 conjugated fluorescence beads (Figure 33).



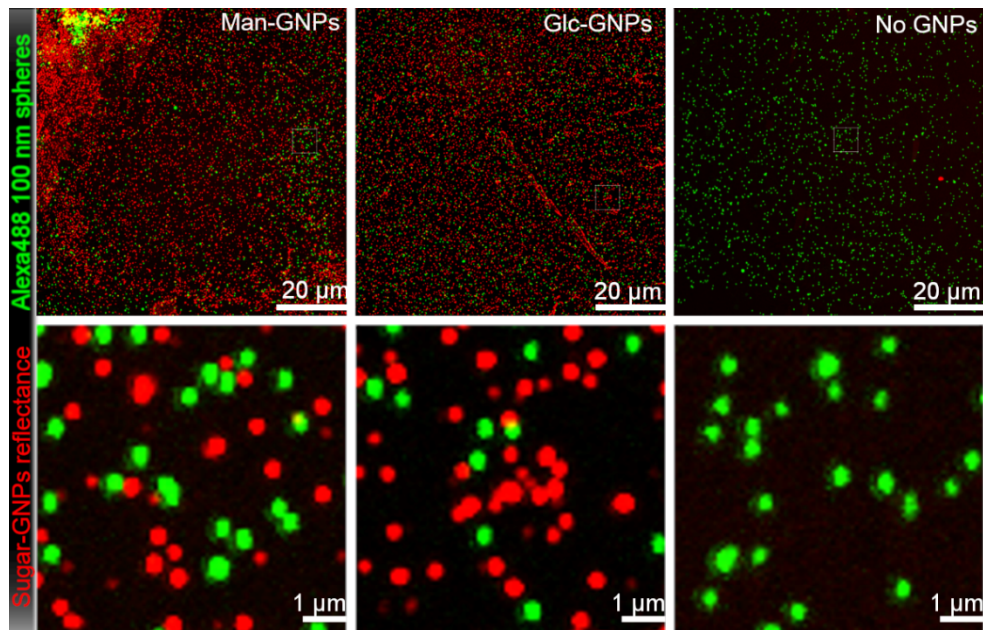


**Figure 33** Set up and test of reflectance confocal microscopy to visualize sugar-GNPs using a confocal microscope.

Sugar-GNPs (red) were captured by reflectance confocal microscopy. Focus and background adjustment done by Alexa488-conjugated beads (100 nm, green, Control images only in presence of Alexa488-conjugated beads presented as No GNPs. Images acquired with a 10x objective (scale bar 20 μm) and a 100x objective (scale bar 1 μm).

Then, the same setting applied on i-hBMECs to investigate Man-GNPs localization. In both conditions i.e., normoxic and hypoxic, nanoparticles were detected in cell soma (Figure 34).

Cytoskeleton organization was altered by hypoxic condition (Figure 32 ,Figure 34B) compared to CTRL group (Figure 34A), as previously reported<sup>22</sup>. However, this strong effect of hypoxia would also mask possible toxic effect of sugar-GNPs since they were accumulated in the cytoplasm of CTRL cells. Therefore CTRL cells were selected and analysed to investigate whether intracellular Man-GNPs presence induced structural changes to the cytoskeleton as shown before with MBL deposition on F-actins filaments<sup>22</sup>.

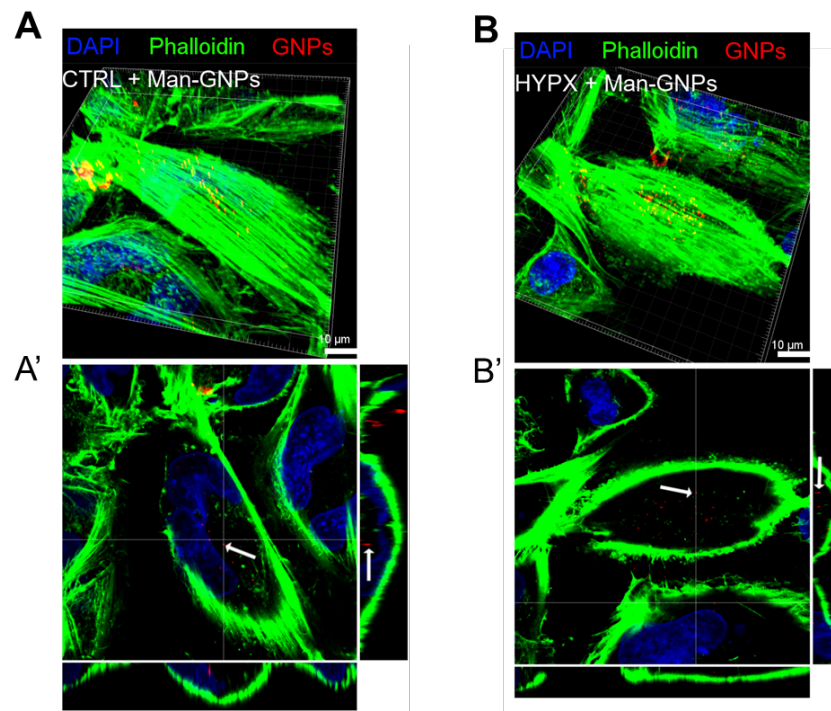


**Figure 34** Mannose-capped gold nanoparticles (Man-GNPs) were localized inside i-hBMECs with or without exposure of hypoxia.

Normoxic (CTRL) or hypoxic (HYPX) i-hBMECs undergone re-oxygenation in the presence of 40  $\mu\text{g}/\text{mL}$  Man-GNPs in 30% HS were analysed by reflectance confocal microscopy for Man-GNPs localization. 3D confocal images show Man-GNPs (red, reflectance microscopy) were clustering on regular (CTRL, A) and distributed (HYPX, B) F-actin layer (phalloidin, green; nuclei are blue (DAPI), scale bar 10  $\mu\text{m}$ ). Man-GNPs were internalized in the cytoplasm of CTRL (A') and HYPX (B') i-hBMECs as pointed with arrows in xy plane and in z projection being within in the same focal plane as F-actin filaments (scale bar 10  $\mu\text{m}$ ).

F-actin filaments were identified on SIM images and quantified by recording their touching with superimposed grid (Figure 35A). Touching per filament in CTRL Man-GNPs-positive cells compared with CTRL Man-GNPs-negative cells did not differ significantly across groups (Figure 35B) and no correlation was found between the touching and Man-GNPs number per  $100\mu\text{m}^3$ .

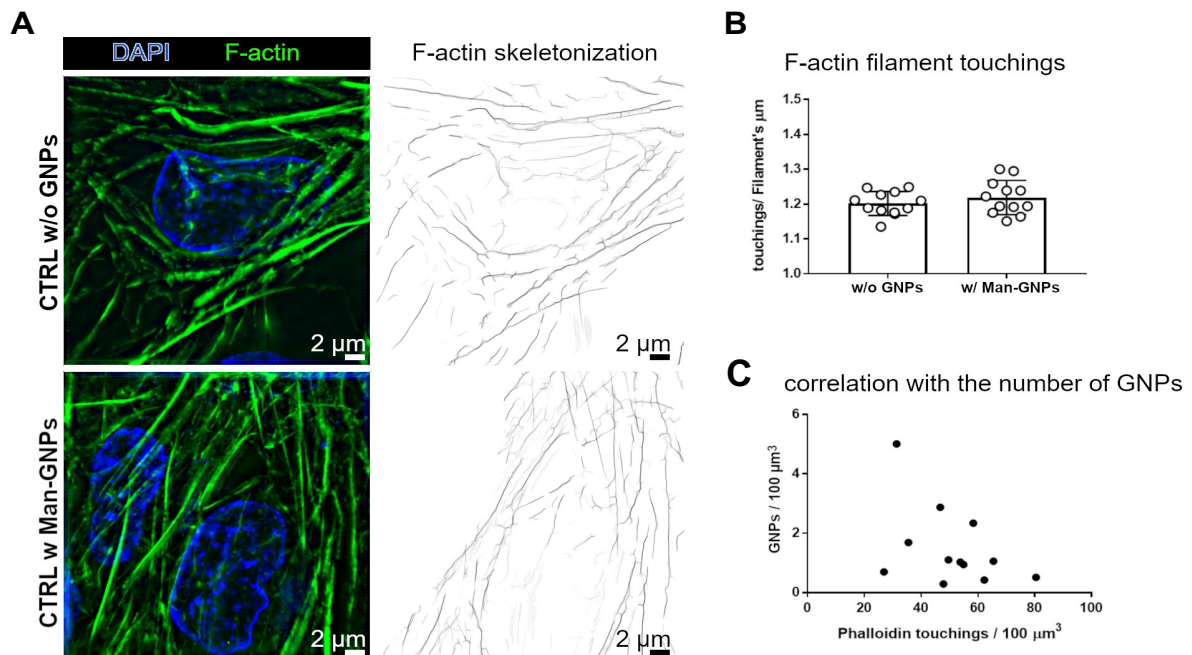


**Figure 35 Cytoskeletal organization of i-hBMECs was not altered in presence of Man-GNPs.**

Cytoskeletal structure of normoxic i-hBMECs treated with (w) or without (w/o) 40  $\mu\text{g}/\text{mL}$  Man-GNPs in presence of 30% HS were analysed by structured illumination microscopy (SIM). SIM images of F-actin (phalloidin, green; nuclei are blue (DAPI) were used to assess the F-actin skeletonization (scale bar 2  $\mu\text{m}$ ) (A). F-actin skeletonization and 1 mm-spaced grid were superimposed. Grid touching per F-actin filament did not vary upon GNP treatment (B). No correlation was found between grid touching and number of Man-GNPs per 100  $\mu\text{m}^3$  (C). Data are reported as mean with individual values  $\pm$  SD (n=12 cells from four wells per condition). Unpaired t test, ns.

These results are strongly suggesting that presence of high concentration of Man-GNPs (40  $\mu\text{g}/\text{mL}$ ) did not affect cell viability (Figure 31) and their internalization had not caused filament loss (Figure 32) as well not disorganized cytoskeleton (Figure 35).

### 3.3.2 Defining protective dose of sugar-GNPs

Proven toxic-free effect of sugar-GNPs, next it was investigated potential protective effect of sugar-GNPs. First possible protective outcome was measured to see if Man-GNPs can reduce inflammatory cascades activated by hypoxia. For that, different hypoxia related inflammatory genes expressed by i-hBMECs, were screened to understand if the hypoxic model presented in this study i.e., 16h of hypoxia and following 4h of reoxygenation is enough for the cells to express any of those inflammatory genes. Among eight different hypoxia related genes as shown in Figure 36, only *IL-1alfa*, *MMP-2* and *ICAM-1* were overexpressed by presence of hypoxia.

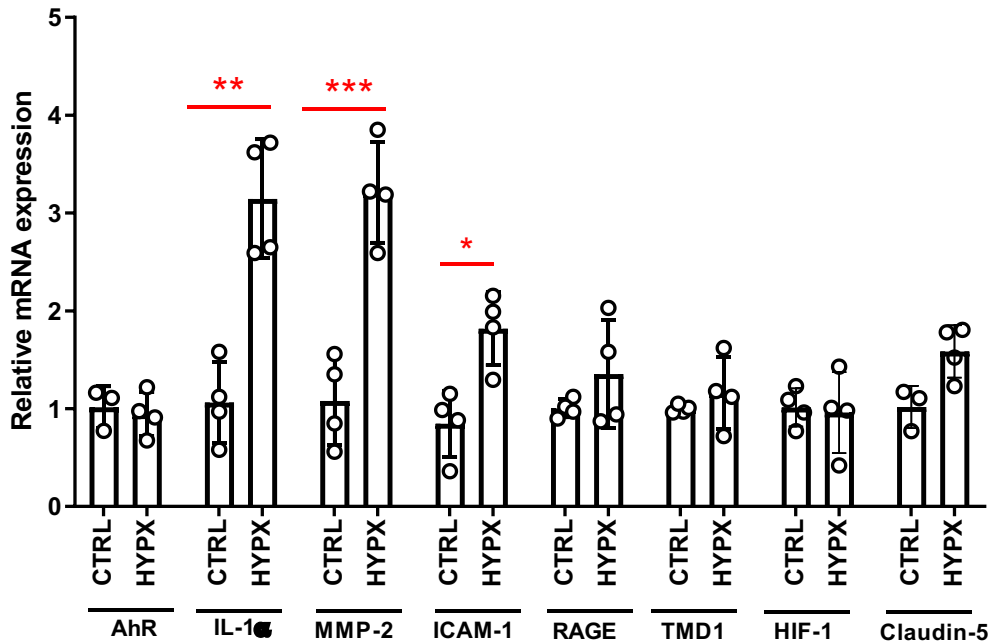


**Figure 36** Characterization of hypoxia-induced inflammatory genes in i-hBMECs after 4h of re-oxygenation in presence of 30% of human serum.

Hypoxic (HYPX) i-hBMECs overexpressed *IL-1 $\alpha$* , *MMP-2* and *ICAM-1* compared to normoxic (CTRL) cells. Data are reported as mean with individual values  $\pm$  SD (n= 4). Two-way ANOVA followed by Sidak's post hoc test for *AhR*, *MMP-2*, *ICAM-1*, *RAGE*, *TMD1*, *HIF-1*, *Claudin-5*, \*\*p<0.01, \*\*\*p<0.001 and Welch corrected t-test applied to *IL-1 $\alpha$* , being variances unequal per Bartlett's test, \*p<0.05, \*\*p<0.01.

Normoxic and hypoxic i-hBMECs treated in presence of Man-GNPs (5-20-40  $\mu$ g/mL) in 30% HS were examined for the gene expression of *ICAM-1*, *MMP-2* and *IL-1 $\alpha$*  (Figure 37). Data obtained from 3 independent experiments, it was showed that *ICAM-1* and *MMP-2* were significantly overexpressed by hypoxia (\*\*p<0.001) but *IL-1 $\alpha$*  was not affected. Only overexpression of *ICAM-1* was significantly (\*\*p<0.001) reduced in presence of 20  $\mu$ g/mL of Man-GNPs as it is reduced by 30% MBL-depleted HS. This is an important observation since MBL was reported to mediate *ICAM-1* overexpression. A partial rescue of the hypoxia-driven *MMP-2* overexpression was also observed with 20  $\mu$ g/mL of Man-GNPs, which showed similar expression levels as compared to the normoxic condition.

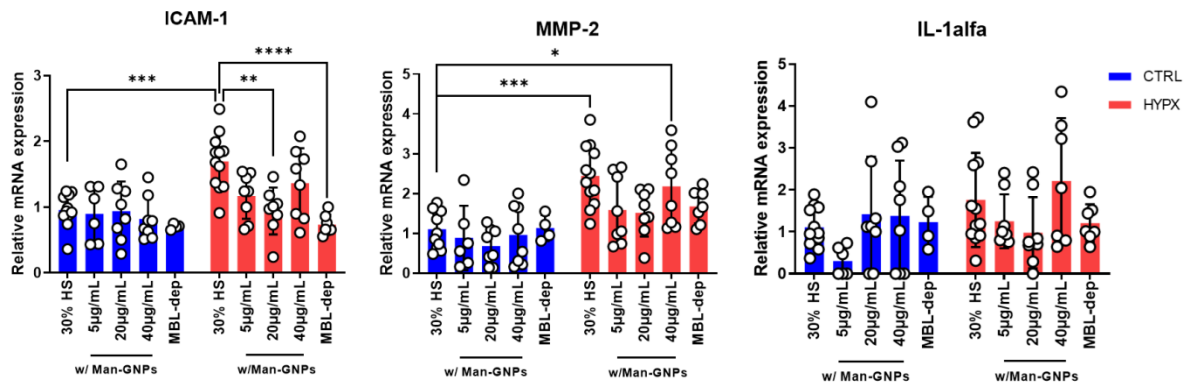


**Figure 37** Normoxic (CTRL) or hypoxic (HYPX) i-hBMECs undergone re-oxygenation in the presence of 5, 20 or 40 µg/mL Man-GNPs in 30% HS (w/Man-GNPs) and analysed for inflammatory gene expression.

Overexpression of ICAM-1 was significantly reduced when i-hBMECs were exposed to 20 µg/mL of Man-GNPs, to a similar extent than exposure to MBL depleted HS 30% (MBL-dep) and 40 µg/mL of Man-GNPs was effective to reduce overexpression of *MMP-2*. *IL-1alfa* expression was not significantly changed in presence of Man-GNPs with or without hypoxia. Data from 3 independent experiments are presented as mean with individual values ± SD (n= 4-12). Two-way ANOVA followed by Tukey's post hoc test, \*\*\*\*p<0.0001, \*\*\*p<0.001, \*\*p<0.01, \*p<0.05.

Consistently to *ICAM-1* result, Figure 38 shows increased MBL deposition on endothelium in the hypoxic i-hBMECs, while this deposition was decreased with a treatment of 5 and 20 µg/mL Man-GNPs.

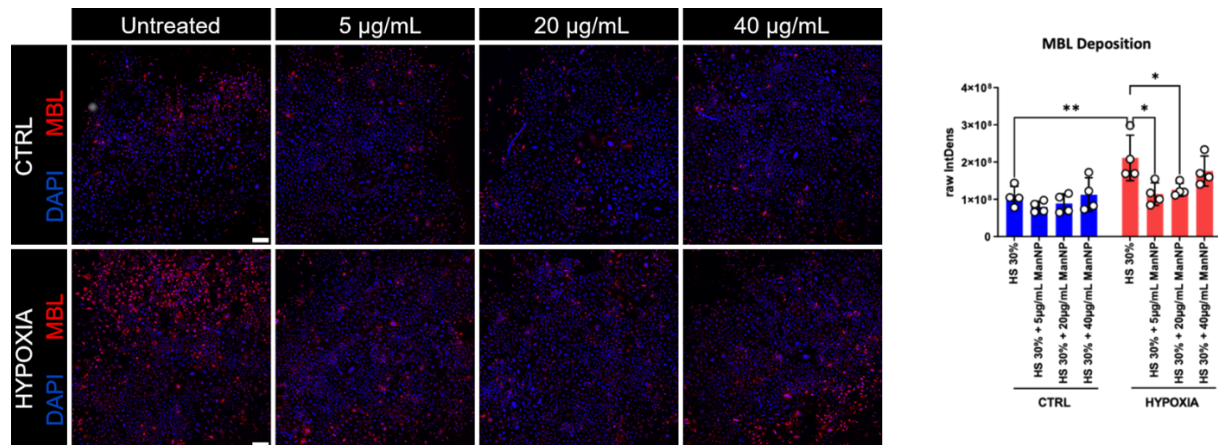


**Figure 38** MBL deposition was significantly increased on endothelium after hypoxia and this deposition was decreased with a re-oxygenation in the presence of 5 and 20 µg/mL Man-GNPs in 30% HS.

Normoxic (CTRL) or hypoxic (HYPX) i-hBMECs undergone re-oxygenation in the presence of 5, 20 or 40 µg/mL Man-GNPs in 30% HS (w/Man-GNPs) and analysed for MBL deposition on cell. MBL (red) deposition was greater on hypoxic than CTRL cells exposed to 30% HS, measured as fluorescence intensity. This increase on MBL deposition was significantly reduced when i-hBMECs were exposed to 5 and 20 µg/mL of Man-GNPs. Nuclei were stained with DAPI (blue). Scale bar is 200 µm. Data are reported as mean with individual values ± SD (n= 4). Two-way ANOVA followed by Tukey's post hoc test, \*\*p<0.001, \*p<0.05.

To understand if deposited MBL was linked to Man-GNPs, colocalization studies between MBL and Man-GNPs were carried out (Figure 39). Immuno-staining of MBL (red) was not merged with Man-GNPs which was acquired with reflectance confocal microscopy (white). This indicates that the scavenging of MBL by Man-GNPs seems to be played in the medium, as Man-GNPs did not bind MBL in the cells.

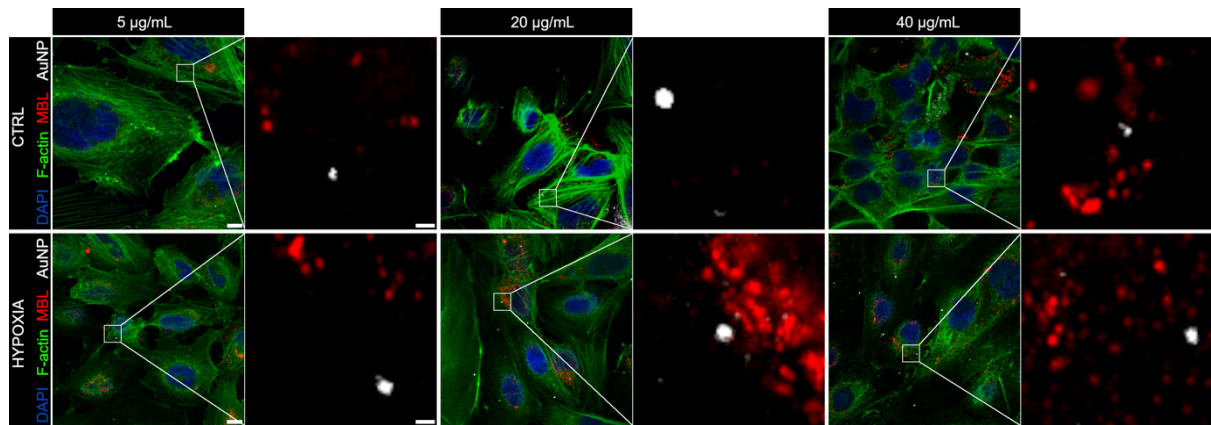


**Figure 39** No-colocalization was found between MBL and of 5, 20 or 40 µg/mL Man-GNPs on hypoxic and normoxic (CTRL) i-hBMECs.

Normoxic (CTRL) or hypoxic (HYPX) i-hBMECs undergone re-oxygenation in the presence of 5, 20 or 40 µg/mL Man-GNPs in 30% HS were analysed by reflectance confocal microscopy for Man-GNPs and MBL co-localization. Confocal images show Man-GNPs (white, reflectance microscopy) and hMBL (red) were depositing on F-actin layer (phalloidin, green; nuclei are blue (DAPI), scale bar 10 µm). Man-GNPs were not co-localized with hMBL (as seen in magnification of white frame, scale bar 1 µm).

Summarizing the data obtained in the in vitro model of ischemia/reperfusion, Man-GNPs were showed that they are not toxic to the cells with high concentrations (40 µg/ml). 20 µg/ml Man-GNPs significantly reduced the over-expression of inflammatory genes and MBL deposition on ischemic endothelium. The scavenging of MBL by Man-GNPs seems to be played in the medium, as Man-GNPs did not bind MBL in the cells.

## 3.4 In vivo ischemic mouse model

### 3.4.1.1 Introduction

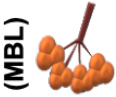
In vitro binding (3.1) and cell assay (3.3) were used to screen inhibition of either recombinant or endogenous human MBL isoform (hMBL) with sugar-GNPs. There are two main reasons to use hMBL; 1) to have better clinical translation of preclinical data, 2) evolutionary differences i.e., structural and functional differences between human and mouse MBL isoforms as explained in

Figure 40. Briefly, humans are carrying one isoform of MBL, while mice are expressing two isoforms (MBL-A and MBL-C)<sup>39,71</sup>. Human MBL isoform is encoded by different functional gene compare to mice<sup>85</sup>, showing only 59.92% with MBL-A and 60.25% with MBL-C similarity of amino acid sequences (available in Uniprot accession No. MBL-C: P41317, MBL-A: P39039, hMBL P11226). Additionally, these isoforms show different affinity to different sugars (see Table B of

Figure 40). Therefore, in vivo studies were carried out with a humanized mouse model which expresses human MBL [hMBL2 knock in (KI)] but does not express murine MBL isoforms (mMBL1<sup>-/-</sup>, mMBL2<sup>-/-</sup>), in order to prevent any alteration on sugar-GNPs inhibitions. First, hMBL KI mice were characterized as an in vivo ischemic model and then sugar-GNPs were screened for their protective functions after iv administration.



**Mannose Binding Lectin (MBL)**



**Table A**

MBL Isoforms		
Human Isoform	Mice Isoforms	Similarity%
hMBL	MBL-A	59.92%
	MBL-C	60.25%

**Table B**

MBL isoforms	Mannose ( $I_{50}$ , mM)	GlcNAc ( $I_{50}$ , mM)	Glucose ( $I_{50}$ , mM)
MBL-A	1.5	1.5	2
MBL-C	4	11	29
hMBL	14	16	63

**Figure 40 Evolutionary differences in MBL isoforms between rodents and humans.**

MBL shows different isoform between humans i.e., human MBL, hMBL and mice i.e., MBL-A and MBL-C with a 59.92% and 60.25% similarity of amino acid sequence respectively (Table A). These isoforms having different affinity to sugars as different concentration (mM) of monosaccharide required for 50% inhibition ( $I_{50}$ ) of MBL binding to Mannan (see reported in *Hansen et al., J Immunol 2000, Table B*).

### 3.4.2 Characterization of hMBL knock-in (KI) mice

Humanized mice only expressed hMBL, keeping all the physiological system unique for mice. This genetical modification is especially important for lectin pathway (LP) activation, since MBL requires a complex structural formation with MBL-associated serine proteases (MASP)—as its binding partner— to initiate LP. Therefore, WB analyses with non-reducing condition were run to investigate single and complex structure of MBL over blood samples collected 2d before and 90 min, 48 h after tMCAo. Figure 41 shows that hMBL had different oligomerizations (Figure 41A) and among these oligomerizations only trimers of trimers ( $3 \times \text{MBL}_3$ ) were slightly changed on a time depended manner (Figure 41B).

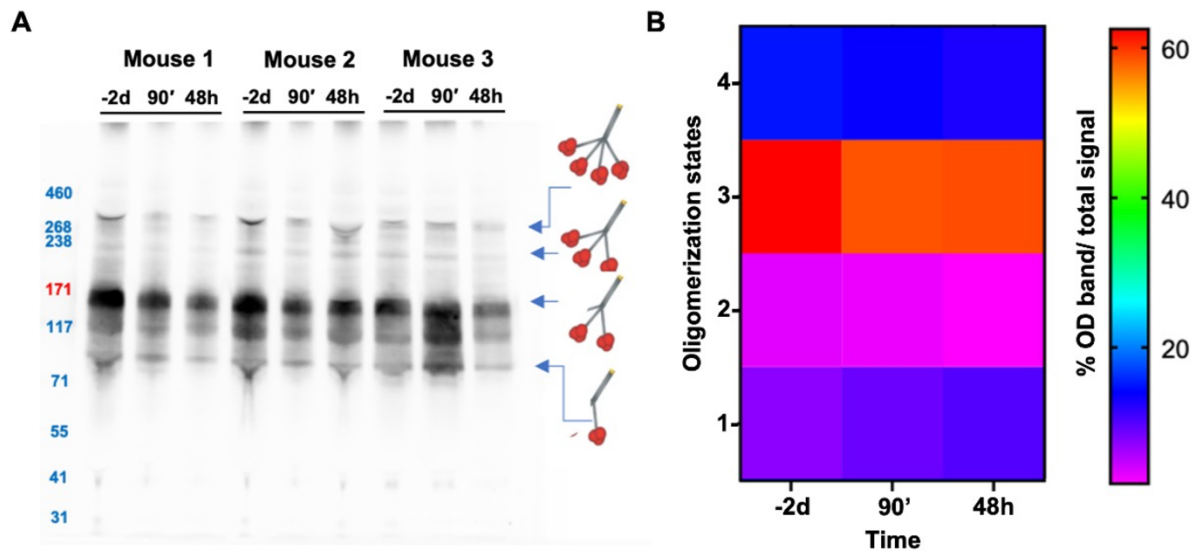


**Figure 41 Human MBL has little changes in oligomerization and was consumed after tMCAo**

Western blot analysis for MBL oligomerization was run in non-reducing condition over plasma samples of hMBL KI mice collected 2 days before (-2d) and 90 min (90') or 48h after tMCAo. hMBL expressed by ischemic hMBL KI mice showed four different oligomerization states, within major distinct band range of 77-308 kDa, with the 77 kDa representing trimers of structural monomers, each made up of three identical 25.5 kDa polypeptide chains monomer (A). Heat map analysis of these different oligomerization states of hMBL was performed by calculating the percentage of the OD band signal of each oligomerization state over the total signal for that sample (%OD band). The heat map presents the ratio of %OD band signals (scaled with colours) for each oligomerization state (see the numbers on the left side of the heat map; 1 is for the trimers ( $MBL_3$ ); 2 is for dimer of trimers ( $2 \times MBL_3$ ); 3 is for the trimer of trimers ( $3 \times MBL_3$ ); 4 is for the tetramers of trimers ( $4 \times MBL_3$ ) of three mice at the different time points (-2d, 90', 48h). The most represented state is  $3 \times MBL_3$ , higher than 60% at -2d, and decreasing thereafter.

Next, complex structure of human MBL with MASP as binding partner of MBL was investigated, since these partners were from two different species—MBL from human and MASP from mouse—and presence of their complex structure in plasma is fundamental for lectin pathway activation. There are three different MASP proteases (MASP-1, MASP-2, and MASP-3), but in this study, only MASP-2 was investigated due to its critical contribution to post-ischemic brain injury.<sup>86</sup> Therefore, a non-reducing western blot assay was carried out on hMBL and mouse MASP-2 (mMASP-2). Fluorescence signals from human MBL merge with mouse-MASP-2 (Figure 42) between 117-171 kDa. These results were especially important as they suggested that the human isoform of MBL was complexed with murine MASP-2, which is key for MBL-s function as a complement system activator.

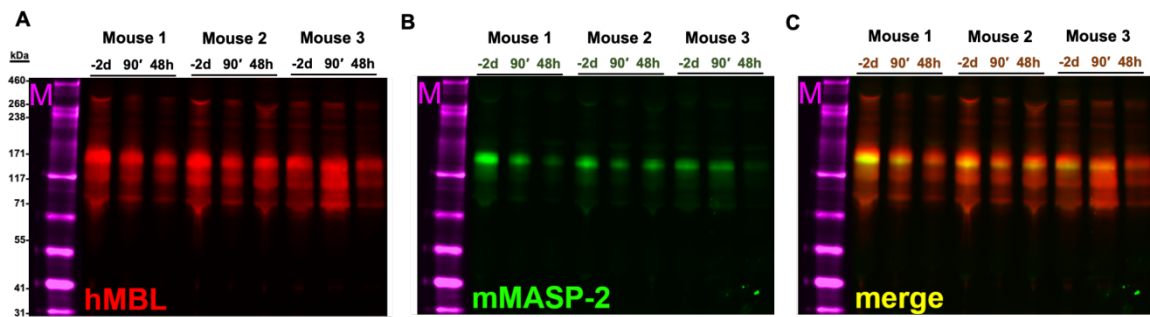


**Figure 42** hMBL expressed by hMBL KI mice was circulating with mMASP-2 after tMCAo.

Plasma sample of hMBL KI mice collected 2d before and 90 min (90'), 48h after tMCAo were used in non-reduced western blot analyses. hMBL stained with anti-hMBLaB (red, A) and mMASP-2 with (green, B) were merged (yellow, C) between 117 and 171 kDa.

Following characterization was performed for DAMPs exhibition on ischemic side of the brain (ipsilateral hemisphere) compared to healthy side (contralateral hemisphere). Exhibition of DAMPs on ischemic brain endothelium was already shown above in *in vitro* QCM studies with different lectins, via overexpression of sugars on ischemic glycocalyx. Among all the sugars, mannose shows highest affinity which makes it primary MBL target. Therefore, ipsi- and contralateral hemispheres of brain slices collected from wild and hMBL KI mice with 30 min of tMCAo, were stained with fluorescence ConA—plant lectin which has high affinity to mannose—to examine presence of mannose on DAMPs. Both mouse types were similarly overexpressed (mannose on ipsilateral hemisphere compared to contralateral hemisphere (Figure 43)).

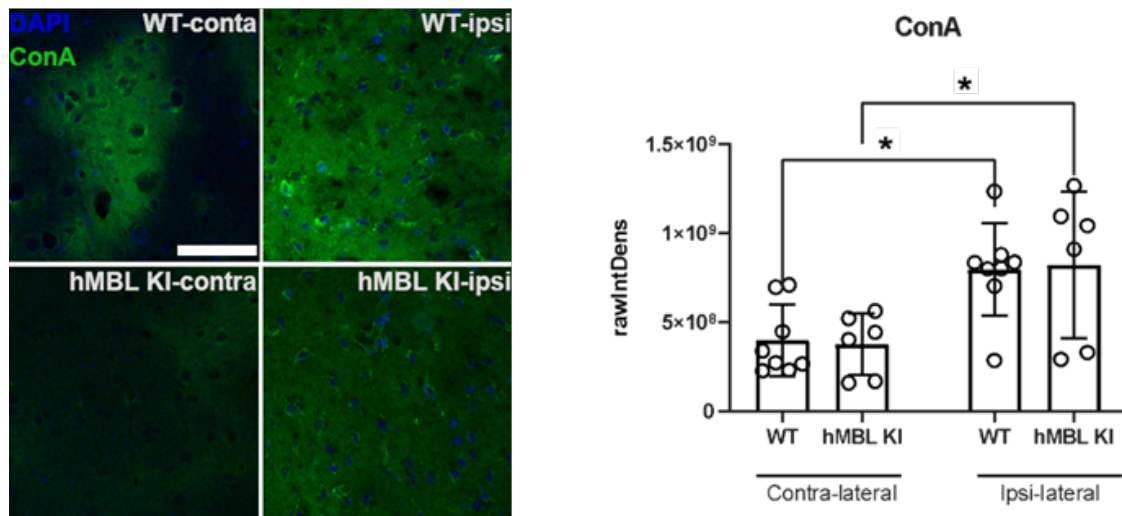


**Figure 43 Brain glycoalyx characterization via mannose staining with fluorescent ConA (ConA).**

ConA labelling (green) after 48 h of reperfusion was greater on ischemic ipsilateral cortex than healthy contralateral cortex (nuclei are blue (DAPI), scale bar 50  $\mu$ m) (A). ConA labelling was measured as fluorescence intensity (B). Data are reported as mean with individual values  $\pm$  SD (WT n=8, hMBL KI n=6). Two-way ANOVA followed by Sidak's post hoc test, \*p<0.05.

After finding overexpressed MBL target (i.e., mannose) in the ischemic part of the brain, it was next investigated whether MBL could be also detected in the ischemic brain of the humanized mouse model. It was assessed the presence of hMBL in hMBL KI mice with 30 min of tMCAo (Figure 44). hMBL was not detected on contralateral vessels (Figure 44B) but was detected on ipsilateral vessels of ischemic mice and deposited on the luminal side of the vessels after tMCAo (Figure 44A), as evidenced by single plane (Figure 44A') and three-dimensional images (Figure 44A''). Coronal sections of vessels were obtained by clipping the three-dimensional renderings (Figure 44A''') and further confirmed the intraluminal deposition of hMBL.

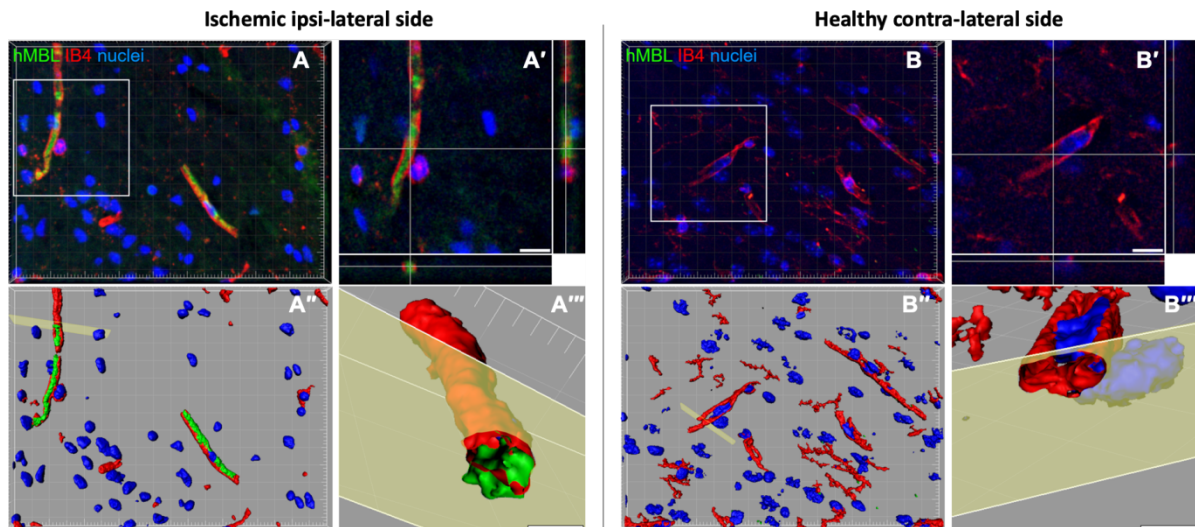


**Figure 44** hMBL targeted the brain vessels pertinent to the ischemic territory

Representative images for hMBL (green), vessels (IB4, red) and nuclei (Hoechst, blue) were stained on the brain sample of hMBL KI mice collected after 48h of tMCAo. hMBL was showed deposition on ischemic vessels of ipsi-lateral side (A). Single xy plane views with z projections of the white boxes in A confirmed that hMBL were located in the luminal space of vessels (A'). 3D renderings (A'') and clipped volumes (A''': clipping in correspondence of the yellow planes) further demonstrated intraluminal deposition of hMBL. No localization (B, B') and intraluminal deposition (B'', B''') detected on the vessels of healthy contra-lateral side. Confocal analysis, scale bar 20  $\mu\text{m}$  (A, B) and 5  $\mu\text{m}$  (A', B').

After structural convenience of the hMBL KI model, its role on lectin pathway (LP) activation was investigated. LP activation encompasses tight sequential activation of complement cascades through the cleavage of the complement component C3, which releases the complement C3a and C3b fragments. These fragments possess pro-inflammatory properties<sup>86</sup>. Therefore, role of MBL on complements pathway activation was tested in mouse plasma (pools from 5 mice belonging to the same experimental group) using an *in vitro* assay<sup>71,87</sup> with mannan-coated plates, through the presence of C3b complement fragments. Both wild type and hMBL KI mice followed similar pattern of lectin activation i.e., reduction 90min and increased 48h after tMCAo compared to plasma samples collected 2d before tMCAo (Figure 45).

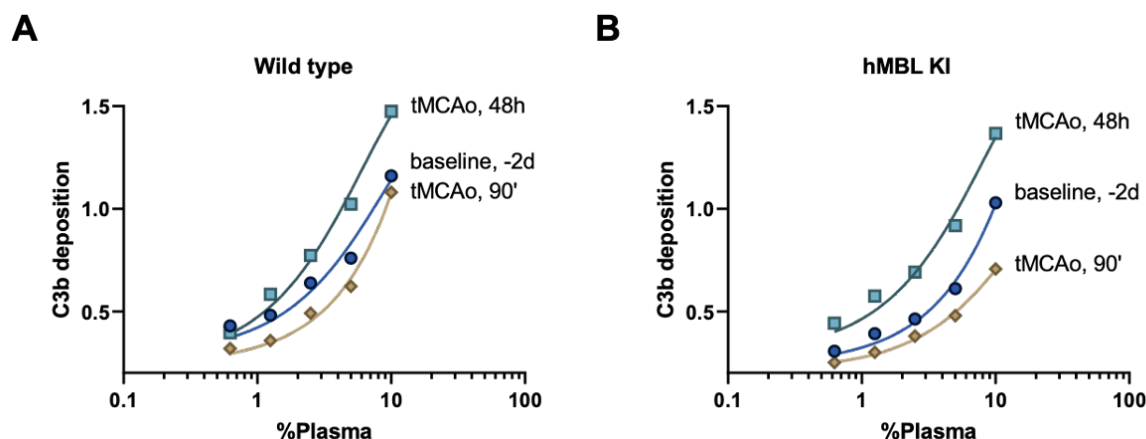


**Figure 45** Systemic activation of the complement system after 48h, 90' and 2d of tMCAo in wild and hMBL KI mice.

LP activity assay was carried out on mannan-coated plate measuring C3b deposition over plasma of mice belonging to the same ischemic experimental group. The in vitro assay for LP activation on mannans showed similar activation in plasma from wild (A) and hMBL KI (B) mice. The data refer to pools of plasma from 5 mice per group, and plasma concentrations are reported on a logarithmic scale.

### 3.4.3 In vivo protective effect Man-GNPs on the ischemic mouse model

Characterized hMBL KI mice for ischemic model, was used for screening inhibitory effect of sugar-GNPs in pathological condition. Since 20  $\mu\text{g/mL}$  concentration of Man-GNPs showed the most protective effect (reducing inflammation and MBL deposition after hypoxia) in vitro, hMBL KI mice was treated with 20  $\mu\text{g/mL}$  of Man-GNPs 3h after tMCAo. Same treatment applied for the control group with Glc-GNPs. Each mouse was rated on neurologic function scales by examining their behavioral deficits. 48h after the tMCAo mice were examined by sensorimotor deficits (neuroscore) as the primary outcome (Figure 10C). To measure long-term anxiety level of mice, EPM analyses were carried out 8d after tMCAo to avoid possible anxiety interference due to blood withdrawer at day 7. No differences on neuroscore (Figure 46A) and EPM (Figure 46B) analyses were detected between Man- or Glc-GNPs treated mice, which would be acute pharmacokinetic loss of the nanoparticles in liver<sup>88</sup>. However further understanding and analyses are required to enlighten this argument.

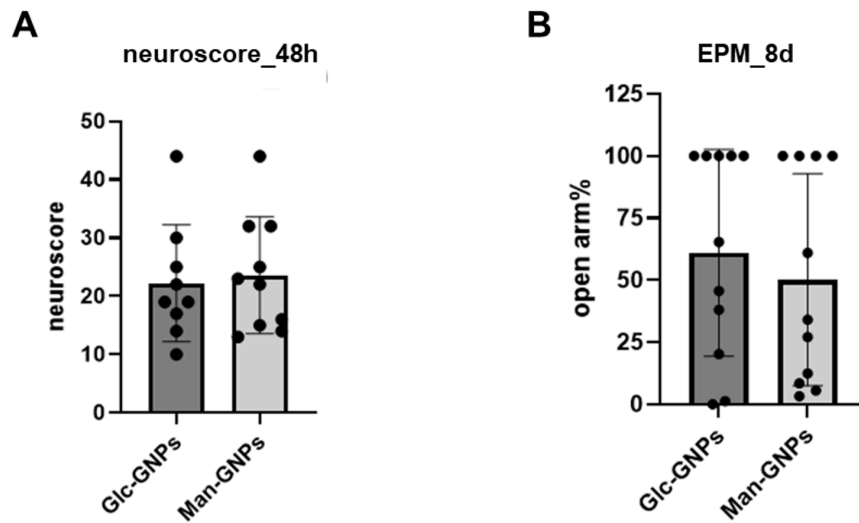


**Figure 46** Evaluation of behavioural deficits, neuroscore after 48 h and EPM after 8d of reperfusion in hMBL KI mice with a treatment of sugar-GNPs (20 µg/mL).

No effect of treatment with Man-GNPs was observed over mice treated with Glc-GNPs. Neuroscore (A) and EPM (B) evaluations were not changed significantly between the groups. All mice meeting inclusion criteria (intraischemic deficits) were included. If sacrificed for humane endpoint, they were given the worst behavioral score. The data are shown as bars + SDs (n = 9 for Glc-GNPs treatment, n = 10 for Man-GNPs); 1:1 gender ratio, unpaired t-test, ns.

## Chapter 4 : Discussion

---

In this thesis, a pipeline for pre-clinical screening of hMBL inhibitors, which includes *in vitro* binding and cell assays up to *in vivo* studies, was developed and characterized.

The new SPR-based assay was designed to mimic the endothelium-exposed DAMPs (carbohydrate patterns) exposed to flowing (circulating) MBL, with the aim to screen compounds inhibiting the MBL-DAMPs binding. Among the putative inhibitors, mannose-coated nanoparticles (Man-GNPs) were identified as the most promising candidate, due to their strong binding to hMBL, also present properties in sera. In order to assess the potential toxic and protective effects of Man-GNPs, studies were carried out in a model of ischemic immortalized human brain microvascular endothelial cells (i-hBMECs).

As last, neuroprotective effect of Man-GNPs were screened *in vivo* in a humanized mice model of ischemic stroke.

*In vitro* binding studies with SPR were first aimed to prepare the surface mimicking the mannosylated pattern of DAMPs and showing optimal MBL binding properties, to be used subsequently to screen MBL inhibitors. For this, Man-linker-SH molecules were selected, to form a self-assembled monolayer (SAM) between the bare gold surface of the chip and thiol group<sup>74,89</sup>. At first, it was tried to prepare the monolayer inside the instrument, i.e., flowing the molecule within the microfluidic channels. This protocol would have had important advantages: to control the amount of immobilized molecule by measuring the SPR signal in real time and to immobilize different SH-molecules in each parallel strip of the same sensor chip. Unfortunately, this approach was not successful, because the exposure of the bare gold to the flowing molecules was too short to saturate the whole surface, so leaving a significant proportion of unfunctionalized gold (a problem for the following injections of MBL). This is consistent with literature data<sup>90-92</sup>, indicating that the formation of well-organized and complete SAM requires exposure of the chip to the solution for hours, which was not feasible, since the flowing solution could not be recycled and therefore an excessive amount of material would have been required.

Therefore, in order to allow longer-lasting exposure of the chip to the molecule, surface functionalization was carried out outside the SPR instrument. Moreover, a method for efficient and complete cleaning/regeneration of a previously used chip was also developed, allowing multiple uses. This was accomplished by sequential cleaning with piranha solution followed by UV exposure<sup>93</sup>. While several studies<sup>90,94,95</sup> have used piranha solution for chip cleaning, no data was found in literature that combines this process with UV exposure. The latter step is likely to convert the alkyl



thiolates to water-soluble alkyl sulfonates, that can be removed from the surface thorough washing<sup>93</sup>, thus allowing a more efficient removal of the sulfur contamination. It was also demonstrated that this cleaning/regeneration method achieves complete removal of the immobilized SH-glycopolymer, while maintaining the surface properties for subsequent functionalization, hence very good reproducibility after different regeneration/functionalization steps. This protocol can be applied to different SH-ligands and therefore it might be useful in different research areas.

The best MBL-capturing molecule was found as Man-EG<sub>6</sub>C<sub>11</sub>S, because MBL bound in a concentration-dependent manner with a high, nanomolar affinity and the binding was specific to MBL since no binding was observed with other lectins with different sugar selectivity<sup>39</sup>. This high-affinity binding suggests a multivalent interaction, i.e., each MBL molecule binds through its different CRD domains to different mannose residues on the chip<sup>15</sup>.

This novel method also proved able to measure native MBL in human serum, which is a very important feature not accomplished with our previous approach<sup>33</sup>. Since human serum gives quite a high non-specific signal, a second injection with an anti-MBL antibody was required to specifically recognize the serum MBL captured during the first injection.

Next, the SPR assay was exploited for screening MBL inhibitors. It is important here to highlight that SPR overcome the disadvantages of other assays carried out at equilibrium (e.g. mannan immunoassay)<sup>39</sup>. With these latter assays, the long incubation of MBL-containing solution in sugar-coated microtiter wells may reduce the binding between the inhibitor and MBL, due to the equilibrium shift induced by the high-affinity binding of free MBL to immobilized sugars. This potential artifact, leading to underestimation of the compound's inhibitory effect, is minimized during the very short flow of plasma over the mannose-coated SPR surface. Another worthwhile advantage of the SPR assay is that it does not need any labeled reagent and uses less antibody than for microtiter wells.

With the SPR approach, monomeric mannose inhibited MBL binding to immobilized sugars with an IC<sub>50</sub> in the mM range, as expected<sup>96,97</sup>. A new oligo-mannose glycan was also tested which had three times higher inhibitory potency than monomeric mannose presumably because of the multivalency effect. Finally, new sugar-NPs, i.e., Mannose-EG<sub>6</sub>C<sub>11</sub>S-coated GNPs (Man-GNPs) and Glucose-EG<sub>6</sub>C<sub>11</sub>S-coated GNPs (Glc-GNPs) were developed, and within them Man-GNPs proved to be extremely potent with a potency of at least 2–3 orders of magnitude higher than monomeric mannose, presumably a result of the multivalence effect provided by the Man-GNPs<sup>3,98</sup>. As expected, Glc-EG<sub>6</sub>C<sub>11</sub>S-coated GNPs (Glc-GNPs)—control group of the experiment since MBL shows low affinity to glucose<sup>39</sup>—had much less potency (> 25-fold).

Then, the binding of Man-GNPs to endogenous (native) hMBL was evaluated even in human serum. In fact, endogenous MBL shows a higher degree of oligomerization (from  $3 \times \text{MBL}_3$  to  $5 \times \text{MBL}_3$ ) in comparison to rhMBL (from MBL to  $\text{MBL}_3$ ). This might allow native MBL to have more carbohydrate binding domains that could increase the binding affinity to Man-GNPs. Indeed, endogenous hMBL showed a strong binding to Man-GNPs (hard corona) but not to Glc-GNPs. Consistently, SPR studies showed that Man-GNPs (6.5  $\mu\text{g/mL}$ ) was effective in inhibiting the binding of serum MBL to mannosylated sensor surface.

These *in vitro* results indicated Man-GNPs as a promising MBL inhibitor and therefore following studies in the pipeline were planned to confirm its potential protective properties in cells model of ischemia. For this, immortalized human brain microvascular endothelial cells (i-hBMECs) were exposed to hypoxia<sup>22</sup> which, according to previous data, show an increased deposition of MBL. Even though these data indicate a hypoxia-induced alteration of glycocalyx, there were no data on the sugars involved. This was addressed here by using the QCM technology, allowing to study cells on-a-chip biosensor. In particular two different approaches were used, i.e., capturing cells on the chip by immobilized PHAL lectins, or directly growing cells on the chip. The latter was more complicated, but it showed higher binding of lectins, suggesting that monolayer formation of cells provide better binding surface for lectins. Hypoxia induced an increased binding of all lectins, including wheat germ agglutinin and concavalin A, which bind mannose and N-acetylglucosamine respectively, i.e., the same target of MBL.

The next step of the pipeline was focused at evaluating of Man-GNPs in preventing the hypoxia-induced effects on i-hBMECs. At first, it was evaluated if the sugar-GNPs, with or without hypoxia, were toxic to the cells. For this, 1.5 times more of highest concentration (25  $\mu\text{g/mL}$ ) of *in vitro* SPR binding studies was chosen, considering further *in vivo* mouse studies where the total blood volume of a mouse is 1.5-2 times more than total blood volume of a human.

Cell viability was measured with cell counting since other techniques<sup>22,99</sup> requires fluorometric readings which would interfere with quenching effect of gold nanoparticles<sup>100</sup>. No significant cytotoxic effect of sugar-GNPs were observed with this method. Further analyses were carried out by measuring F-actin layer density, which was reduced by hypoxia as expected<sup>22</sup>. With this approach too, no effect of sugar-GNPs was observed. The localization of sugar-GNPs on i-hBMECs was investigated by reflectance confocal microscopy (RCM) as a label-free imaging technique since labeling nanoparticles with fluorescent dyes<sup>101-103</sup> may affect their physicochemical properties and subsequent *in vivo* behavior<sup>88,104</sup>. Additionally, photobleaching effect of metallic surface of sugar-GNPs creates problem on detection of fluorescent signals<sup>104,105</sup>. Sugar-GNPs were detected in normoxic and hypoxic cell soma with no toxicity. While the exact mechanisms of sugar-GNPs

internalization is not known, it can be speculated that nanoparticles may be taken by endocytosis<sup>106</sup> or by recognizing molecules on cell surfaces such as the glucose transporter, Glut-1<sup>107</sup> for Glc-GNPs.

In summary, sugar-GNPs did not show any toxicity. So next, they were tested for their efficacy, starting from their effect on hypoxia-induced over-expression of the inflammatory genes *MMP-2*, *IL-1alfa* and *ICAM-1*. Among these genes, over-expression of *ICAM-1* was significantly reduced with the treatment of 20 µg/mL Man-GNPs, which is especially important because *ICAM-1* is a transmembrane protein expressed by activated endothelial cells and is involved in the recruitment of inflammatory cells to the injured brain e.g. facilitates leukocyte endothelial transmigration<sup>108</sup>. Indeed the connection of *ICAM-1* and MBL was shown before in vivo as *ICAM-1* expression is downstream to the MBL deposition on ischemic endothelium<sup>70</sup>. The results obtained with the cellular model of hypoxic i-hBMECs for MBL deposition on ischemic endothelium are consistent with the in vivo results, thus supporting the specificity of the inhibitory effects of 20 µg/mL Man-GNPs on MBL-driven pathological mechanisms on the ischemic endothelium. However, no inhibitory effect of Man-GNPs was observed at the highest dose tested here (40 µg/mL). It may be speculated that this was due to aggregation of the nanoparticles at this concentration, thus lowering their available functionalized surface to MBL binding.

To clarify if Man-GNPs may target MBL in the cells, co-localization studies were carried out. The binding of Man-GNPs to MBL, and thus the above-mentioned effects due to MBL scavenging, are likely to occur in the extracellular space, since no co-localization of the two was observed at the intracellular level. To validate our co-localization studies, the quenching effects of gold nanoparticles were not be taking into account which could hide the signal of MBL. Because the distance between the fluorophore which conjugated to the secondary antibody for detecting MBL and the GNP, exceeds the maximum radius of gold-driven quenching.

The last part of the project was aimed at evaluating if the promising properties of Man-GNPs, highlighted by in vitro binding studies and by functional cell assays, are maintained in vivo. For this, a mouse model of ischemia, induced by transient (30 min) occlusion of the medial cerebral artery (tMCAo) followed by reperfusion was used. Furthermore, a hMBL KI mouse model was used, for the first time, under brain ischemic conditions, and this required a preliminary characterization. It was found that hMBL showed a similar oligomerization before and after tMCAo, which is important for more reliable translation of the results since in vitro affinity studies of Man-GNPs were carried on serum samples collected from healthy donors. Indeed, hMBL oligomerization states may alter the availability of their carbohydrate binding sites to the Man-GNPs. Moreover, it was confirmed that circulating hMBL is actually associated with MASP-2—mannose-binding lectin-associated serine protease-2, the first enzymatic component for the lectin pathway of complement activation<sup>109,110</sup> —

<sup>26,111</sup> Moreover, it was confirmed that ischemia induces, in the brain vessel endothelium of these mice, the exposure of mannose-containing DAMPs (as observed with fluorescent ConA) and the deposition of MBL, with activation of the LP pathway (as observed by measuring C3b 48h post-ischemia).

After the characterization of the hMBL KI mouse model of ischemia, that confirmed the relevance of MBL and the lectin pathway in the ischemic stroke model, it was evaluated if the consequences of ischemia could be prevented by Man-GNPs, administered iv to have plasma concentrations of 20 µg/mL, 3h after reperfusion. Unfortunately, no improvement was observed in the animals treated with Man-GNPs as regards to the ischemia-induced sensorimotor deficits, in comparison with animals treated with Glc-GNPs (not binding to MBL). The lack of efficacy could be due to a very rapid removal of Man-GNPs from the circulation, i.e. for a very fast elimination and/or accumulation in organs <sup>88,112,113</sup> i.e. liver, kidney, spleen. In this regard unpublished observations from the NanoCarb network showed a quick liver accumulation of the GNPs after systemic injection, which may limit their bioavailability in blood. Further pharmacokinetic studies are needed to clarify this point.

## Chapter 5 : Conclusion

---

The studies reported in this thesis describe the development, characterization and exploitation of a stepwise, comprehensive pre-clinical pipeline for the identification of inhibitors of MBL, as potential drugs to ameliorate brain injury after ischemic stroke. Pipeline starts from binding studies between the drug and its molecular target by a novel SPR-based biosensor, allowing to determine the affinity constants. This original SPR method can be also easily applied in different research areas by using different tailored SH-linkers, and allows reproducible and affordable assays. The most interesting MBL ligand/inhibitor identified with SPR is a mannosylated nanoparticle, so that studies on the formation of protein corona on nanoparticles surface were added in the pipeline. Additionally, our results confirmed the importance of using endogenous (native) form of proteins, since the recombinant form might show significant structural differences, as found in our studies with MBL. The following step in the pipeline involved studies in cells, and for them it is crucial to select correct cell lines and disease models. In our study, human brain microvascular endothelial cells exposed to hypoxia were used to study alterations of brain vessels induced by ischemia, and in particular to study the molecular features underlying the deposition of MBL to damage-associated mannosylated patterns. For that, an original cell-on-a-chip QCM binding assay was developed and exploited. Moreover, the same cells can be – and were - exploited to test the most promising MBL inhibitors, to evaluate their intrinsic toxicity and their protective efficacy. These studies indeed confirmed the promising properties of an MBL inhibitor, and so its neuroprotective properties can be evaluated in the most expensive and time-consuming *in vivo* preclinical studies. In order to have more relevant results for clinical translation, here for the first time a new mouse model of stroke were characterized, that is a mouse expressing the human form of MBL only, exposed to a transient occlusion of the cerebral artery. This model can be then exploited to screen new potential drugs, as it was done in this thesis with the mannosylated nanoparticles.

In conclusion, not only the work of this thesis allowed to develop an original pre-clinical pipeline for drug discovery, but also applied it to test a new neuroprotective therapeutic strategy, based on sugar-coated nanoparticles, for a still unmet medical need, i.e., the injury caused by brain ischemia.

## Chapter 6 : References

1. Varki, A. Biological roles of glycans. *Glycobiology* **27**, 3–49 (2017).
2. Ramachandraiah, G., Chandra, N. R., Surolia, A. & Vijayan, M. Computational analysis of multivalency in lectins: structures of garlic lectin–oligosaccharide complexes and their aggregates. *Glycobiology* **13**, 765–775 (2003).
3. Becer, C. R. The Glycopolymer Code: Synthesis of Glycopolymers and Multivalent Carbohydrate–Lectin Interactions. *Macromol. Rapid Commun.* **33**, 742–752 (2012).
4. Müller, C., Despras, G. & Lindhorst, T. Organizing multivalency in carbohydrate recognition. *Chem. Soc. Rev.* **45**, 3275–3302 (2016).
5. Sharon, N. & Lis, H. Microbial lectins and their glycoprotein receptors. *New Compr. Biochem.* **29**, 475–506 (1997).
6. Kotecha, H. & Poduval, P. B. Chapter 9 - Microbial lectins: Roles and applications. in *Advances in Biological Science Research* (eds. Meena, S. N. & Naik, M. M.) 135–147 (Academic Press, 2019). doi:10.1016/B978-0-12-817497-5.00009-4.
7. Nizet, V., Varki, A. & Aebi, M. 37 Microbial Lectins: Hemagglutinins, Adhesins, and Toxins. 12.
8. De Hoff, P. L., Brill, L. M. & Hirsch, A. M. Plant lectins: the ties that bind in root symbiosis and plant defense. *Mol. Genet. Genomics* **282**, 1–15 (2009).
9. Pryme, I. F. & Aarra, T. M. Exhaustive Overview of Dietary Plant Lectins: Prospective Importance in the Mediterranean Diet. *Am. J. Biomed. Sci. Res.* **13**, 339 (2021).
10. Lannoo, N. & Van Damme, E. J. M. Lectin domains at the frontiers of plant defense. *Front. Plant Sci.* **5**, (2014).
11. Manikandan, S. B. An overview on human serum lectins. 25 (2020).

12. Lepenies, B. & Lang, R. Editorial: Lectins and Their Ligands in Shaping Immune Responses. *Front. Immunol.* **10**, (2019).
13. Mason, C. P. & Tarr, A. W. Human Lectins and Their Roles in Viral Infections. *Molecules* **20**, 2229–2271 (2015).
14. Raposo, C. D., Canelas, A. B. & Barros, M. T. Human Lectins, Their Carbohydrate Affinities and Where to Find Them. *Biomolecules* **11**, 188 (2021).
15. Eddie Ip, W. K., Takahashi, K., Alan Ezekowitz, R. & Stuart, L. M. Mannose-binding lectin and innate immunity. *Immunol. Rev.* **230**, 9–21 (2009).
16. Ricklin, D., Hajishengallis, G., Yang, K. & Lambris, J. D. Complement - a key system for immune surveillance and homeostasis. *Nat. Immunol.* **11**, 785–797 (2010).
17. Ricklin, D., Reis, E. S. & Lambris, J. D. Complement in disease: a defence system turning offensive. *Nat. Rev. Nephrol.* **12**, 383–401 (2016).
18. Mn, B., V, P., K, T. & Gl, S. Myocardial ischemia and reperfusion injury is dependent on both IgM and mannose-binding lectin. *Am. J. Physiol. Heart Circ. Physiol.* **297**, H1853-9 (2009).
19. Walsh, M. C. *et al.* Mannose-Binding Lectin Is a Regulator of Inflammation That Accompanies Myocardial Ischemia and Reperfusion Injury. *J. Immunol.* **175**, 541–546 (2005).
20. de Vries, B. *et al.* The mannose-binding lectin-pathway is involved in complement activation in the course of renal ischemia-reperfusion injury. *Am. J. Pathol.* **165**, 1677–1688 (2004).
21. Hart, M. L. *et al.* Gastrointestinal Ischemia-Reperfusion Injury Is Lectin Complement Pathway Dependent without Involving C1q. *J. Immunol.* **174**, 6373–6380 (2005).
22. Neglia, L. *et al.* Mannose-binding lectin has a direct deleterious effect on ischemic brain microvascular endothelial cells. *J. Cereb. Blood Flow Metab.* **40**, 1608–1620 (2020).
23. Orsini, F. *et al.* Targeting Mannose-Binding Lectin Confers Long-Lasting Protection With a Surprisingly Wide Therapeutic Window in Cerebral Ischemia. *Circulation* **126**, 1484–1494 (2012).

24. De Blasio, D. *et al.* Pharmacological inhibition of mannose-binding lectin ameliorates neurobehavioral dysfunction following experimental traumatic brain injury. *J. Cereb. Blood Flow Metab.* **37**, 938–950 (2017).
25. Longhi, L. *et al.* Mannose-binding lectin is expressed after clinical and experimental traumatic brain injury and its deletion is protective. *Crit. Care Med.* **42**, 1910–1918 (2014).
26. Fumagalli, S. & De Simoni, M.-G. Lectin Complement Pathway and Its Bloody Interactions in Brain Ischemia. *Stroke* **47**, 3067–3073 (2016).
27. Johnson, W., Onuma, O., Owolabi, M. & Sachdev, S. Stroke: a global response is needed. *Bull. World Health Organ.* **94**, 634-634A (2016).
28. Feigin, V. L. *et al.* World Stroke Organization (WSO): Global Stroke Fact Sheet 2022. *Int. J. Stroke* **17**, 18–29 (2022).
29. Abdu, H., Tadese, F. & Seyoum, G. Comparison of Ischemic and Hemorrhagic Stroke in the Medical Ward of Dessie Referral Hospital, Northeast Ethiopia: A Retrospective Study. *Neurol. Res. Int.* **2021**, 1–9 (2021).
30. Kleindorfer, D. O. *et al.* 2021 Guideline for the Prevention of Stroke in Patients With Stroke and Transient Ischemic Attack: A Guideline From the American Heart Association/American Stroke Association. *Stroke* **52**, e364–e467 (2021).
31. Aguiar de Sousa, D. *et al.* Access to and delivery of acute ischaemic stroke treatments: A survey of national scientific societies and stroke experts in 44 European countries. *Eur. Stroke J.* **4**, 13–28 (2019).
32. Gjelstrup, L. C. *et al.* The Role of Nanometer-Scaled Ligand Patterns in Polyvalent Binding by Large Mannan-Binding Lectin Oligomers. *J. Immunol.* **188**, 1292–1306 (2012).
33. Stravalaci, M. *et al.* A New Surface Plasmon Resonance Assay for In Vitro Screening of Mannose-Binding Lectin Inhibitors. *J. Biomol. Screen.* **21**, 749–757 (2016).



34. Soares, S., Sousa, J., Pais, A. & Vitorino, C. Nanomedicine: Principles, Properties, and Regulatory Issues. *Front. Chem.* **6**, (2018).
35. Choi, Y. H. & Han, H.-K. Nanomedicines: current status and future perspectives in aspect of drug delivery and pharmacokinetics. *J. Pharm. Investig.* **48**, 43–60 (2018).
36. Jain, K. K. Nanomedicine: Application of Nanobiotechnology in Medical Practice. *Med. Princ. Pract.* **17**, 89–101 (2008).
37. Pelaz, B. *et al.* Diverse Applications of Nanomedicine. *ACS Nano* **11**, 2313–2381 (2017).
38. Erol, G. *et al.* New nanostructures inhibiting human mannose binding lectin identified by a novel surface plasmon resonance assay. *Sens. Actuators B Chem.* **360**, 131661 (2022).
39. Hansen, S., Thiel, S., Willis, A., Holmskov, U. & Jensenius, J. C. Purification and Characterization of Two Mannan-Binding Lectins from Mouse Serum. *J. Immunol.* **164**, 2610–2618 (2000).
40. Pavlov, V. I. *et al.* Human Mannose-Binding Lectin Inhibitor Prevents Myocardial Injury and Arterial Thrombogenesis in a Novel Animal Model. *Am. J. Pathol.* **185**, 347–355 (2015).
41. Rich, R. L. & Myszka, D. G. Higher-throughput, label-free, real-time molecular interaction analysis. *Anal. Biochem.* **361**, 1–6 (2007).
42. Canovi, M. *et al.* Applications of Surface Plasmon Resonance (SPR) for the Characterization of Nanoparticles Developed for Biomedical Purposes. *Sensors* **12**, 16420–16432 (2012).
43. Beeg, M., Diomede, L., Stravalaci, M., Salmona, M. & Gobbi, M. Novel approaches for studying amyloidogenic peptides/proteins. *Curr. Opin. Pharmacol.* **13**, 797–801 (2013).
44. Šípová, H. & Homola, J. Surface plasmon resonance sensing of nucleic acids: A review. *Anal. Chim. Acta* **773**, 9–23 (2013).
45. Beeg, M. *et al.* A Surface Plasmon Resonance-based assay to measure serum concentrations of therapeutic antibodies and anti-drug antibodies. *Sci. Rep.* **9**, (2019).

46. Castellano, G. *et al.* Therapeutic targeting of classical and lectin pathways of complement protects from ischemia-reperfusion-induced renal damage. *Am. J. Pathol.* **176**, 1648–1659 (2010).
47. Møller-Kristensen, M. *et al.* Mannan-Binding Lectin Recognizes Structures on Ischaemic Reperfused Mouse Kidneys and is Implicated in Tissue Injury. *Scand. J. Immunol.* **61**, 426–434 (2005).
48. Pavlov, V. I. *et al.* Endogenous and Natural Complement Inhibitor Attenuates Myocardial Injury and Arterial Thrombogenesis. *Circulation* **126**, 2227–2235 (2012).
49. McMullen, M. E. *et al.* Mannose-binding lectin binds IgM to activate the lectin complement pathway in vitro and in vivo. *Immunobiology* **211**, 759–766 (2006).
50. Orsini, F., De Blasio, D., Zangari, R., Zanier, E. R. & De Simoni, M.-G. Versatility of the complement system in neuroinflammation, neurodegeneration and brain homeostasis. *Front. Cell. Neurosci.* **8**, (2014).
51. Duni, A. *et al.* The Endothelial Glycocalyx as a Target of Ischemia and Reperfusion Injury in Kidney Transplantation—Where Have We Gone So Far? *Int. J. Mol. Sci.* **22**, 2157 (2021).
52. Bongoni, A. K. *et al.* Complement-mediated Damage to the Glycocalyx Plays a Role in Renal Ischemia-reperfusion Injury in Mice. *Transplant. Direct* **5**, e341 (2019).
53. Mitra, R. *et al.* Glycocalyx in Atherosclerosis-Relevant Endothelium Function and as a Therapeutic Target. *Curr. Atheroscler. Rep.* **19**, 63 (2017).
54. Bruegger, D. *et al.* Shedding of the endothelial glycocalyx during cardiac surgery: On-pump versus off-pump coronary artery bypass graft surgery. *J. Thorac. Cardiovasc. Surg.* **138**, 1445–1447 (2009).
55. Rubio-Gayosso, I., Platts, S. H. & Duling, B. R. Reactive oxygen species mediate modification of glycocalyx during ischemia-reperfusion injury. *Am. J. Physiol.-Heart Circ. Physiol.* **290**, H2247–H2256 (2006).

- 56.van Golen, R. F. *et al.* The Mechanisms and Physiological Relevance of Glycocalyx Degradation in Hepatic Ischemia/Reperfusion Injury. *Antioxid. Redox Signal.* **21**, 1098–1118 (2014).
- 57.Haeger, S. M., Yang, Y. & Schmidt, E. P. Heparan Sulfate in the Developing, Healthy, and Injured Lung. *Am. J. Respir. Cell Mol. Biol.* **55**, 5–11 (2016).
- 58.Nian, K., Harding, I. C., Herman, I. M. & Ebong, E. E. Blood-Brain Barrier Damage in Ischemic Stroke and Its Regulation by Endothelial Mechanotransduction. *Front. Physiol.* **11**, (2020).
- 59.Jin, J. *et al.* The Structure and Function of the Glycocalyx and Its Connection With Blood-Brain Barrier. *Front. Cell. Neurosci.* **15**, (2021).
- 60.Peiris, D. *et al.* Cellular glycosylation affects Herceptin binding and sensitivity of breast cancer cells to doxorubicin and growth factors. *Sci. Rep.* **7**, 43006 (2017).
- 61.Li, X. *et al.* Real-time and label-free analysis of binding thermodynamics of carbohydrate-protein interactions on unfixed cancer cell surfaces using a QCM biosensor. *Sci. Rep.* **5**, 14066 (2015).
- 62.Shao, C. *et al.* Facile fabrication of glycopolymer-based iron oxide nanoparticles and their applications in the carbohydrate–lectin interaction and targeted cell imaging. *Polym. Chem.* **7**, 1337–1344 (2016).
- 63.Elmlund, L., Käck, C., Aastrup, T. & Nicholls, I. A. Study of the Interaction of Trastuzumab and SKOV3 Epithelial Cancer Cells Using a Quartz Crystal Microbalance Sensor. *Sensors* **15**, 5884–5894 (2015).
- 64.von Tiedemann, B. & Bilitewski, U. Characterization of the vascular endothelial growth factor-receptor interaction and determination of the recombinant protein by an optical receptor sensor. *Biosens. Bioelectron.* **17**, 983–991 (2002).
- 65.Pei, Z., Saint-Guirons, J., Käck, C., Ingemarsson, B. & Aastrup, T. Real-time analysis of the carbohydrates on cell surfaces using a QCM biosensor: a lectin-based approach. *Biosens. Bioelectron.* **35**, 200–205 (2012).

66. Peiris, D., Markiv, A., Curley, G. P. & Dwek, M. V. A novel approach to determining the affinity of protein-carbohydrate interactions employing adherent cancer cells grown on a biosensor surface. *Biosens. Bioelectron.* **35**, 160–166 (2012).
67. Angeloni, S. *et al.* Glycoprofiling with micro-arrays of glycoconjugates and lectins. *Glycobiology* **15**, 31–41 (2005).
68. Kutuzov, N., Flyvbjerg, H. & Lauritzen, M. Contributions of the glycocalyx, endothelium, and extravascular compartment to the blood–brain barrier. *Proc. Natl. Acad. Sci.* **115**, E9429–E9438 (2018).
69. Beyer, S. *et al.* Lectin Staining of Microvascular Glycocalyx in Microfluidic Cancer Cell Extravasation Assays. *Life* **11**, 179 (2021).
70. Orsini, F. *et al.* Mannose-Binding Lectin Drives Platelet Inflammatory Phenotype and Vascular Damage After Cerebral Ischemia in Mice via IL (Interleukin)-1 $\alpha$ . *Arterioscler. Thromb. Vasc. Biol.* **38**, 2678–2690 (2018).
71. Neglia, L., Oggioni, M., Mercurio, D., De Simoni, M.-G. & Fumagalli, S. Specific contribution of mannose-binding lectin murine isoforms to brain ischemia/reperfusion injury. *Cell. Mol. Immunol.* **17**, 218–226 (2020).
72. Rajagopalan, R., Salvi, V. P., Jensenius, J. Chr. & Rawal, N. New insights on the structural/functional properties of recombinant human mannan-binding lectin and its variants. *Immunol. Lett.* **123**, 114–124 (2009).
73. Barrientos, Á. G., de la Fuente, J. M., Rojas, T. C., Fernández, A. & Penadés, S. Gold Glyconanoparticles: Synthetic Polyvalent Ligands Mimicking Glycocalyx-Like Surfaces as Tools for Glycobiological Studies. *Chem. - Eur. J.* **9**, 1909–1921 (2003).
74. Martínez-Ávila, O. *et al.* Gold Manno -Glyconanoparticles: Multivalent Systems to Block HIV-1 gp120 Binding to the Lectin DC-SIGN. *Chem. - Eur. J.* **15**, 9874–9888 (2009).

75. Silvestri, A. *et al.* Design of functionalized gold nanoparticle probes for computed tomography imaging: Design of Tailored Engineered AuNPs as CT Contrast Agents. *Contrast Media Mol. Imaging* **11**, 405–414 (2016).
76. Percie du Sert, N. *et al.* The IMPROVE Guidelines (Ischaemia Models: Procedural Refinements Of in Vivo Experiments). *J. Cereb. Blood Flow Metab.* **37**, 3488–3517 (2017).
77. Garred, P., Larsen, F., Seyfarth, J., Fujita, R. & Madsen, H. O. Mannose-binding lectin and its genetic variants. *Genes Immun.* **7**, 85–94 (2006).
78. Guo, L. *et al.* A Universal Photochemical Method to Prepare Carbohydrate Sensors Based on Perfluorophenylazide Modified Polydopamine for Study of Carbohydrate-Lectin Interactions by QCM Biosensor. *Polymers* **11**, 1023 (2019).
79. Honoré, C. *et al.* Tethering of Ficolin-1 to cell surfaces through recognition of sialic acid by the fibrinogen-like domain. *J. Leukoc. Biol.* **88**, 145–158 (2010).
80. Lu, J. H., Thiel, S., Wiedemann, H., Timpl, R. & Reid, K. B. Binding of the pentamer/hexamer forms of mannan-binding protein to zymosan activates the proenzyme C1r2C1s2 complex, of the classical pathway of complement, without involvement of C1q. *J. Immunol.* **144**, 2287–2294 (1990).
81. Jensen, P. H. *et al.* Characterization of the Oligomer Structure of Recombinant Human Mannan-binding Lectin \*. *J. Biol. Chem.* **280**, 11043–11051 (2005).
82. Monopoli, M. P., Pitek, A. S., Lynch, I. & Dawson, K. A. Formation and Characterization of the Nanoparticle–Protein Corona. in *Nanomaterial Interfaces in Biology: Methods and Protocols* (eds. Bergese, P. & Hamad-Schifferli, K.) 137–155 (Humana Press, 2013). doi:10.1007/978-1-62703-462-3\_11.

83. Liangsupree, T., Multia, E., Forssén, P., Fornstedt, T. & Riekkola, M.-L. Kinetics and interaction studies of anti-tetraspanin antibodies and ICAM-1 with extracellular vesicle subpopulations using continuous flow quartz crystal microbalance biosensor. *Biosens. Bioelectron.* **206**, 114151 (2022).
84. Goumenou, A., Delaunay, N. & Pichon, V. Recent Advances in Lectin-Based Affinity Sorbents for Protein Glycosylation Studies. *Front. Mol. Biosci.* **8**, 746822 (2021).
85. Seyfarth, J., Garred, P. & Madsen, H. O. The ‘involution’ of mannose-binding lectin. *Hum. Mol. Genet.* **14**, 2859–2869 (2005).
86. Orsini, F. *et al.* Mannan binding lectin-associated serine protease-2 (MASP-2) critically contributes to post-ischemic brain injury independent of MASP-1. *J. Neuroinflammation* **13**, 213 (2016).
87. Schwaeble, W. J. *et al.* Targeting of mannan-binding lectin-associated serine protease-2 confers protection from myocardial and gastrointestinal ischemia/reperfusion injury. *Proc. Natl. Acad. Sci.* **108**, 7523–7528 (2011).
88. Arms, L. *et al.* Advantages and Limitations of Current Techniques for Analyzing the Biodistribution of Nanoparticles. *Front. Pharmacol.* **9**, 802 (2018).
89. Guesmi, H., Luque, N. B., Santos, E. & Tielens, F. Does the S–H Bond Always Break after Adsorption of an Alkylthiol on Au(111)? *Chem. - Eur. J.* **23**, 1402–1408 (2017).
90. Altintas, Z. Surface plasmon resonance based sensor for the detection of glycopeptide antibiotics in milk using rationally designed nanoMIPs. *Sci. Rep.* **8**, (2018).
91. Spampinato, V., Parracino, M. A., La Spina, R., Rossi, F. & Ceccone, G. Surface Analysis of Gold Nanoparticles Functionalized with Thiol-Modified Glucose SAMs for Biosensor Applications. *Front. Chem.* **4**, (2016).
92. Whitesides, G. M., Kriebel, J. K. & Love, J. C. Molecular engineering of Surfaces Using Self-Assembled Monolayers. *Sci. Prog.* **88**, 17–48 (2005).

93. Worley, C. G. & Linton, R. W. Removing sulfur from gold using ultraviolet/ozone cleaning. *J. Vac. Sci. Technol. Vac. Surf. Films* **13**, 2281–2284 (1995).
94. Lee, J. M. *et al.* Direct Immobilization of Protein G Variants with Various Numbers of Cysteine Residues on a Gold Surface. *Anal. Chem.* **79**, 2680–2687 (2007).
95. Park, K. *et al.* Combination of cysteine- and oligomerization domain-mediated protein immobilization on a surface plasmon resonance (SPR) gold chip surface. *The Analyst* **136**, 2506 (2011).
96. Jensenius, H. *et al.* Mannan-Binding Lectin: Structure, Oligomerization, and Flexibility Studied by Atomic Force Microscopy. *J. Mol. Biol.* **391**, 246–259 (2009).
97. Miller, A., Phillips, A., Gor, J., Wallis, R. & Perkins, S. J. Near-planar Solution Structures of Mannose-binding Lectin Oligomers Provide Insight on Activation of Lectin Pathway of Complement. *J. Biol. Chem.* **287**, 3930–3945 (2012).
98. Yilmaz, G. & Remzi Becer, C. Glyconanoparticles and their interactions with lectins. *Polym. Chem.* **6**, 5503–5514 (2015).
99. Rampersad, S. N. Multiple Applications of Alamar Blue as an Indicator of Metabolic Function and Cellular Health in Cell Viability Bioassays. *Sensors* **12**, 12347–12360 (2012).
100. Veksler, B. A., Lemelle, A., Kozhevnikov, I. S., Akchurin, G. G. & Meglinski, I. V. Improving image quality in reflection confocal microscopy involving gold nanoparticles and osmotically active immersion liquids. *Opt. Spectrosc.* **110**, 483–488 (2011).
101. S. Wolfbeis, O. An overview of nanoparticles commonly used in fluorescent bioimaging. *Chem. Soc. Rev.* **44**, 4743–4768 (2015).
102. Chou, L. Y. T. & Chan, W. C. W. Fluorescence-Tagged Gold Nanoparticles for Rapidly Characterizing the Size-Dependent Biodistribution in Tumor Models. *Adv. Healthc. Mater.* **1**, 714–721 (2012).

103. Fokkema, J. *et al.* Fluorescently Labelled Silica Coated Gold Nanoparticles as Fiducial Markers for Correlative Light and Electron Microscopy. *Sci. Rep.* **8**, 13625 (2018).
104. Robson, A.-L. *et al.* Advantages and Limitations of Current Imaging Techniques for Characterizing Liposome Morphology. *Front. Pharmacol.* **9**, (2018).
105. Guggenheim, E. J. *et al.* Comparison of Confocal and Super-Resolution Reflectance Imaging of Metal Oxide Nanoparticles. *PLOS ONE* **11**, e0159980 (2016).
106. Wang, S.-H., Lee, C.-W., Chiou, A. & Wei, P.-K. Size-dependent endocytosis of gold nanoparticles studied by three-dimensional mapping of plasmonic scattering images. *J. Nanobiotechnology* **8**, 33 (2010).
107. Gromnicova, R. *et al.* Glucose-Coated Gold Nanoparticles Transfer across Human Brain Endothelium and Enter Astrocytes In Vitro. *PLOS ONE* **8**, e81043 (2013).
108. del Zoppo, G. J. & Mabuchi, T. Cerebral Microvessel Responses to Focal Ischemia. *J. Cereb. Blood Flow Metab.* **23**, 879–894 (2003).
109. Gál, P. *et al.* A true autoactivating enzyme. Structural insight into mannose-binding lectin-associated serine protease-2 activations. *J. Biol. Chem.* **280**, 33435–33444 (2005).
110. Stover, C. *et al.* The human gene for mannan-binding lectin-associated serine protease-2 (MASP-2), the effector component of the lectin route of complement activation, is part of a tightly linked gene cluster on chromosome 1p36.2–3. *Genes Immun.* **2**, 119–127 (2001).
111. Kozarcanin, H. *et al.* The lectin complement pathway serine proteases (MASPs) represent a possible crossroad between the coagulation and complement systems in thromboinflammation. *J. Thromb. Haemost.* **14**, 531–545 (2016).
112. Chen, Y.-S., Hung, Y.-C., Liao, I. & Huang, G. S. Assessment of the In Vivo Toxicity of Gold Nanoparticles. *Nanoscale Res. Lett.* **4**, 858–864 (2009).



113. Arvizo, R., Bhattacharya, R. & Mukherjee, P. Gold nanoparticles: Opportunities and Challenges in Nanomedicine. *Expert Opin. Drug Deliv.* **7**, 753–763 (2010).

## Appendix

---

### A. Declaration of Competing Interest

The authors declare the following financial interests/personal relationships which may be considered as potential competing interests, Daniel I. R. Spencer reports a relationship with Ludger Ltd that includes employment. The authors based at Ludger Ltd work in commercializing analytical assays for use in the field of glycomics and the analysis of biopharmaceuticals.

### B. Publications

Title: New nanostructures inhibiting human mannose binding lectin identified by a novel surface plasmon resonance assay

G Erol et al. Science Direct, Sensors and Actuators B: Chemical, 2022, IF 7.3

Link: <https://doi.org/10.1016/j.snb.2022.131661>

### C. Funding

This project has received funding from the European Union's Horizon 2020 research and innovation programme under the Marie Skłodowska-Curie grant agreement No [814236](#).